Leaking chaotic systems

Eduardo G. Altmann

Max Planck Institute for the Physics of Complex Systems, 01187 Dresden, Germany

Jefferson S. E. Portela

Max Planck Institute for the Physics of Complex Systems, 01187 Dresden, Germany and Fraunhofer Institute for Industrial Mathematics ITWM, 67663 Kaiserslautern, Germany

Tamás Tél

Institute for Theoretical Physics-HAS Research Group, Eötvös University, Pázmány Péter sétány 1/A, Budapest, H-1117, Hungary

(published 29 May 2013)

There are numerous physical situations in which a hole or leak is introduced in an otherwise closed chaotic system. The leak can have a natural origin, it can mimic measurement devices, and it can also be used to reveal dynamical properties of the closed system. A unified treatment of leaking systems is provided and applications to different physical problems, in both the classical and quantum pictures, are reviewed. The treatment is based on the transient chaos theory of open systems, which is essential because real leaks have finite size and therefore estimations based on the closed system differ essentially from observations. The field of applications reviewed is very broad, ranging from planetary astronomy and hydrodynamical flows to plasma physics and quantum fidelity. The theory is expanded and adapted to the case of partial leaks (partial absorption and/or transmission) with applications to room acoustics and optical microcavities in mind. Simulations in the limaçon family of billiards illustrate the main text. Regarding billiard dynamics, it is emphasized that a correct discrete-time representation can be given only in terms of the so-called true-time maps, while traditional Poincaré maps lead to erroneous results. Perron-Frobenius-type operators are generalized so that they describe true-time maps with partial leaks.

DOI: 10.1103/RevModPhys.85.869 PACS numbers: 05.45.Mt, 05.45.Gg

CONTENTS

I. INTRODUCTION

A. Motivation

Perhaps the most important distinction in the temporal evolution of a dynamical system is between persistent (asymptotic) and transient (finite-time) dynamics. The dynamical systems theory reflects this division and has developed specialized methods and tools to investigate persistent (e.g., strange attractors, asymptotic Lyapunov exponents) and transient (e.g., chaotic saddle, escape rates) chaotic dynamics (Ott, 1993; Tél and Gruiz, 2006; Lai and Tél, 2011). These two approaches become connected when considering the effect of opening up a hole (or introducing a leak) in an otherwise closed chaotic system, converting by this persistent into transient chaos. Transient and persistent dynamics appear in both conservative and dissipative systems, and it is important to distinguish leakage (escape or removal of trajectories) from dissipation (contraction in the phase space). Introducing a leak never generates an extra phase-space contraction and, e.g., a conservative system remains conservative after becoming leaky.

More than a tool to investigate the relationship between different theories, problems described by a closed chaotic system with a leak appear nowadays in a great variety of fields.

- Room acoustics: The decay of the sound energy characterized traditionally by the so-called reverberation time can be considered a consequence of leaks: openings and absorbing surfaces on the room's boundary (Bauer and Bertsch, 1990; Legrand and Sornette, 1990b, 1991a; Mortessagne, Legrand, and Sornette, 1993). Absorbing surfaces provide examples of partial leaks.
- Chemical reactions: Unimolecular decay of excited chemical species has been modeled as an escape from a (chaotic) reactant region through a leak (Dumont and Brumer, 1992; Ezra, Waalkens, and Wiggins, 2009).
- Hydrodynamical flows and environmental sciences: The fact that certain regions of flows have special hydrodynamical features and might therefore change the properties of particles advected into these regions can be described by the so-called resetting mechanism (Pierrehumbert, 1994), which is a kind of leak from the point of view of chaotic advection (Neufeld, Haynes, and Picard, 2000; Schneider, Fernández, and Hernández-Garcia, 2000; Schneider, Tél, and Neufeld, 2002; Schneider and Tél, 2003; Tuval *et al.*, 2004; Schneider, Schmalzl, and Tél, 2007).
- Planetary science and cosmology: The (inelastic) collision of a small body with larger planetary objects leads to a drastic change in its dynamics compared to that in a point mass approximation of the larger bodies. In a first approximation the problem can be treated as a loss due to leaks (Nagler, 2004, 2005). Similar ideas apply in cosmology (Motter, 2001).
- Optical microcavities: Light rays in dielectric materials are partially transmitted and reflected (with the exception of regions where total internal reflection takes place). Chaotic cavities can be constructed to provide a strong directionality of emission through such a partial leak, a requirement for the laser application (Nöckel and Stone, 1997; Lee *et al.*, 2004; Schwefel *et al.*, 2004; Ryu *et al.*, 2006; Wiersig and Hentschel, 2008; Altmann, 2009; Dettmann *et al.*, 2009; Shinohara *et al.*, 2009, 2010, 2011; Yan *et al.*, 2009; Harayama and Shinohara, 2011).
- Plasma physics: Particles in magnetic confinement devices are lost through collisions with sensors, antennas, or the chambers wall itself. These regions therefore play the role of a leak (Evans, Moyer, and Monat, 2002; Portela *et al.*, 2007; Wingen *et al.*, 2007; Portela, Caldas, and Viana, 2008; Viana *et al.*, 2011).
- Wave and quantum signatures of open systems: Features related to that of a leaking classical dynamics appear in properties such as the (fractal) distribution of eigenstates (Casati, Maspero, and Shepelyanski, 1999a; Kuhl, Stöckmann, and Weaver, 2005; Keating *et al.*, 2006; Nonnenmacher and Schenk, 2008; Ermann, Carlo, and Saraceno, 2009; Pedrosa *et al.*, 2009; Novaes, 2012), the survival probability in simulations and experiments (Alt *et al.*, 1995, 1996; Fendrik and Wisniacki, 1997; Casati, Maspero, and Shepelyansky, 1999b; Friedman *et al.*, 2001; Kaplan *et al.*, 2001), and in the fractal Weyl's law (Lu, Sridhar, and Zworski, 2003; Schomerus and Tworzydło, 2004; Shepelyansky, 2008; Wiersig and Main, 2008; Ramilowski *et al.*, 2009; Ermann and Shepelyansky, 2010; Kopp and Schomerus, 2010; Nonnenmacher, 2011).

In dynamical-systems theory, the idea of leaking an otherwise closed chaotic systems was first proposed by Pianigiani and Yorke as early as 1979:

> Picture an energy conserving billiard table with smooth obstacles so that all trajectories are unstable with respect to the initial data. Now suppose a small hole is cut in the table so that the ball can fall through. We would like to investigate the statistical behavior of such phenomena (Pianigiani and Yorke, 1979).

Their main motivation was precisely to investigate transient chaos as opposed to persistent chaos. The leakage procedure was therefore a tool to create transiently chaotic systems. Interestingly, the development of the theory of transient chaos happened not to follow this line over decades.

The importance of this mathematical approach becomes apparent when one realizes the multitude of situations in which the leak region has a well-defined physical interpretation. This aspect was first emphasized by Smilansky and coworkers, who pointed out that any measurement (both classical and quantum) leads unavoidably to a leakage of the system. They wrote in 1992:

A discrete spectrum is a property of a closed system. However, the process of measuring the spectrum of a bounded system consists of coupling the system to an external continuum. Thus, for the purpose of measurement, the closed system is turned into a scattering system (Doron and Smilansky, 1992a).

Physical realizations of the leak can thus be either the effect of measurement devices or intrinsic properties of the system, such as, e.g., absorbing boundaries.

Apart from physical leaks, there are also different *theoretical* motivations for considering leaking systems:

- Leakage is a tool to understand the dynamics of closed systems, providing thus a sort of *chaotic spectroscopy* (Doron and Smilansky, 1992a, 1992b). More generally, systems with leaks help monitoring or *peeping at* chaos (Bunimovich and Dettmann, 2007) [see also Nagler *et al.* (2007)]. In this context, as in Pianigiani and Yorke (1979), billiards with leaks were the first systems investigated because they allow a natural connection between the classical and quantum pictures (Bauer and Bertsch, 1990; Alt *et al.*, 1995, 1996).
- Leaking systems have been explored in the context of synchronization of chaotic oscillators (Jacobs, Ott, and Hunt, 1998), and of the control of chaos (Paar and Pavin, 1997; Paar and Buljan, 2000; Buljan and Paar, 2001).
- Leakage reveals the foliations inside the closed system (Schneider, Tél, and Neufeld, 2002; Aguirre and Sanjuán, 2003; Sanjuán, Horita, and Aihara, 2003; Aguirre, Viana, and Sanjuán, 2009) that lead, e.g., to fractal exit boundaries (Bleher *et al.*, 1988; Ree and Reichl, 2002; Portela *et al.*, 2007).
- The distribution of Poincaré recurrences, which is commonly used to quantify properties of closed Hamiltonian dynamics (Chirikov and Shepelyansky, 1984; Zaslavsky, 2002), is equivalent to the survival probability in the same system with a leak (Altmann and Tél, 2008).
- Several quantifications of wave or quantum chaos, such as Loschmidt echo (Gorin, Prosen, and Seligman, 2006; Jacquod and Petitjean, 2009) or fidelity decay (Peres, 1984), can be realized physically in configurations that are analogous to introducing a localized leak in a closed system (Goussev and Richter, 2007; Goussev *et al.*, 2008; Höhmann, Kuhl, and Stöckmann, 2008; Ares and Wisniacki, 2009; Köber *et al.*, 2011).

The common feature in all applications and theoretical procedures listed above is that one has some freedom when choosing the opening, i.e., the leak in a well-defined closed chaotic system (Schneider, Tél, and Neufeld, 2002). This should be contrasted to genuinely open systems in which the openness is intrinsic, and only slight parametric changes are physically realistic, which typically do not allow one to go to the closed-system limit. Although both classes of systems are dynamically open, one of our aims is to emphasize the benefits of considering leaking systems, which are more precisely defined by two key elements:

(i) the existence of a well-defined closed system which can be used as a comparison, and
(ii) the possibility of controlling (some) properties of the leak such as position, size, shape, or reflectivity.

Property (i) guarantees that one can compare transient and asymptotic dynamics and can be considered as a particular case of (ii) if the possibility of reducing the leak size to zero is assured. Leaking systems can be both dissipative and conservative (Hamiltonian). Within this latter category, we consider the problem of chaotic scattering [as typically defined, e.g., by Gaspard (1998)] to be beyond the scope of this review because it lacks properties (i) and (ii) above.[1]

Our main approach in this review article is based on transient chaos theory, which is applied to the case of leaky systems and connected to different recent applications. Our aim is to be understandable by nonspecialists interested in learning what the implications of dynamical-systems theories are to specific applications. At the same time, we emphasize how specific applications pose new questions to the theory. Thus, we devote special attention to developing a theory consistent with the following two aspects required by different applications:

- Leaks are not necessarily full holes; they might be "semipermeable," i.e., the energy content of trajectories entering a leak is partially transmitted and partially reflected. In such cases the leak is called a *partial* leak.
- Discrete-time maps of open flows might lead to a loss of information over the temporal properties, and therefore it is essential to use the generalized concept of *true-time maps* (Kaufmann and Lustfeld, 2001), which will be defined in Sec. I.C.

We note here that even though our focus and numerical illustrations are on billiards (Hamiltonian systems), the theoretical framework and many of the specific results can be naturally extended to systems with dissipation.

In the remainder of this section we motivate the general problem through a historical example and a simple simulation. In Sec. II we confront the simplest theory, based on the properties of the closed system, with the appropriate transient chaos theory for open systems. A generalization of this theory to partial leaks is also given. Section III is devoted to a Perron-Frobenius–type operator formalism that is able to describe any kind of leaking dynamics. The main implications of transient chaos theory are explored in Sec. IV, including the case of multiple leaks and emission. In Sec. V we discuss how to describe the generic situation of weakly chaotic Hamiltonian systems (mixed phase space). Finally, in Sec. VI we use our results to give a detailed view on some of the problems we started this section with. Our conclusions appear in Sec. VII. In Appendixes A, B, C, and D we discuss some important but technical aspects of open billiards (like, e.g., different types of measures and algorithms).

[1]In some scattering cases it is possible to "close" the inside of the scattering region (e.g., in the three disk problem, when the disks touch). However, in these cases the closing procedure is either arbitrary or unnatural from the point of view of scattering (e.g., the incoming trajectories are unable to enter the chaotic region).

B. Classical leaking: Kinetic theory and Sabine's law

Historically, perhaps the first problem involving systems with leaks was one related to the kinetic theory of gases. Consider a container filled with ideal gas. How is the container emptied after a *small* leak I is introduced on its boundary?

The answer can be obtained from an elementary application of the kinetic theory. Here we follow basically the treatment of Joyce (1975) and Bauer and Bertsch (1990). Let I be a disk of area ΔA on the surface of the container and $f(\mathbf{v}, t)$ be the phase-space density of the particles, for which

$$\int f(\mathbf{v}, t) d^3\mathbf{v} = \frac{N(t)}{V}, \tag{1}$$

where $N(t)$ is the number of particles in the container of volume V at time t. The number of particles with velocity $\mathbf{v}$ leaving the system over a short time interval dt is then $dN = dt\Delta A\mathbf{v}\mathbf{n} f(\mathbf{v}, t) d^3\mathbf{v}$, where $\mathbf{n}$ is the normal vector of the surface at the leak I. The total number is then obtained by carrying out an integration over all velocities. Thus, the time derivative of the number $N(t)$ of particles inside the container is

$$\frac{dN(t)}{dt} = -\Delta A \int \mathbf{v}\mathbf{n} f(\mathbf{v}, t) d^3\mathbf{v}, \tag{2}$$

where the minus sign indicates that particles are escaping.

Molecular chaos, a basic ingredient of kinetic theory, implies that an *equilibrium* phase-space density exists. In our problem it is *homogeneous* (location independent) and *isotropic*: all velocity directions are equally probable. In the limit of small ΔA we can expect that there is a quasiequilibrium distribution $f(\mathbf{v}, t)$ in the open system which sets in on a time scale shorter than the average lifetime. This quasiequilibrium distribution shares the properties of that of closed systems. In this case, isotropy guarantees that the phase-space density depends only on the modulus v of the velocity, and it is, therefore, convenient to use spherical coordinates for the integration. With θ being the angle between velocity and the normal vector, $\mathbf{v} \cdot \mathbf{n} = v\cos\theta$, Eq. (2) reads as

$$\frac{dN(t)}{dt} = -\Delta A \int_0^\infty v f(v, t) v^2 dv \int_0^{\pi/2} \cos\theta \sin\theta d\theta \int_0^{2\pi} d\phi. \tag{3}$$

The spherical symmetry of the phase-space density applied to Eq. (1) leads to

$$\int_0^\infty f(v, t) v^2 dv 4\pi = \frac{N(t)}{V}, \tag{4}$$

and implies that $w(v) = 4\pi f(v, t) v^2 V/N(t)$ is the probability density for the velocity modulus v in the gas.

Substituting this into Eq. (3), the first integral is found to be proportional to the average $\langle v\rangle$ of the velocity modulus. By carrying out all integrals, we find

$$\frac{dN(t)}{dt} = -\frac{\Delta A\langle v\rangle}{4V} N(t). \tag{5}$$

As long as $\langle v\rangle$ is independent of time[2] the decay of the particle number is thus exponential of the form of $\exp(-\kappa t)$, with an *escape rate*

$$\kappa = \frac{\Delta A\langle v\rangle}{4V}. \tag{6}$$

For simplicity we focus here on an ensemble of identical particles with the *same* velocity v colliding elastically, in which case $\langle v\rangle \mapsto v$ in Eq. (6).[3] The reciprocal of the escape rate, which turns out to be the average lifetime, can then be written as

$$\langle\tau\rangle = \frac{1}{\kappa} = \frac{4V}{\Delta A v}. \tag{7}$$

This is the time needed for the decay of the survivors by a factor of e. Since the result is linear in ΔA, and the velocity distribution is not only isotropic but also homogeneous, i.e., independent of the position along the wall, the expression remains valid for small leaks I of any shape, and ΔA is then the total leaking area. Since ΔA is small, $\langle\tau\rangle$ is large, and hence the assumption of a quasiequilibrium distribution becomes justified *a posteriori*.

An interesting, historically independent development is Sabine's law, a central object of architectural acoustics. This law says that the residual sound intensity in a room decays exponentially with time (Joyce, 1975; Mortessagne, Legrand, and Sornette, 1993). The duration to decay below the audible intensity is called the reverberation time T_r and was found experimentally by W. C. Sabine in 1898 to be

$$T_r = 6\ln(10)\frac{4V}{\Delta A c}. \tag{8}$$

Here c is the sound velocity, and ΔA is the area of the union of all openings of the room (or of all energy absorbing surfaces after proper normalization). With $c = 340$ m/s, the numerical value of T_r in SI units is $T = 0.16V/\Delta A$. Sabine's experiments also showed that the reverberation time for a pleasant sound perception is on the order of a few seconds for a good auditorium, and he designed concert halls (like, e.g., the Boston Music Hall) according to this principle.

A comparison of Eqs. (7) and (8) reveals that Sabine's law is nothing but an application of the exponential decay of the particle number evaluated with $v = c$ as the particle velocity. What is leaving the system in this problem is however not particles, but the energy of the sound waves. In the geometrical limit of room acoustics, one can consider the decay of energy as the problem of particles which travel along sound rays and lose part of their energy upon hitting the leak or the absorbing surface. The most remarkable property of Eq. (8) is its universality: the reverberation time is *independent* of the location of the sound source and of the shape of the room, provided the absorption is weak and sound disperses

[2]In a thermodynamical system the decay of particles eventually leads to a reduction in the pressure and temperature inside the container and thus to a reduction of v. Here we are interested in systems with constant v. The exponential decay is then valid for any $t > 0$.

[3]Note that the dynamics of elastic collisions of identical particles is equivalent to the dynamics of independent particles, as can be seen by exchanging particle labels at collision.

uniformly around the room, e.g., due to roughness or irregular geometry of the walls (Mortessagne, Legrand, and Sornette, 1993). The prefactor $6\ln(10)$ in Eq. (8) results from the fact that in the acoustic context the decay below the audible intensity implies 60 dB, i.e., a decay factor of 10^6, instead of a factor of e in Eq. (8). Sabine's law (8), dated back to 1898, appears thus to be the first application of leaking chaotic dynamical systems in the history of science.

We now take a closer look at the assumptions in the derivations above from the perspective of the dynamics. In terms of the modern theory of dynamical systems, the isotropy and homogeneity of the velocity distribution are a consequence of the following two hypotheses:

H1: the leak size is small, so that the phase-space distribution does not change due to the openness; and

H2: the particle dynamics inside the room is *chaotic*, more technically, the dynamics is *ergodic and strongly mixing* (implying exponential decay of correlations in time).

Under these assumptions, the exponential decay is valid also in other dimensions. For instance, the escape rate in two-dimensional billiards is then found to be

$$\kappa = \frac{\Delta A v}{\pi V}, \tag{9}$$

where ΔA is the length of the leak along the perimeter, and V is the two-dimensional volume, the area, of the billiard table. The replacement of the factor of 4 by π is due to the geometrical change from spherical to planar polar coordinates.

It should be noted that in both cases the survival probability $P(t)$ up to time t is

$$P(t) = e^{-\kappa t}, \tag{10}$$

as obtained from Eq. (5), with initial condition $P(0) = 1$. The probability $p(\tau)$ to leave around the escape time $\tau = t$ is the negative derivative of $P(t)$ and thus

$$p(\tau) = \kappa e^{-\kappa\tau}, \tag{11}$$

and $P(t) = \int_t^\infty p(\tau)d\tau$. Since the exponential decay holds from the very beginning, the average lifetime

$$\langle\tau\rangle = \int_0^\infty t' p(t')dt' = \int_0^\infty P(t')dt' \tag{12}$$

is found to be $\langle\tau\rangle = 1/\kappa$, which was used in Eq. (7). The symbol $\langle\cdots\rangle$ can be interpreted as an ensemble average.

Finally, it is instructive to write both Eqs. (6) and (9) of the escape rate as

$$\kappa = \frac{\mu(I)}{\langle t_{\rm coll}\rangle}, \tag{13}$$

where $\mu(I) = \Delta A/A$ is the relative size of the leak compared to the full wall surface and can therefore be considered as the *measure* of the leak (taken with respect to the Lebesgue measure). The denominator has the dimension of time and is given by

$$\langle t_{\rm coll}\rangle = \frac{4V}{Av} \quad \text{and} \quad \langle t_{\rm coll}\rangle = \frac{\pi V}{Av}, \tag{14}$$

in the three- and two-dimensional cases, respectively. These $\langle t_{\rm coll}\rangle$'s turn out to be the precise expressions of the *average collision time* between collisions with the wall (or, after a multiplication by v, the mean-free path), well known for three- and two-dimensional *closed* rooms or billiards. As emphasized by Joyce (1975) and Mortessagne, Legrand, and Sornette (1993), these results were obtained already in the late 19th century by Czuber and Clausius. It is the average collision time that sets the characteristic time with which the average lifetime should be compared: for small leaks $\langle\tau\rangle \gg \langle t_{\rm coll}\rangle$, i.e., the time scales strongly separate.

By definition, $\langle t_{\rm coll}\rangle$ can be expressed as the average over the local collision times $t_{\rm coll}(\mathbf{x})$ for the phase-space coordinates $\mathbf{x}$ along the wall as

$$\langle t_{\rm coll}\rangle = \int t_{\rm coll}(\mathbf{x})d\mu, \tag{15}$$

where μ is the uniform phase-space (Lebesgue) measure characteristic of conservative systems. All equations found are taken with respect to the distributions characteristic of the *closed* system. This is consistent with the small leak assumption (H1 above) so that the escape rates obtained can be considered as a leading order result in a perturbation expansion where averages can yet be taken with respect to distributions characterizing the unperturbed (closed) system.

In the modern applications mentioned in Sec. I.A, however, conditions H1 (small leaks) and H2 (strong chaos) are typically not met. Here we discuss in detail what happens in such cases. For instance, in any practical application the leak size is not, or cannot be made, infinitesimally small so that H1 is violated and perturbation expansions break down.

We shall see that an exponential decay of the survival probability typically remains valid for finite leak sizes, at least after some initial period. The estimation of the escape rate can be greatly improved by considering a similar expression as in Eq. (13), the measure of the leak divided by the average collision time, however, both taken with respect to a *different* measure:

$$\mu(I) \to \mu_c(I), \quad \langle t_{\rm coll}\rangle \to \langle t_{\rm coll}\rangle_c = \int t_{\rm coll}(\mathbf{x})d\mu_c. \tag{16}$$

The new relevant measure μ_c differs from the original Lebesgue measure μ since many particles have left the system by the time of observation, and what counts is the set of long-lived particles. With finite leaks, the decay differs substantially from the naive estimate obtained by using the original Lebesgue measure, as illustrated for our billiard example in Fig. 1. Even if precise definitions and further details appear only later, the conceptual difference between μ and μ_c is clear [compare Figs. 3(b) and 6 for an illustration of the dramatic changes in the phase space of the billiard].

The theory of open dynamical systems tells us that this new measure is the so-called *conditionally invariant measure* (c measure for short) introduced by Pianigiani and Yorke (1979), which is didactically introduced and investigated in Secs. A, B, C, and D and Appendix A. The violation of hypothesis H2 of strong chaos leads to even more radical changes, e.g., to a deviation from the exponential decay for long times. This case will be investigated in Sec. V.

C. Billiard dynamics and true-time maps

In dynamical-systems theory, the kinetic problem with fixed velocities and Sabine's picture of room acoustics are described as billiard systems, as noticed already by Joyce

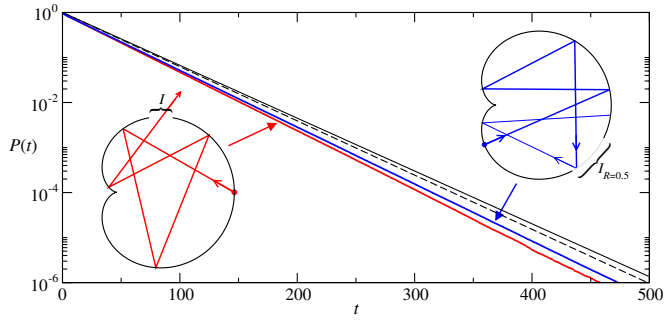

FIG. 1 (color online). Escape of particles in a billiard with a finite leak. The survival probability $P(t)$ for the strongly chaotic cardioid billiard [see Eq. (19) with $\varepsilon = 1$] is shown for two different configurations of the leak I (same effective size $2\Delta s$ but different leak positions s_l and reflectivity R). The first (bottom) line corresponds to a full leak [see Eq. (20)] centered at the top of the billiard, $s_l = 0.5$, with size $2\Delta s = 0.1$ (5% of the perimeter) as shown in the left inset. The second (next to the bottom) line corresponds to a partial leak with $R = 0.5$ [see Eq. (21)] centered at $s_l = -0.25$ with a size $2\Delta s = 0.2$ as shown in the right inset. The observed escape rates are $\kappa = 0.030\,02 \pm 0.000\,07$ (full leak) and $\kappa = 0.029\,04 \pm 0.000\,03$ (partial leak), clearly different from the predictions $\kappa = 0.0270$ (upper full line) based on Sabine's law (13) and (14), and the naive estimate $\kappa^* = 0.0277$, Eq. (23) (dashed line) with $\mu(I) = 0.05$. Initial conditions were uniformly distributed in the phase space (s, $p = \sin\theta$, see Fig. 3).

(1975). Billiards are defined as bounded volumes or areas inside which particles move in a straight line with constant velocity v between collisions at the boundary, where they experience specular, elastic reflection (i.e., the angle of incidence is equal to the angle θ of reflection and the absolute value of the velocity v is conserved) (Chernov and Markarian, 2006). A recent sample of the research on billiards can be found in Leonel, Beims, and Bunimovich (2012).

For numerical and visualization convenience, we illustrate our results in two-dimensional billiards. In this case the dynamics can be described in a two-dimensional phase space, achieved by replacing the continuous-time dynamics by a corresponding discrete-time system $\mathbf{f}$ that maps the position s along the boundary and angle θ of the nth collision into those of the $(n+1)$th collision at the boundary. By convention, the map f connects the momenta right *after* the collisions. This procedure corresponds to a Poincaré surface of section. The dimension of the full (four-dimensional) phase space is reduced by 2 (using momentum conservation and the condition of collision). The shape of the billiard's boundary uniquely defines the dynamics of the particles, and system-specific properties depend sensitively on this shape. It is convenient to write the phase space of the map in terms of Birkhoff coordinates $\mathbf{x} = (s, p \equiv \sin\theta)$ in which case

$$\mathbf{f}: (\mathbf{x}_n) \mapsto (\mathbf{x}_{n+1}) \tag{17}$$

is area preserving (Berry, 1981; Chernov and Markarian, 2006).

A faithful representation of the temporal dynamics of billiards requires augmenting Eq. (17) by keeping track of the information about the time of each trajectory:

$$t_{n+1} = t_n + t_{\text{coll}}(\mathbf{x}_{n+1}), \tag{18}$$

where t_n denotes the time of the nth collision at the boundary of the billiard, and t_{coll} denotes the time between two subsequent collisions. In what follows we associate t_{coll} with the Birkhoff coordinates of the *later* collision ($\mathbf{x}_{n+1}$) in order to be able to speak about the collision times within the leak when systems with leaks are considered [see Eq. (20)].

Equations (17) and (18) are called a true-time map as coined by Kaufmann and Lustfeld (2001), which is also frequently used in the billiard context [see, e.g., Bunimovich and Dettmann (2007)]. More generally, true-time maps provide a link between discrete-time maps and continuous-time flows in the same spirit as described by the mathematical concepts of *suspended* flows, *special* flows, or *flows under a function* (Katok and Hasselblatt, 1995; Gaspard, 1998). They have also been used in the context of transport models (Matyas and Klages, 2004; Matyas and Barna, 2011).

A true-time map is equivalent to the continuous-time representation, but leads to faster and more reliable results than a direct integration of the billiard flow. The different collision times can be taken into account also in the Perron-Frobenius representation of the dynamics, as shown in Sec. III.D.

In contrast, the often used Poincaré map, represented by Eq. (17) alone, provides a distorted image of time. It implies associating with each pair of collision the same time interval and thus loses contact with the temporal dynamics of the continuous-time physical system (e.g., it can overestimate the importance of events with short collision times). The Poincaré map generates a measure different from that of the true-time map and thus leads to erroneous results. When talking about maps in the billiard context, we, therefore, always mean true-time maps. (Poincaré maps of billiards will be mentioned again in Table II and Appendix D to illustrate the difference to true-time maps.)

D. Example in a chaotic billiard

The main properties of two-dimensional billiards can be illustrated by the family of limaçon billiards introduced by Robnik (1983) whose borders are defined in polar coordinates $(\mathfrak{r}, \phi)$ by limaçon-like curves

$$\mathfrak{r}(\phi) = S(1 + \varepsilon\cos\phi), \tag{19}$$

where S scales the size and ε controls the shape of the billiard. The ratio S/v defines the unit in which time t is measured, which is the only effect of S and v on the dynamics. We therefore set $S = v = 1$ in what follows, which implies that the perimeter length is $A = 8$, the billiard's area is $V = 3\pi/2$, and the mean collision time (14) is thus $\langle t_{\text{coll}}\rangle = 3\pi^2/16$. For convenience, throughout we use the convention that the perimeter coordinate s is parametrized between -1 and $+1$ (see, e.g., Figs. 2 and 3).

For $\varepsilon = 0$ we recover the circular billiard, exhibiting regular dynamics. For $\varepsilon = 1$, Eq. (19) defines the *cardioid* billiard, which is ergodic and strongly mixing (Robnik, 1983; Wojtkowski, 1986), satisfying the hypothesis of strong chaos H2 (Sec. I.B). For $0 < \varepsilon < 1$, the billiard typically shows the coexistence of chaotic and regular components in the phase space (Dullin and Baecker, 2001), and exhibits weak chaos. The collision time $t_{\text{coll}}(\mathbf{x})$ needed for the

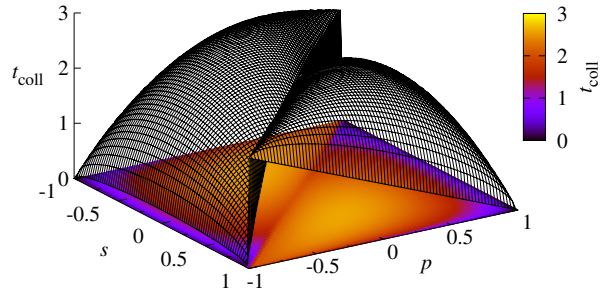

FIG. 2 (color online). Collision time $t_{coll}(\mathbf{x})$ as a function of the phase-space coordinates $\mathbf{x} = (s, p)$ in the cardioid billiard, Eq. (19) with $\varepsilon = 1$. Consistent with the convention in Eq. (18), $t_{coll}(\mathbf{x})$ is defined as the distance (or time, since $v \equiv 1$) between $\mathbf{x}$ and the *previous* collision $f^{-1}(\mathbf{x})$. The discontinuity close to the diagonal reflects the billiard's cusp at $s = \pm 1$; see Fig. 3(a).

true-time map (17) and (18) can be determined numerically and is shown in Fig. 2 for the cardioid case ($\varepsilon = 1$).

We now introduce a leak in such a closed billiard and test the limitations of Sabine's prediction. For concreteness, consider removing 5% of the perimeter of the strongly chaotic cardioid billiard, as shown in the left inset of Fig. 1. Numerical simulations of the survival probability of trajectories in this system yield an escape rate $\kappa = 0.030$, which differs substantially from the escape rate $\kappa = 0.8/3\pi^2 = 0.027$ obtained from Sabine's original estimate (13) by using $\mu(I) = 0.05$ and $\langle t_{coll}\rangle = 3\pi^2/16$. In fact, Sabine's estimates holds for infinitesimally small leaks only, and a naive extension for finite leaks will be presented in Sec. II.A and leads to Eq. (23), which is a generalization of Sabine's prediction. This yields $\kappa^* = 0.0277$ which is still about 10% below the observed one. Although this difference appears to be small, it shows up in the exponent of an exponential time dependence. After 500 time units, the number of observed survivors is a factor of $e^{0.003\times 500} = e^{1.5} \approx 4.5$ times smaller than the one based on the closed-system estimate. In Fig. 1 it corresponds to the difference between the dashed (generalized Sabine's formula) and the bottom solid (direct simulations) lines.

This very basic observation is just the simplest temporal manifestation of a series of discrepancies that will be discussed and that are all originated in the difference between the dynamics of the closed and of the leaky systems (see Figs. 3 and 4 for the illustration of the change in the phase space). All these illustrate the need for a deeper theoretical understanding of systems with leaks, beyond the results obtained under simplifying assumptions such as those used to obtain Sabine's law in Sec. I.B.

Before exposing the theory in Sec. II, we define in full generality the problem of introducing a leak in an otherwise closed system. We emphasize that our motivation for using two-dimensional billiards is visual convenience and direct connection to applications. The idea of introducing leaks in dynamical systems applies to a much broader class of systems where the results of this paper can also be applied, such as, e.g., non-billiard-type Hamiltonian systems, dissipative systems, and also in higher dimensions.

E. Definition of the leak

Consider a closed system described by a map $\mathbf{f}_{closed}(\mathbf{x})$. Here we are mainly interested in maps $\mathbf{f}_{closed}$ that admit chaotic motion, but the introduction of a leak is independent of this requirement. Choose the leak I as a subset of the phase space Ω. In its simplest version, a particle is regarded as having escaped the system after entering the region I. The dynamics can thus be described by the following map:

$$\mathbf{x}_{n+1} = \mathbf{f}(\mathbf{x}_n) = \begin{cases} \mathbf{f}_{closed}(\mathbf{x}_n), & \text{if } \mathbf{x}_n \notin I, \\ \text{escape}, & \text{if } \mathbf{x}_n \in I. \end{cases} \tag{20}$$

Since escape is considered to occur one step after entering I, map $\mathbf{f}$ is defined in I.

In the example shown in the left inset of Fig. 1, the leak I is centered at the boundary point $s_l = 0.5$ with width $2\Delta s = 0.1$. In general, a leak I can be centered at any phase-space position $\mathbf{x}_l = (s_l, p_l) \in \Omega$. The leak mentioned above corresponds thus to $I = [s_l - \Delta s, s_l + \Delta s] \times [-1, 1]$, representing a rectangular strip parallel to the p axis. A prominent physical example of leaks represented by strips parallel to the s axis is that of dielectric cavities. In this case light rays coming from a medium with higher refractive index ($n_{in} > n_{out}$) are totally reflected if they collide with $|p| > p_{critical} = n_{out}/n_{in}$, where $p_{critical} = \sin(\theta_{critical})$ is the critical

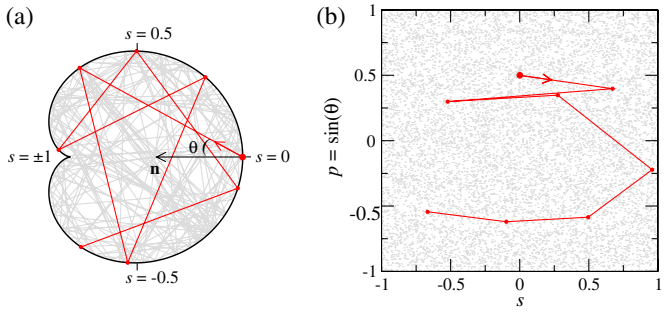

FIG. 3 (color online). Dynamics in the closed cardioid billiard [see Eq. (19) with $\varepsilon = 1$]. (a) Configuration space with parametrization of the perimeter $s \in [-1, +1]$ and collision angle θ. (b) Phase space depicted in Birkhoff coordinates $\mathbf{x} = (s, p = \sin(\theta))$ obtained at the collisions with the boundary. Two trajectories are shown in (a) and (b), one long and one short.

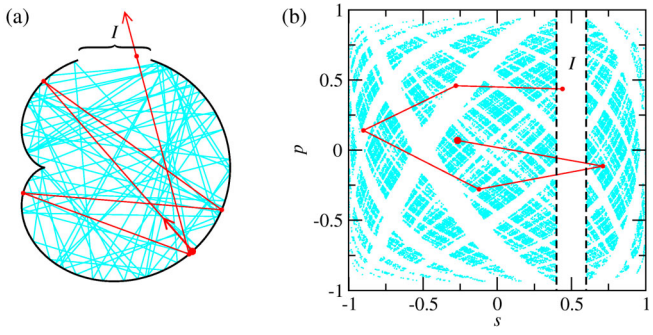

FIG. 4 (color online). Dynamics in a leaky cardioid billiard [see Eq. (19) with $\varepsilon = 1$]. (a) Configuration space with the leak I centered around $s_l = 0.5$ with $\Delta s = 0.1$ (in the momentum space $p_l = 0$ and $\Delta p = 1$). One short-lived and one long-lived orbit are shown. (b) Phase space of the true-time map with the chaotic saddle (dots) and the short-lived trajectory.

momentum (θ_{critical} is the critical angle). The leak is then $|p| < p_{\text{critical}}$, s arbitrary.

A general leak I can have arbitrary shape (e.g., circular, square, oval, etc.) and can also be composed of disjoint regions $I = \cup I_i$. In this last case, a natural question is that of the nature of the set of initial conditions which lead to each I_i, i.e., of the properties of the escape basins B_i. This problem will be discussed in Sec. IV.B. For presentational convenience we focus on leaks at the billiard's boundary, in which case we can still faithfully represent the phase space with Birkhoff coordinates. (For leaks inside the billiard, a representation in the full phase space is needed.)

There are also physically relevant types of leaks that go beyond the definition in Eq. (20). For instance, in room acoustics, or in the above mentioned dielectric cavities, it is very natural to consider objects with partial reflection and partial absorption (or transmission). In this case we associate each particle with an intensity J that monotonically decays due to collisions at the leak. The dynamics of particles is given by the closed map $\mathbf{x}_{n+1} = f_{\text{closed}}(\mathbf{x}_n)$, but the intensity of each particle will change as

$$J_{n+1} = \begin{cases} J_n, & \text{if } \mathbf{x}_n \notin I, \\ R(\mathbf{x}_n)J_n, & \text{if } \mathbf{x}_n \in I, \end{cases} \tag{21}$$

where the *reflection coefficient* $0 \le R < 1$ might also depend on the phase-space position $\mathbf{x}$ within the leak. The full leak defined in Eq. (20) is recovered by taking $R \equiv 0$ ($J_n \equiv J_0$) in Eq. (21). Altogether, a leak I is defined by its size, position, shape, and reflectivity. In Sec. IV we show that all these different characteristics of the leak affect the observable quantities of interest.

II. THEORY FOR FINITE LEAKS

A. Theory based on closed-system properties

The spirit behind Sabine's theory described in Sec. I.B is to calculate the observable quantities of the open system based on the properties of the closed system. While the results of this theory are exact only for infinitesimally small leaks, it is natural to extend them to systems with finite leaks. As already shown, the dynamics of two-dimensional billiards can be conveniently represented by the true-time map (17) and (18). Since for limaçon billiards both s and p change in $[-1, 1]$, $\mathbf{f}$ preserves the measure $d\mu = \frac{1}{4}\cos(\theta)d\theta ds$. Figure 3 illustrates how this map is applied in the case of the cardioid billiard. Upon the nth collision with the wall the length s_n along the perimeter is determined (measured from the point lying farthest from the cusp) along with $p_n = \sin\theta_n$. Any trajectory in the configuration space [like the ones in Fig. 3(a)] is thus mapped on a sequence of points in discrete time in Fig. 3(b), and the time is monitored via Eq. (18) in the knowledge of $t_{\text{coll}}(\mathbf{x})$ shown in Fig. 2.

This billiard is strongly chaotic and the measure μ is the Lebesgue measure. This means that the predictions of the theory based on the closed system are extremely simple: trajectories are assumed to follow the natural invariant density of the closed system, $\rho_\mu(\mathbf{x}) = \frac{1}{4}$, i.e., they are uniformly distributed in $\mathbf{x} = (s, p)$.

We apply this theory to estimate the escape rate of a chaotic system with a finite leak. The average collision time $\langle t_{\text{coll}}\rangle$ for the closed system [see Eq. (15)] is independent of the leak size, and Eq. (14) remains valid. The escape rate resulting from this estimation will be denoted κ^*. It again depends only on the size (measure) of the leak $\mu(I)$, but this time we do not assume $\mu(I)$ to be small. For instance, a leak $I = [s_l - \Delta s, s_l + \Delta s] \times [p_l - \Delta p, p_l + \Delta p]$ has size $2\Delta s$ along the s axis, height $2\Delta p$ in p, area $4\Delta s\Delta p$, and a measure $\mu(I) = \Delta s\Delta p$. This is the measure of trajectories escaping on the time scale $\langle t_{\text{coll}}\rangle$ of one collision. The survival probability after $n = t/\langle t_{\text{coll}}\rangle$ collisions can be estimated as

$$P(t) = [1 - \mu(I)]^{t/\langle t_{\text{coll}}\rangle} = e^{-\kappa^* t}, \tag{22}$$

which yields a *naive estimate* for the escape rate

$$\kappa^* = \frac{-\ln[1 - \mu(I)]}{\langle t_{\text{coll}}\rangle}. \tag{23}$$

This can be considered a generalization of Sabine's law because it is a natural extension of Eq. (13) to finite $\mu(I)$. Equation (23) is usually attributed to Eyring's work in 1930 (Mortessagne, Legrand, and Sornette, 1993), but see Joyce (1975) for a detailed historical account. The naive prediction in Fig. 1 was determined with Eq. (23) and still considerably differs from the measured decay. It is important to note that while Sabine's theory is exact for infinitesimally small leaks, Eq. (23) is just an approximation of the finite-size case. Although it leads to an improved understanding of the problem of room acoustics, it neglects the fact that the presence of a large leak essentially changes the dynamics because only a small portion of the closed system's orbits has sufficiently long lifetime to give a considerable contribution to both the escape rate and the average collision time. A precise understanding of the dynamics in systems with finite leaks, including an explanation of the behavior observed in Fig. 1, can be given only if one abandons the approach based on closed systems and adopts a description in terms of the theory of transient chaos (Lai and Tél, 2011).

B. Theory based on transient chaos

The basic idea of transient chaos theory is to look at the invariant set of orbits that never leave the system for both $t \to \pm\infty$. A key statement of the theory is that there is a nonattracting chaotic set in the phase space that is responsible for the transiently chaotic dynamics (Ott, 1993; Tél and Gruiz, 2006; Lai and Tél, 2011). This set is a chaotic saddle and is of course drastically different from the chaotic set of the closed system. To illustrate this difference we present in Fig. 4 a leaky billiard, its chaotic saddle, and a short-lived trajectory. It is apparent that the long-lived orbits are rather exceptional and the saddle is very sparse: it is a measure zero object (with respect to the Lebesgue measure), a set that exhibits a double fractal character. The difference between the closed system's Sabine-type theories and the ones based on transient chaos can pictorially best be expressed by comparing Figs. 3(b) and 4(b). It becomes evident that transient chaos is based on a strongly selected and extremely ordered *subset* of the closed system's trajectories. Hence the measures (μ and μ_c) with

which averages should be taken are fundamentally different in the two cases.

The saddle is responsible for the exponential decay of the survival probability

$$P(t) \sim e^{-\kappa t}, \tag{24}$$

where $\sim$ indicates an asymptotic equality in t. The escape rate κ is a property of the saddle and is independent of the initial distribution of the trajectories used to represent an ensemble.

The invariant set of transient chaos is called a saddle because it possesses a stable and an unstable manifold. The stable (unstable) manifold is composed of all trajectories that approach the chaotic saddle for $t \to \infty$ in the direct (inverted) dynamics. These manifolds of attracting and repelling character are extremely important to understand the properties of the open system. This is the reason why the term chaotic saddle is more appropriate than the often used term repeller [see, e.g., Gaspard (1998)], which suggests (erroneously) that only unstable directions exist.

Here we present, the so-called *sprinkler method* that can be used to calculate not only a chaotic saddle but also its stable and unstable manifolds (Tél and Gruiz, 2006; Lai and Tél, 2011). One starts with $N_0 \gg 1$ trajectories distributed uniformly over the phase space. One then chooses a time $t^* \gg 1/\kappa$ and follows the time evolution of each initial point up to t^*. Only trajectories that do not escape are kept, whose number is approximately $N_0 e^{(-\kappa t^*)}$. If κt^* is sufficiently large (but not too large such that only a few points remain inside), trajectories with this long lifetime come close to the saddle in the course of dynamical evolution, implying that their initial points must be in the immediate vicinity of the stable manifold of the saddle (or of the saddle itself), and their end points must be close to the unstable manifold of the saddle. The latter is so because most points still inside after time t^* are about to leave. The points from the middle of these trajectories ($t \approx t^*/2$) are then in the vicinity of the saddle. In the spirit of true-time maps, we used a generalization of this method (see Appendix C) to generate the chaotic saddle of Fig. 4(b) and the corresponding manifolds plotted in Figs. 5(a) and 5(b).

From the construction above it is clear that the particles being in the process of escape are distributed along the unstable manifold. When compensating the loss due to escape by pumping in new particles according to an appropriate way, which corresponds in practice to multiplying the density by $\exp(\kappa t)$, we obtain an invariant density as the one shown in Fig. 6. This stationary distribution is known to be the conditionally invariant measure.

Traditionally, a measure μ_c is said to be conditionally invariant (c measure for short) if for any subset E of the region of interest Ω (Pianigiani and Yorke, 1979; Demers and Young, 2006)

$$\frac{\mu_c(\mathbf{f}^{-1}(E))}{\mu_c(\mathbf{f}^{-1}(\Omega))} = \mu_c(E). \tag{25}$$

This means that the c measure is not directly invariant under the map $\mu_c(f^{-1}(E)) \neq \mu_c(E)$, but it is preserved under the incorporation of the compensation factor $\mu_c(f^{-1}(\Omega)) < 1$ (the c measure of the set remaining in Ω in one iteration).

Although many c measures exist (Collet, Martínez, and Maume-Deschamps, 2000; Demers and Young, 2006), here we are interested in the *natural* c measure which is concentrated along the saddle's unstable manifold and has been demonstrated to be relevant in several transient-chaos-related phenomena (Lai and Tél, 2011). Figure 6 shows the c measure over the full phase space of the cardioid and indicates that the distribution is rather irregular. This should be compared with the smooth Lebesgue measure characterizing the closed system.

1. Dimensions of the invariant sets

Both the chaotic saddle and its manifolds are fractal sets, as can clearly be seen from Figs. 4(b), 5(a), and 5(b). Commonly, there are (at least) two different dimensions used to quantify the fractality of these sets: the box-counting dimensions D_0 and the information dimensions D_1. The former characterizes the mere geometrical pattern, and the latter also characterizes the distribution of particles on the pattern (Ott, 1993).

The chaotic saddle of a two-dimensional map has a clear direct product structure: it can locally be decomposed into two Cantor-set-like components, one along each manifold. The dimension along the unstable (stable) manifold is called the partial dimension in the unstable (stable) direction and is marked by an upper index 1 (2). None of the partial dimensions can be larger than 1. The dimensions D_0 and D_1 of the

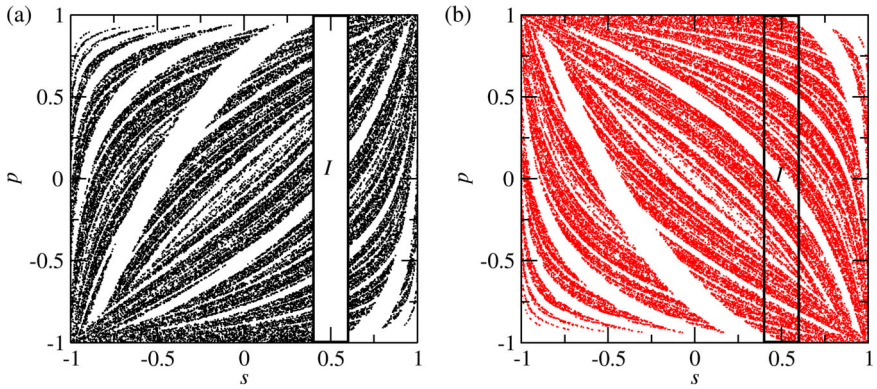

FIG. 5 (color online). (a) Stable and (b) unstable manifolds of the cardioid billiard shown in Fig. 4, obtained by the sprinkler method ($N_0 = 10^8$, $t^* = 120$, $\Delta t^* = 40$, see Appendix C).

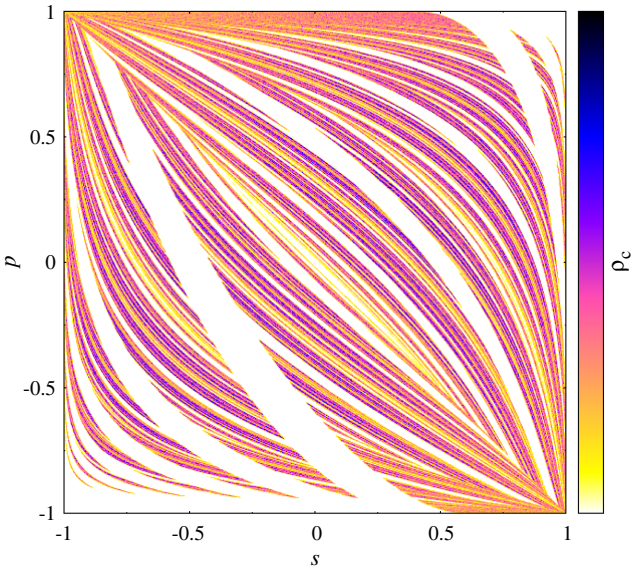

FIG. 6 (color online). Density of trajectories on the unstable manifold shown in Fig. 5(b). This distribution corresponds to the c measure, the measure according to which averages are to be taken in the transient chaos context. Note that the c measure is defined within the leak ($N_0 = 10^8$, $t^* = 80$, $\Delta t^* = 80$, see Appendix C).

chaotic saddle are the sum of the two corresponding partial dimensions (Tél and Gruiz, 2006; Lai and Tél, 2011):

$$D_0 = D_0^{(1)} + D_0^{(2)}, \qquad D_1 = D_1^{(1)} + D_1^{(2)}. \tag{26}$$

The saddle might also contain very rarely visited, and thus atypical, regions. Consequently, the information dimension D_1 cannot be larger than the box-counting dimension D_0, which naturally holds for the partial dimensions too: $D_1^{(j)} \leq D_0^{(j)}$, $j = 1, 2$. The value of the box-counting dimension is often found to be close to that of the information dimension and it is then sufficient to use only one of them.

The manifolds are also of direct product structure, but one component of them is a line segment, an object of partial dimension 1 [see Figs. 5(a) and 5(b)]. Since the saddle can be considered as the intersection of its own manifolds, the dimension $D_{0,1}^{(u(s))}$ of the unstable (stable) manifold is 1 plus the partial dimension in the stable (unstable) direction

$$D_{0,1}^{(u)} = 1 + D_{0,1}^{(2)}, \qquad D_{0,1}^{(s)} = 1 + D_{0,1}^{(1)}. \tag{27}$$

It should be noted that the information dimension $D_1^{(u)}$ of the unstable manifold is nothing but the information dimension of the c measure that sits on this manifold.

A simplifying feature occurs in Hamiltonian systems: due to time reversal symmetry the partial dimensions coincide.[4] Therefore, in Hamiltonian cases, we have

$$\begin{aligned} D_{0,1} &= 2D_{0,1}^{(1)}, \\ D_{0,1}^{(u)} &= D_{0,1}^{(s)} = 1 + D_{0,1}^{(1)} = 1 + D_{0,1}/2, \end{aligned} \tag{28}$$

i.e., all relevant dimensions can be expressed by the partial dimensions $D_{0,1}^{(1)}$ in the unstable direction.

It is an important result of transient chaos theory that this partial information dimension can be expressed in a simple way by the escape rate and the average continuous-time Lyapunov exponent $\bar{\lambda}$ on the chaotic saddle:

$$D_1^{(1)} = 1 - \frac{\kappa}{\bar{\lambda}}. \tag{29}$$

This relation, the Kantz-Grassberger relation (Kantz and Grassberger, 1985), states that the dimension observed along the unstable direction deviates from 1 more, the larger the ratio of the escape rate (a characteristic of the global instability of the saddle) to the average Lyapunov exponent (a characteristic of the local instability on the saddle) is.[5]

2. Implications for systems with leaks

All results described so far are valid for open systems in general; they are not particular to systems with leaks. In the latter case, however, the chaotic saddle and its manifolds depend sensitively on the leak I. This implies that the unstable manifold's dimension, and the c measure in general, might strongly depend on the size, location, and shape of the leak.

We assume throughout this work that (a) I is not too large so that trajectories do not trivially escape after a short time [$P(t) \neq 0$, for any t]; and (b) ergodicity and the chaotic properties of the closed system lead to *one and only one* chaotic saddle after the leak is introduced. We also exclude the possibility of trajectories reentering the billiard after hitting a leak. This assumption is naturally satisfied in a convex billiard, but should be enforced in the limaçon billiard for leaks around the cusp.[6]

We take advantage of the fact that a leaky system is obtained from a strongly chaotic closed system. For instance, it is possible to explicitly construct the chaotic saddle by extracting from the original phase space all the $\mathbf{f}_{\text{closed}}$ images and preimages of the set used as leak I in $\mathbf{f}$. To see this, in Fig. 7 leak I of Figs. 4 and 5 is shown together with its forward and backward images. Compared to Fig. 5, we see that the white regions in the plot of the stable (unstable) manifold correspond to the backward (forward) iterates of the leak.

Because of area preservation and ergodicity of the closed system, the result of removing infinitely many images can be a set of measure zero only. The chaotic saddle in a leaking system is the set of points that remain in the *complement* of the leak I and all its images for both forward and backward iterations. Indeed, the complement of the union of the sets in Figs. 7(a) and 7(b) already provides a good approximation to Figs. 5(a) and 5(b), respectively, and the complement of both panels is a good approximation to Fig. 4(b). The chaotic saddle is a fractal subset of the original chaotic set (the full

[4]This symmetry explains why Figs. 5(a) and 5(b) are mirror images of each other with respect to the s axis (after the leak is removed from the unstable manifold). The closed cardioid has an additional symmetry $(s, p) \mapsto (-s, -p)$.

[5]Equation (29) is valid in dissipative cases as well, but the partial dimension along the stable manifold is then $D_1^{(2)} = D_1^{(1)}\bar{\lambda}/|\bar{\lambda}'|$, where $\bar{\lambda}'$ is the average negative Lyapunov exponent on the saddle.

[6]Physically we can imagine that an absorbing material is placed on the border of the closed billiard so that trajectories crossing the leak are immediately absorbed.

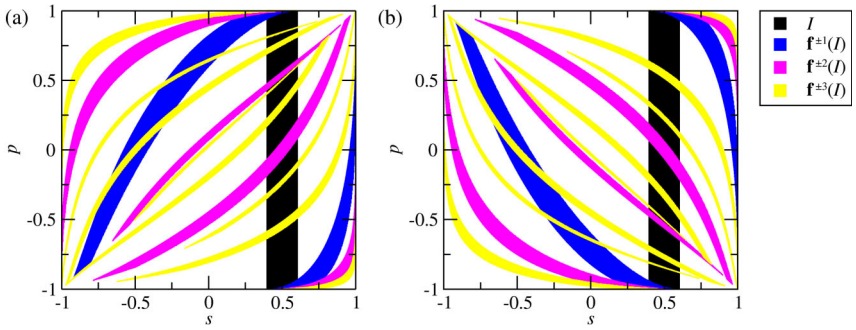

FIG. 7 (color online). Phase space (s, p) of the cardioid billiard showing the (closed system) iterates of the black vertical stripe that corresponds to I in Figs. 4 and 5. (a) Backward iterates. (b) Forward iterates. In both cases the first, second, and third iterates are shown.

phase space in our strongly chaotic example). Furthermore, all invariant sets of the leaky system (periodic orbits, manifolds of the saddle, etc.) are subsets of those in the corresponding closed system.

3. An improved escape rate formula

We now notice that since escape in Eq. (20) is considered to occur one step *after entering* I, the map $\mathbf{f}$ with leak is defined in I and thus the unstable manifold of the chaotic saddle enters I [see Fig. 5(b)]. It is also possible to compute measures of the leak as indicated in Eq. (16). The region of interest in Eq. (25) is identified with the closed system's phase space $\mu_c(\Omega) = 1$, and the compensation factor in this equation is obtained as

$$\mu_c(\mathbf{f}^{-1}(\Omega)) = \mu_c(\Omega \backslash I) = 1 - \mu_c(I). \tag{30}$$

We now recall that the c measure is invariant and is distributed along the unstable manifold. The escape rate can be estimated by the same simple calculations that lead to Eq. (23) by replacing the natural measure $\mu(I)$ by the c measure $\mu_c(I)$ of the leak. Also carrying out the averaging of the collision times with respect to the c measure [see Eq. (16)], we find that

$$\kappa(I) \simeq -\frac{\ln[1 - \mu_c(I)]}{\langle t_{\mathrm{coll}} \rangle_c}, \tag{31}$$

where the subscript c stands for the c measure of the true-time map and $\simeq$ indicates approximate equality. The validity and limitations of the improved escape rate formula [Eq. (31)] are discussed in Sec. III.C, but by now it is instructive to discuss the implications of this equation. It clearly shows that for finite leaks the escape rate cannot be obtained from the properties of the closed system and the c measure should be used, a measure which deviates essentially from that of the closed system. The difference between $\mu(I)$ (the area of I) and $\mu_c(I)$ (the proportion of dots within I) is visually clear from Fig. 5(b).

We now discuss the case of usual open maps, in contrast to true-time maps. Their escape rate we denote by γ (to sharply distinguish from the continuous-time or true-time map escape rate κ) implying that the discrete-time survival probability $P(n)$ decays as $e^{-\gamma n}$. The relation for the escape rate

$$e^{-\gamma(I)} = 1 - \mu_c(I) \rightarrow \gamma(I) = -\ln[1 - \mu_c(I)] \tag{32}$$

has been known since Pianigiani and Yorke (1979) and can also be obtained directly from Eq. (30) for leaky maps (Paar and Buljan, 2000; Altmann and Tél, 2008). It expresses the fact that the c measure μ_c of the leak is the proportion of particles escaping via the leak within an iteration step. Since starting from the c measure the decay is exponential from the very beginning, the proportion of the surviving particles after one time unit is $\exp(-\gamma)$, of those who escape is $1 - \exp(-\gamma)$, and thus $\mu_c(I) = 1 - \exp(-\gamma)$ which is equivalent to Eq. (32).

Equation (31) leads to Eq. (32) when $t_{\mathrm{coll}}(\mathbf{x}) \equiv 1$. It shows also that when using the true time of the system together with a surface of section at the billiard's boundary, it is essential to take into account that the average collision time differs from $\langle t_{\mathrm{coll}} \rangle$ given in Eq. (14). As already anticipated in Eq. (16), with finite leaks the correct average collision time is given by $\langle t_{\mathrm{coll}} \rangle_c = \int t_{\mathrm{coll}}(\mathbf{x}) \rho_c(\mathbf{x}) d\mathbf{x}$, where ρ_c is the density of the c measure characterizing the system in the presence of leak I. We note that different corrections for κ due to the collision times were suggested by Mortessagne, Legrand, and Sornette (1993) and Ryu *et al.* (2006). While Mortessagne, Legrand, and Sornette (1993) used a Gaussian approximation for the distribution of the collision times of long-lived trajectories, Ryu *et al.* (2006) took into account only the collision times inside the leak. None of them is equivalent to Eq. (31) or to the exact expressions in Sec. III.C.

Another general statement we make about systems with leaks is that when the size of the leak goes to zero, the properties of the open system tend to those of the closed system (de Moura and Letelier, 1999; Aguirre and Sanjuán, 2003), i.e., the theory of Sec. II.A becomes correct. In particular, $\mu_c(I) \rightarrow \mu(I) \rightarrow 0$, which implies that κ in Eq. (31) tends to κ^* in Eq. (23) and both tend to Sabine's prediction $\kappa(I) = \mu(I)/\langle t_{\mathrm{coll}} \rangle$, Eq. (13). In terms of dimensions, $D_{0,1} \rightarrow 2$. A nontrivial closed-system approximation $D_1^{*(1)}$ of the information dimension can be obtained from the Kantz-Grassberger relation (29) with $\kappa(I) = \kappa^*$, $\bar{\lambda}(I) = \bar{\lambda}$ (Lyapunov exponent of the closed system) (Neufeld, Haynes, and Picard, 2000).

4. Periodic orbits in maps with leaks

We also review the dynamics in general maps with leaks. Periodic orbits analysis (Cvitanović *et al.*, 2004) is a powerful method to investigate chaotic systems and also clearly illustrates the spirit of leaking systems. Generally, a dense set of

unstable periodic orbits is embedded into the chaotic saddle and this set can be used to obtain an expression for the escape rate of the saddle. As pointed out by Altmann and Tél (2009), in systems with leaks this can be done either using the periodic orbits of the open system (that never hit the leak) or using only the periodic orbits of the closed system that hit the leak. To illustrate the simple arguments that lead to this, we consider the case of computing the escape rate γ of a generic discrete mapping $\mathbf{f}$. First we split the set $\Gamma_n^{(\mathrm{all})}$ of all periodic orbits of length n (i.e., all orbits that have an integer period equal to $n, n/2, n/3, \ldots$) of the closed system into two sets: $\Gamma_n^{(\mathrm{inside})}$, the orbits that have at least one point inside I, and the complementary set $\Gamma_n^{(\mathrm{outside})}$, i.e., all orbits for which all points are outside the leak I. In the limit of large n the following relation holds for hyperbolic systems (Ott, 1993; Dorfman, 1999):

$$e^{-\eta\gamma} = \sum_i \frac{1}{|\Lambda(\Gamma_{i,n}^{(\mathrm{outside})})|}, \tag{33}$$

where the sum is over all points i of periodic trajectories in $\Gamma_n^{(\mathrm{outside})}$, and Λ is the largest eigenvalue of the n-fold iterated map $\mathbf{f}^n$ on the orbit.

Next we notice that in the closed system $\gamma = 0$ (no escape). Therefore,

$$1 = \sum_i \frac{1}{|\Lambda(\Gamma_{i,n}^{(\mathrm{all})})|}, \tag{34}$$

where the sum is over all points i in $\Gamma_n^{(\mathrm{all})}$. Subtracting Eq. (33) from Eq. (34) we obtain

$$1 - e^{-\eta\gamma} = \sum_i \frac{1}{|\Lambda(\Gamma_{i,n}^{(\mathrm{inside})})|}, \tag{35}$$

where the sum now is over all points i in $\Gamma_n^{(\mathrm{inside})}$, i.e., all points that belong to periodic orbits that have at least one point in I. Altogether this means that even if we are allowed to probe the system only through the leak, the identification of the periodic orbits entering I suffices for the computation of the main properties of the chaotic saddle that exists inside the system. This can be applied also to more efficient methods based on expansions of the zeta function (Artuso, Aurell, and Cvitanovic, 1990).

A simple relation can be obtained in uniformly expanding (piecewise linear) maps in which leaks are selected as elements of a Markov partition. In this case it is possible to prove that for two different leaks I_1 and I_2, the relation $\gamma(I_1) > \gamma(I_2)$ holds if and only if the shortest periodic orbit in I_1 is shorter than the one in I_2 (Bunimovich, 2012). This follows also from Eq. (35) with constant Λ (as in piecewise linear maps with constant slope).

C. Initial conditions and average escape times

Typical observable quantities in transient chaos theory, such as κ and the fractal dimensions, are independent of the choice of the density of initial conditions $\rho_0(\mathbf{x})$ because they are directly related to the properties of the invariant chaotic saddle. More precisely, the underlying assumption is that $\rho_0(\mathbf{x})$ overlaps the stable manifold of this saddle. The stable manifold of the chaotic saddle typically spreads through the phase space in a filamentary pattern [e.g., as in Fig. 5(a)] and therefore smooth $\rho_0(\mathbf{x})$'s typically fulfill this requirement. Even in this typical case, there are important quantities that depend on $\rho_0(\mathbf{x})$ such as any quantity averaged over a large number N of trajectories. The dependence on initial conditions and the universal asymptotic decay of the survival probability $P(t) \sim e^{-\kappa t}$ can be reconciled by noticing that for short times $t < t_s$, the escape of trajectories is nonuniversal, and $P(t) \neq e^{-\kappa t}$. Even if t_s is short, a large fraction of the trajectories may escape for $t < t_s$.

Here we discuss in more detail the simplest yet representative case of the average lifetimes (Altmann and Tél, 2009)

$$\langle\tau\rangle_{\rho_0} \equiv \lim_{N\to\infty}\frac{1}{N}\sum_{i=1}^{N}\tau_i = \int_0^\infty \tau p(\tau)d\tau = \int_0^\infty P(t')dt', \tag{36}$$

obtained with different initial densities $\rho_0(\mathbf{x})$, and hence with different survival probabilities $P(t)$, where τ_i is the lifetime of trajectory i. Here we used $p = -dP/dt$ [see Eq. (12)], $P(0) = 1$, and $P(t) \to 0$ faster than $1/t$.

For maps, the averaged discrete lifetime is

$$\langle\nu\rangle_{\rho_0} = \sum_{n'=0}^{\infty} n' p(n'), \tag{37}$$

where $p(n)$ is the probability to escape in the nth step. Note that for true-time maps [Eqs. (17) and (18)], in general, $\langle\tau\rangle_{\rho_0} \neq \langle\nu\rangle_{\rho_0}\langle t_{\mathrm{coll}}\rangle_c$, with $\langle t_{\mathrm{coll}}\rangle_c$ given by Eq. (16). Instead,

$$\begin{aligned}\langle\tau\rangle_{\rho_0} &= \lim_{N\to\infty}\frac{1}{N}\sum_{i=1}^{N}\sum_{j=1}^{\nu_i} t_{\mathrm{coll}}(\mathbf{x}^{(i,j)}) \\ &= \lim_{N\to\infty}\frac{1}{N}\sum_{i=1}^{N}\nu_i\bar{t}_{\mathrm{coll}}^{(i)} = \langle\nu\bar{t}_{\mathrm{coll}}\rangle_{\rho_0},\end{aligned}$$

where ν_i is the total number of collisions along the ith trajectory, $\mathbf{x}^{(i,j)}$ is the position of the jth collision ($j = 1, \ldots, \nu_i$) of trajectory i that has initial condition $\mathbf{x}^{(i,0)}$, $\bar{t}_{\mathrm{coll}}^{(i)} \equiv (1/\nu_i)\sum_{j=1}^{\nu_i} t_{\mathrm{coll}}(\mathbf{x}^{(i,j)})$ is the mean collision time of trajectory i, and the average $\langle\cdots\rangle$ is taken over $i = 1, \ldots, N$ trajectories. The reason for this difference is that for short times $\bar{t}_{\mathrm{coll}}^{(i)}$ differs significantly from $\langle t_{\mathrm{coll}}\rangle_c$.

We want to see if $\langle\tau\rangle_{\rho_0}$ and $\langle\nu\rangle_{\rho_0}$ can be expressed as a function of other easily measurable quantities. We also try to find a relation between $\langle\tau\rangle_{\rho_0}$ and $\langle\nu\rangle_{\rho_0}$ for the following particular initial densities $\rho_0(\mathbf{x})$.

1. Conditionally invariant density ρ_c

We take initial conditions according to the c measure $\rho_0(\mathbf{x}) = \rho_c(\mathbf{x})$. As explained in Sec. II.B, $\rho_c(\mathbf{x})$ describes the escaping process and is achieved by rescaling the surviving trajectories from an arbitrary smooth initial density. Therefore, for $\rho_0(\mathbf{x}) = \rho_c(\mathbf{x})$ we find $p(t) = \kappa e^{-\kappa t}$ for all $t > 0$ and from Eqs. (31) and (36) the simple relation

$$\langle\tau\rangle_c = \frac{1}{\kappa} \simeq -\frac{\langle t_{\mathrm{coll}}\rangle_c}{\ln[1-\mu_c(I)]} \tag{38}$$

follows.

For maps with escape rate γ, the normalization of $p(n)$ implies $\sum_{n=1}^{\infty} p(n) = 1$, and thus $p(n) = (e^{\gamma} - 1)e^{-\gamma n}$ (since $e^{\gamma} - 1 \approx \gamma$ for $\gamma \ll 1$). This leads to a different result (Altmann and Tél, 2009)

$$\langle \nu \rangle_c = \frac{1}{1 - e^{-\gamma}} = \frac{1}{\mu_c(I)}. \tag{39}$$

In the last equality we used Eq. (32). It is important to note that for maps obtained from flows, the c densities ρ_c of the map and flow (or true-time map) are usually different due to the nontrivial collision time distribution.

2. Recurrence density ρ_r

As pointed out by Altmann and Tél (2008, 2009), there is an initial density $\rho_0(\mathbf{x}) = \rho_r(\mathbf{x})$ connected to the problem of *Poincaré recurrences* that leads to simple results for $\langle \tau \rangle_r$ and $\langle \nu \rangle_r$. The Poincaré recurrence theorem asserts that in a closed dynamical system with an invariant measure μ, almost any trajectory (with respect to μ) chosen inside a region I with $\mu(I) > 0$ will return to I an infinite number of times. The times T_i's between two consecutive returns are called Poincaré recurrence times, a central concept in dynamical-systems theory (Haydn, Lacroix, and Vaienti, 2005). The (cumulative) distribution of recurrence times $P_r(T)$ is also used to quantify chaotic properties of specific systems (Chirikov and Shepelyansky, 1984). Figure 8 illustrates the Poincaré recurrence setup in billiard systems. Using the notation introduced in Fig. 8, the average recurrence time $\bar{T}$ of a single long trajectory is calculated as

$$\bar{T} = \frac{1}{N}\sum_{i=1}^{N} T_i = \frac{t_{\text{total}}}{N} = \frac{N_{\text{coll}}\langle t_{\text{coll}} \rangle}{N} = \frac{\langle t_{\text{coll}} \rangle}{\mu(I)}, \tag{40}$$

where T_i is the ith recurrence time along the trajectory, $\langle t_{\text{coll}} \rangle$ is the average collision time of a typical trajectory starting inside the leak that, due to ergodicity, coincides with the closed system $\langle t_{\text{coll}} \rangle$ given by Eq. (15), N_{coll} is the total number of collisions up to time t_{total}, N is the number of such collisions inside I, and $\mu(I) = N/N_{\text{coll}}$ is the fraction of collisions on I. Equation (40) is valid for large t_{total}, N, and N_{coll}.

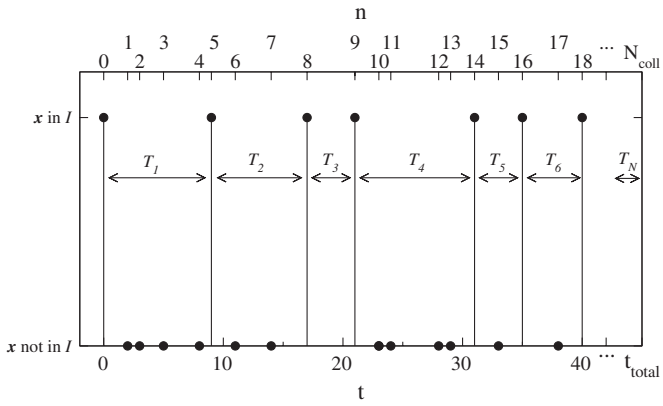

FIG. 8. Schematic illustration of Poincaré recurrences in a closed billiard. The symbols indicate the times t of the nth collision with the boundary of a single trajectory. The recurrence times T_i's are defined as the times between successive collisions in I. In the total time t_{total} there are N_{coll} collisions, out of which N collisions are inside the region I.

For maps, analogously, we obtain that the average discrete recurrence time $\bar{\mathcal{N}}$ is given by

$$\bar{\mathcal{N}} = \frac{1}{\mu(I)}. \tag{41}$$

The inverse relation between measure and recurrence time shown in Eqs. (40) and (41) is known as Kac's lemma (Kac, 1959; Zaslavsky, 2002). For higher moments of the return time distribution see Cristadoro, Knight, and Degli Esposti (2012).

The connection to systems with leaks is achieved by *identifying* the recurrence region and the leak I. One can find an appropriate initial density $\rho_0(\mathbf{x}) = \rho_r(\mathbf{x})$ for the open case for which the survival probability in the presence of leak I coincides with the recurrence time distribution to I in the closed system

$$P_r(T) = P(t) \tag{42}$$

for any $t = T$. This can be done by using the positions $\mathbf{x} \in I$ of the N recurrent points as initial conditions (see Fig. 8). Because of the ergodicity of the closed chaotic system, in the limit of long times, the points of this single trajectory are distributed according to the natural density $\rho_\mu(\mathbf{x})$ of the closed system, justifying the notation $\mu(I)$ in the equation above. In the case of the billiard systems discussed here, $\rho_r(\mathbf{x})$ corresponds to initial conditions in the leak, uniformly distributed in $\mathbf{x} = (s, p)$, but with velocities pointing inward, i.e., not escaping through the leak. Physically, this corresponds to shooting trajectories into the billiard through the leak.

If time is counted discretely, $\rho_r(\mathbf{x})$ corresponds to the next iteration of the uniform distribution [natural measure of closed system $\rho_\mu(\mathbf{x})$] of initial conditions in $\mathbf{x} \in I$. In the general case of an invertible map $\mathbf{f}$ this is obtained by applying the Perron-Frobenius (Gaspard, 1998; Dorfman, 1999) operator as (Altmann and Tél, 2009)

$$\rho_r(\mathbf{x}) = \frac{\rho_\mu(\mathbf{f}^{-1}(\mathbf{x}) \cap I)}{\mathcal{J}(\mathbf{f}^{-1}(\mathbf{x}) \cap I)\mu(I)} \quad \text{for } \mathbf{x} \in f(I), \tag{43}$$

where $\mathbf{f}^{-1}(x) \cap I$ denotes the points that come from I, $\mathcal{J}$ is the Jacobian of the map, and the factor $\mu(I)$ ensures normalization. Note that the single iteration introduced in the definition of ρ_r is *compensated* at the end because the escape is considered also one time step after entering I; see Eq. (20). With $\rho_0(\mathbf{x}) = \rho_r(\mathbf{x})$, $P(t) = P_r(T = t)$ for all $t \geq 0$, showing that the problem of Poincaré recurrence can be interpreted as a specific problem of systems with leaks. In particular, $P_r(T) \sim e^{-\kappa T}$ with the escape rate κ of the system opened up in I. The average lifetime is given by Eq. (40) as

$$\langle \tau \rangle_r = \bar{T} = \frac{\langle t_{\text{coll}} \rangle}{\mu(I)} \neq \frac{\langle t_{\text{coll}} \rangle_c}{\mu_c(I)} \neq -\frac{\langle t_{\text{coll}} \rangle_c}{\ln[1 - \mu_c(I)]}.$$

For maps, Eq. (41) implies that

$$\langle \nu \rangle_r = \bar{\mathcal{N}} = \frac{1}{\mu(I)} \neq \frac{1}{\mu_c(I)}.$$

Note that both relations above reveal that for ρ_r there is no difference in the dependence on the measure for maps and

flows, in contrast to Eqs. (38) and (39) obtained with ρ_c as the initial density.

3. Closed-system density ρ_μ, or any smooth ρ_s

The most popular initial condition for systems with leaks is by far ρ_μ. This corresponds to introducing the leak after the trajectories have reached equilibrium inside the system. While this is sometimes implicitly assumed as natural, the results of this section show that ρ_μ is not the only possibility and certainly not the simplest one. For ρ_μ and any other smooth initial distribution $\rho_0 = \rho_s$, the surviving trajectories relax toward the c density $\rho_c(\mathbf{x})$, the natural density of the open system. The numerical investigations of Altmann and Tél (2009) indicate that results with ρ_μ or other smooth densities ρ_s are usually similar to those obtained by ρ_c, and more different from those obtained by ρ_r. This can be understood by noting that the hyperbolicity of the chaotic saddle leads to a fast convergence $\rho_0(\mathbf{x}) \to \rho_c(\mathbf{x})$. While a convergence also holds for ρ_r, it is made much slower by ρ_r's lack of any overlap with the chaotic saddle, with orbits taking, therefore, a longer time to approach the saddle (Altmann and Tél, 2009).

The results of this section are summarized in Table I. All formulas here were confirmed within a 3% error in the cardioid billiard with a finite leak (see Table II). In the limit of a small leak, the simple case $\langle\tau\rangle = 1/\kappa$ discussed in Eq. (12) and Sabine's law in the form of Eq. (13) are recovered, independent of the initial distribution.

D. Extension to partial leaks

So far we have restricted our theory to the case of full leaks that completely transmit the trajectories falling on them. At the end of Sec. I.E we emphasized the need to extend the theory to leaks that partially transmit and partially reflect trajectories. This problem can be handled by associating with each trajectory i an intensity $J_n^{(i)}$ that decreases with time $J_{n+1}^{(i)} = R(\mathbf{x})J_n^{(i)}$ due to collisions at the leak regions with reflectivity $R(\mathbf{x}) < 1$, as described by Eq. (21). Here we show how the results of Sec. II.B can be extended to this case.

For simplicity, we consider that all N trajectories of the initial ensemble start with intensity $J_0 = 1$. Nonhomogeneous energy intensities can be achieved by manipulating the density of initial trajectories $\rho_0(\mathbf{x})$, as discussed in Sec. II.C. For longer times the energy density depends not only on the density of trajectories $\rho(\mathbf{x}, t)$ but also on their intensities, which can be thought of as weights $0 \le J \le 1$ attributed to each trajectory. The survival probability $P(t)$ of trajectories is physically reinterpreted as the fraction $\tilde{P}(t)$ of the total energy still inside the system. In strongly chaotic systems, $\tilde{P}(t)$ is expected to decay asymptotically as

$$P(t) \sim e^{-\tilde{\kappa}t},$$

with $\tilde{\kappa}$ as the *energy escape rate*. In practice, $\tilde{P}(t)$ can be obtained as a sum over all N trajectories

$$\tilde{P}(t) \approx \frac{1}{N}\sum_{i=1}^{N} J_t^{(i)} = \int_\Omega J_t(\mathbf{x})\rho(\mathbf{x}, t)d\mathbf{x} \equiv \int_\Omega \tilde{\rho}(\mathbf{x}, t)d\mathbf{x}, \tag{44}$$

where $\rho(\mathbf{x}, t)$ is the density and $J_t(\mathbf{x})$ is the intensity of trajectories in $\mathbf{x}$ at time t. The intensity of each trajectory i at time t is given by $J_t^{(i)} = \Pi_{j=1}^{\nu_i(t)} R(\mathbf{x}_j^{(i)})$, with $\nu_i(t)$ the number of collisions of trajectory i until time t and $\mathbf{x}_j^{(i)}$ the position of these collisions. We defined the combined density

$$\tilde{\rho} \equiv \rho J, \tag{45}$$

which is, by convention, not normalized for $t > 0$. The appearance of $\tilde{\rho}$ in Eq. (44) reflects the more general fact that the division between trajectories and intensities has no observable consequence, despite their natural interpretation in physical terms and their natural implementation in ray simulations. It is only their combination, Eq. (45), that leads to a physically relevant density for the case of partial leaks, both for the c measure and for estimations based on μ. A mathematical description coherent with this interpretation considers operators acting on densities and is given in Sec. III. In the remainder of this section we consider how partial leaks modify the closed system (see Sec. II.A) and transient chaos (see Sec. II.B) theories discussed above.

We start with a straightforward extension of the naive estimate of the escape rate. When estimating the transmission happening through the leak one has to account for the partial transmission because for a trajectory in $\mathbf{x} \in I$ only a fraction $1 - R(\mathbf{x})$ of its intensity is lost. Therefore, the measure of the leak $[\mu(I) = \int_I d\mu]$ used in Eq. (23) to compute the naive estimate $\kappa = \kappa^*$ has to be replaced by

TABLE I. Dependence of the average lifetime $\langle\tau\rangle$ and $\langle\nu\rangle$ for flows and maps, respectively, on the initial distribution $\rho_0(\mathbf{x})$, and expressions for the escape rate κ, γ. The natural invariant measure of the leak (closed system) $\mu(I)$ and the conditionally invariant measure $\mu_c(I)$ of the leak I coincide only in the limit of small leaks. From Altmann and Tél, 2009.

		Large leaks Finite $\mu(I) \neq \mu_c(I)$		Limit of small leaks $\mu_c(I) = \mu(I) \to 0$
$\rho_0(\mathbf{x})$	c measure: ρ_c	Recurrence: ρ_r	Natural, smooth: $\rho_{\mu,s}$	$\rho_{r,c,\mu,s}$
Mean time				
Continuous, t	$\langle\tau\rangle_c = \frac{1}{\kappa} \simeq \frac{-\langle t_{\rm coll}\rangle_c}{\ln[1-\mu_c(I)]}$	$\langle\tau\rangle_r = \frac{\langle t_{\rm coll}\rangle}{\mu(I)} = \langle\nu\rangle_r\langle t_{\rm coll}\rangle \neq \frac{1}{\kappa}$	$\langle\tau\rangle_{\mu,s} \approx \frac{1}{\kappa}$	$\langle\tau\rangle = \frac{\langle t_{\rm coll}\rangle}{\mu(I)}$
Discrete, n	$\langle\nu\rangle_c = \frac{1}{1-e^{-\gamma}} = \frac{1}{\mu_c(I)}$	$\langle\nu\rangle_r = \frac{1}{\mu(I)}$	$\langle\nu\rangle_{\mu,s} \approx \frac{1}{\mu_c(I)}$	$\langle\nu\rangle = \frac{1}{\mu(I)} = \frac{1}{\gamma}$
Escape rate				
Continuous, t		$\kappa \simeq -\frac{\ln[1-\mu_c(I)]}{\langle t_{\rm coll}\rangle_c} \neq \frac{\ln[1-\mu(I)]}{\langle t_{\rm coll}\rangle} = \kappa^*$		$\kappa = \frac{\mu(I)}{\langle t_{\rm coll}\rangle} = \frac{1}{\langle\tau\rangle}$
Discrete, n		$\gamma = -\ln[1-\mu_c(I)] \neq -\ln[1-\mu(I)] \equiv \gamma^*$		$\gamma = \mu(I) = \frac{1}{\langle\nu\rangle}$

TABLE II. Numerical results for the average lifetime in the cardioid billiard with a leak $s_l = 0.5$, $\Delta s = 0.1$ (as in Figs. 4–6 and 42–44). Other data: $\langle t_{\rm coll}\rangle = 1.850\,55$, $\mu(I) = 0.1$, $\mu_c(I) = 0.1175$, and $\langle t_{\rm coll}\rangle_c = 1.916$. In order to illustrate the case of maps, instead of the true-time map, exclusively for this simulation we have used the Poincaré map of the billiard. In order to minimize the effect of sliding orbits (see Appendix D) we used in all simulations the following restrictions: a cutoff in the maximum collision time at 83 collisions ($t = 158$ in Fig. 43), and ρ_s is taken to be constant in $s \in [-1, 1]$, $p \in [-0.9, 0.9]$. ρ_c was built by iterating ρ_s. For $\gamma_{P\rm map}$ we used a more restrictive cutoff $2\langle\tau\rangle_{\mu,s}$, because it is more sensitive to the sliding orbits. The quantities $\mu_c(I)$ and $\langle t_{\rm coll}\rangle_c$ were calculated using Eq. (B3).

$\rho_0(\mathbf{x})$	ρ_c	ρ_r	$\rho_{\mu,s}$
Mean time			
Continuous, t	$\langle\tau\rangle_c = 15.24$	$\langle\tau\rangle_r = 18.50$	$\langle\tau\rangle_{\mu,s} = 14.23$
Discrete, n	$\langle\nu\rangle_c = 8.28$	$\langle\nu\rangle_r = 10.0$	$\langle\nu\rangle_{\mu,s} = 7.78$
Escape rate			
Continuous, t	$\kappa = 0.065\,59 \neq \kappa^* = 0.056\,93$		
Discrete, n	$\gamma_{P\rm map} = 0.1286 \neq \gamma^* = 0.1054$		

$$\mathfrak{m}(I) = \int_I [1 - R(\mathbf{x})]d\mu = \int_I [1 - R(s,\theta)]\frac{1}{4}\cos\theta d\theta ds, \tag{46}$$

where $R(\mathbf{x})$ is the (position dependent) reflection coefficient. The argument of Sec. II.A leads to the naive estimate

$$\tilde{\kappa}^* = \frac{-\ln[1 - \mathfrak{m}(I)]}{\langle t_{\rm coll}\rangle}; \tag{47}$$

see also Joyce (1975) and Ryu *et al.* (2006). This shows that the closed-system estimation for a leak with $R = 0.5$ is the same as the one for a leak of half the size, which was tested in Fig. 1 (and proved to be inaccurate).

The essential extension of the transient chaos theory is to consider a (modified) c density $\tilde{\rho}_c$ which should be normalized. As ρ_c, $\tilde{\rho}_c$ can also be achieved by rescaling. Here the *intensity* should be multiplied by a factor $e^{\tilde{\kappa}t}$ to compensate the global decay of $\tilde{P}(t)$. This rescaling implies that the c measure $\tilde{\mu}_c(E)$ of a region $E \in \Omega$ in a partially open system is the fraction of the intensity at time $t \to \infty$ that is in E. A more proper estimate of the escape rate $\tilde{\kappa}$ from this measure has to include, as in Eq. (46), the partial transmission through the leak as (Altmann, 2009)

$$\mathfrak{m}_c(I) = \int_I [1 - R(\mathbf{x})]d\tilde{\mu}_c = \int_I [1 - R(\mathbf{x})]\tilde{\rho}_c(\mathbf{x})d\mathbf{x}. \tag{48}$$

The analog of the improved escape rate formula (31) for a system with partial leaks is thus

$$\tilde{\kappa} \simeq -\frac{\ln[1 - \mathfrak{m}_c(I)]}{\langle t_{\rm coll}\rangle_{\tilde{c}}}, \tag{49}$$

where $\tilde{c}$ in $\langle t_{\rm coll}\rangle_{\tilde{c}}$ indicates the average taken with respect to $\tilde{\rho}_c$.

The complete extension of the transient chaos theory presented in Sec. II.B is considerably more subtle and requires the extension of the invariant sets discussed above (chaotic saddle and its invariant manifolds). We illustrate our general considerations introducing uniform reflectivity $R = 0.1$ in the leak of the cardioid billiard of Figs. 4 and 5. The procedures used previously (see Figs. 4–6) were employed to obtain Fig. 9, but now the intensities of the trajectories were used as weights attached to each trajectory; see Appendix B for details. The energy escape rate was found numerically to be $\tilde{\kappa} = 0.058$, obviously less than $\kappa = 0.066$ for the full leak case of the same size. The support of the regions with non-negligible densities shown in Fig. 9 shows the stable manifold, chaotic saddle, and unstable manifold, respectively. In the case of partial leaks it is important to distinguish the manifold of the trajectories from the manifold of the (trajectories weighted with) intensities J. Whenever the reflection coefficient is nonvanishing, $R(\mathbf{x}) \neq 0$ for all $\mathbf{x} \in \Omega$, trajectories survive forever (and correspond thus to that of the closed problem). The chaotic set of trajectories is then the full phase space; its manifolds are also space filling and are not very informative. The interesting patterns present in all panels of Fig. 9 motivate us to interpret the results in terms of manifolds of the (trajectories weighted with) intensities. This generalizes the case of full leak ($R = 0$ for $\mathbf{x} \in I$).

Consider first the case of the stable manifold W^S. While in the full leak case $W^S_{\rm full}$ is obviously outside the leak [e.g., in Fig. 5(a)], in the partial leak case $\tilde{W}^S$ should certainly include trajectories which start in the leak and never return. These new trajectories are nothing but the closed map preimage of $W^S_{\rm full}$ in I. Indeed, in Fig. 9(a) the filamentary structure extends inside I (with much lower intensity). These new trajectories modify the manifolds in the whole phase space because their preimages can be outside the leak. More generally, it is natural to consider $W^S_{\rm full}$ as the set of all points that carry a nonvanishing intensity J for arbitrarily large t (Altmann, 2009)

$$\mathbf{x} \in \tilde{W}^S \Leftrightarrow \text{ for } t \to +\infty, \quad J_t(\mathbf{x}) \to J_{+\infty}(\mathbf{x}) > 0, \tag{50}$$

where $J_\infty(\mathbf{x})$ is the asymptotic intensity. The same reasoning applies to the unstable manifold $\tilde{W}^U$, in which case the limit $t \to -\infty$ is taken in Eq. (50). The presence of new orbits, compared to the case with full leak, is clearly seen when comparing Figs. 6 and 9(c). Figure 9(c) shows the c density $\tilde{\rho}_c(\mathbf{x})$ of the partial leak case. The chaotic saddle (CS) is shown in Fig. 9(b) and should be compared to Fig. 4(b). Again, it can be thought of as $CS = \tilde{W}^S \cap \tilde{W}^U$, i.e., the points that remain with $J > 0$ for $t \to \pm\infty$. The natural extensions of the concepts of chaotic saddle and its invariant manifolds are expected to hold in all systems with partial leaks [see also Wiersig and Main (2008)].

A complete description of distributions such as those shown in Fig. 9 cannot be achieved by simply including the new trajectories mentioned above. For instance, trajectories that collide infinitely many times with $R < 1$ but still less frequently than other trajectories might also contribute to the asymptotic properties. Indeed, it appears natural that the support of the distributions such as those shown in Fig. 9 fills an area of the phase space and therefore has a trivial fractal dimension $D_0 = 2$ (the same as that of the chaotic set of the trajectories). Given the peaked structures of the densities, we speculate that the information dimension D_1 and the generalized dimension D_q with $q > 0$ might be below 2 [see Tél and Gruiz (2006) for simple examples of sets with trivial D_0

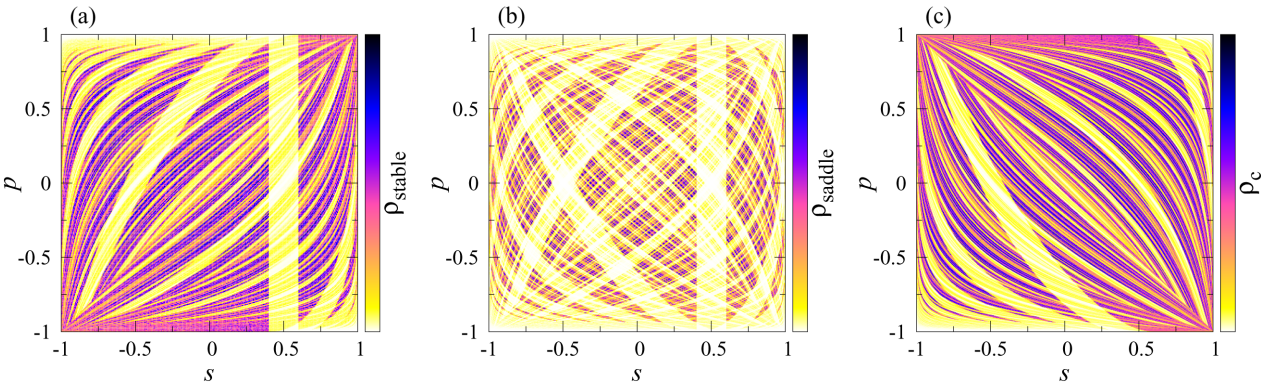

FIG. 9 (color online). Invariant densities for the cardioid billiard considered in Figs. 4–6 with partial leak $R = 0.1$ for $\mathbf{x} \in I$. The different panels show the densities associated with (a) the stable manifold, (b) the chaotic saddle, and (c) the unstable manifold. The densities were obtained considering the intensity weighted trajectories at times $1/\tilde{\kappa}^* < 60 < t < 80$ and plotting at (a) their initial conditions, (b) their positions around the time $t/2$, and (c) their positions over the time interval $60 < t < 80$. See Appendix C for details.

and nontrivial D_1]. It remains, however, to be verified whether Eqs. (27)–(29) are applicable to systems with partial leaks.

In Sec. III we introduce a formalism based on Perron-Frobenius operators that directly calculates the (normalized) density $\tilde{\rho}_c$ and the artificial (nonobservable) distinction between J and ρ_c becomes superfluous.

III. OPERATOR FORMALISM

In the previous sections we used extended trajectories which depend not only on the phase-space coordinate $\mathbf{x}$ of the map but also on the true-time t and on the intensity J. These two quantities are labels which are attached to each trajectory and change depending on (but do not affect) the sequence of collisions $\mathbf{x}_i$, $i = 0, \ldots, n$. Here we develop a more elegant formalism based on operators acting on densities $\rho(\mathbf{x}, t)$ that naturally accounts for both of these aspects, allowing for a more rigorous treatment. In the spirit of systems with leaks, and similarly to Sec. II, we start with the case of closed systems that will be used for comparison with the leaking case.

Before discussing how densities evolve in time, it is essential to clarify the relationship between the different characteristic densities in billiard systems. Here we search for exact relationships between the measure μ_F of the flow and the measure μ of the true-time map (for more details see Appendix B). In closed Hamiltonian systems the natural measure μ is the Lebesgue measure.

A trajectory of the billiard flow can be represented by the Birkhoff coordinates $\mathbf{x} = (s, p)$ of its next collision with the boundary and the time r after the previous collision, as illustrated in Fig. 10 [see Chernov and Markarian (2006) for a rigorous mathematical formulation]. We call r the coordinate time and it also corresponds to a distance in the billiard, since the velocity of the particle has been chosen to be unity. Of course, the coordinate time fulfills $0 \le r \le t_{\text{coll}}(\mathbf{x})$, where the collision time $t_{\text{coll}}(\mathbf{x})$ is defined as the time t between the collision in $\mathbf{x}$ and the last collision.[7]

[7]These definitions are convenient because they assure that $t_{\text{coll}}(\mathbf{x})$ and the c measure are defined inside the leak $\mathbf{x} \in I$.

A. Closed system

In the time-continuous representation, let $\rho_F(\mathbf{x}, r)$ denote the probability density for finding a flow trajectory at $(\mathbf{x}, r)$. The corresponding invariant measure $d\mu_F$ of the flow can then be written as

$$d\mu_F = \rho_F(\mathbf{x}, r) d\mathbf{x} dr. \tag{51}$$

Consider now the true-time map in standard Birkhoff coordinates $\mathbf{x} = (s, p)$. Let $\rho_\mu(\mathbf{x})$ denote the probability density of the invariant measure in this map, which is a constant as seen in Fig. 3. The corresponding measure $d\mu$ is

$$d\mu = \rho_\mu(\mathbf{x}) d\mathbf{x}. \tag{52}$$

We want to connect μ to μ_F. Since the dynamics between collisions is a uniform motion of unit velocity, ρ_F is independent of r and, therefore, the flow density in variable $\mathbf{x}$ is proportional to that of the map

$$\rho_F(\mathbf{x}, r) = A \rho_\mu(\mathbf{x}), \tag{53}$$

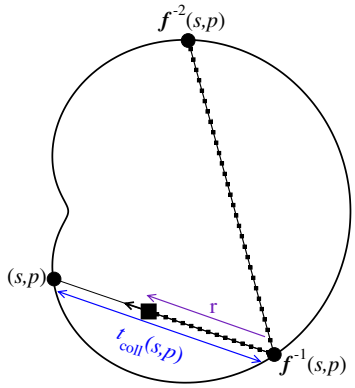

FIG. 10 (color online). Schematic illustration of flow and map coordinates for billiards. We use the convention that a particle in the flow (■) has coordinates $(s, p, r) = (\mathbf{x}, r)$. Note that $\mathbf{x}$ is the end point of a flight within the billiard. Because of the specular nature of the reflection, the p coordinate does not change during a collision, $\mathbf{x} \equiv (s, p)$ corresponds thus to the map coordinate denoted by ● at the boundary of the billiard defined right after collisions. Smaller dots represent other particles in the flow that move along the same trajectory.

where A is a constant. Its value follows from the normalization of the measure $\int d\mu_F = 1$:

$$\int \rho_F(\mathbf{x}, r) dr d\mathbf{x} = \iint_0^{t_{\rm coll}(\mathbf{x})} A\rho_\mu(\mathbf{x}) dr d\mathbf{x} = A \int t_{\rm coll}(\mathbf{x})\rho_\mu(\mathbf{x}) d\mathbf{x} = 1. \tag{54}$$

Since the integral in the last equality equals the average collision time in the closed system's true-time map, we have

$$A = \frac{1}{\langle t_{\rm coll}\rangle}. \tag{55}$$

From this relation, and Eqs. (51)–(53), it follows that the flow measure and the map measure are related as

$$d\mu_F = \frac{dr}{\langle t_{\rm coll}\rangle} d\mu. \tag{56}$$

This is a well-known relation connecting flows and maps in closed billiards [see, e.g., Chernov and Markarian (2006)]. Recalling that $\langle t_{\rm coll}\rangle$ can be related to simple geometric properties of the billiard as in Eq. (14), this formula shows that the mean collision time provides a simple and elegant connection between properties of the flow and the map. For instance, Lyapunov exponents of the flow are equal to those of the true-time map divided by $\langle t_{\rm coll}\rangle$.

From Eq. (56) one can also estimate the escape rate by assuming that the existence of such a leak does not influence the validity of this relation. The rate of change of μ_F over coordinate time r is in this type of perturbation approach

$$\mathcal{F} = \frac{d\mu_F}{dr} = \frac{d\mu}{\langle t_{\rm coll}\rangle}, \tag{57}$$

and this rate is independent of coordinate time r. The fraction of trajectories escaping through leak I over a time unit can be computed as $\mathcal{F}(I) = \int_I d\mathbf{x}\mathcal{F}$. Consider a time interval of the length of the average collision time $\langle t_{\rm coll}\rangle$. The decay of surviving trajectories is exponential $P(t) = e^{-\kappa t}$ for any time t for trajectories distributed according to the c density, which is then approximately $\rho_\mu(\mathbf{x})$. We can thus estimate κ using Eq. (57) and writing the proportion of particles that escape the billiard in a time $t = \langle t_{\rm coll}\rangle$ as $1 - e^{-\kappa\langle t_{\rm coll}\rangle}$:

$$\mathcal{F}(I)\langle t_{\rm coll}\rangle = \mu(I) = 1 - e^{-\kappa\langle t_{\rm coll}\rangle}. \tag{58}$$

This leads to the naive estimate $\kappa^* = -\ln[1 - \mu(I)]/\langle t_{\rm coll}\rangle$ stated in Eq. (23).

Finally, the dynamics of densities in closed maps can be rewritten in terms of the Perron-Frobenius operators (Gaspard, 1998; Dorfman, 1999; Lai and Tél, 2011)

$$\rho_{n+1}(\mathbf{x}') = \frac{\rho_n(\mathbf{x})}{|\mathcal{J}(\mathbf{x})|_{\mathbf{x}\in\mathbf{f}^{-1}(\mathbf{x}')}}, \tag{59}$$

where $\mathcal{J}(\mathbf{x})$ is the Jacobian at point $\mathbf{x}$. In Hamiltonian systems $\mathcal{J}(\mathbf{x}) = 1$, and the constant Lebesgue density $\rho_\mu(\mathbf{x}) = \text{const}$ is a stable fixed point of Eq. (59). Since there is no escape, the largest eigenvalue of the Perron-Frobenius operator is unity. In the next section we repeat the procedures presented above for systems with large leaks, i.e., we derive a connection between flow and map measures, an expression for the escape rate, and establish a Perron-Frobenius formalism. A direct connection between the Perron-Frobenius operator Eq. (59) of the open and leaky systems has recently been investigated for cases with Markov partitions by Froyland and Stancevic (2010).

B. Flow and map measures in billiards with leaks

From the point of view of the escape process, the analog of the natural measure is the c measure. Even if the c-measure definition in Eq. (25) applies for maps ($\mathbf{x}$ coordinates), it is essential to extend this concept to flows and true-time maps ($\mathbf{x}$ and r coordinates) in order to take the real time of trajectories into account. Indeed, it is known that averages taken with respect to flows (or true-time maps) and to traditional maps differ considerably in open systems (Kaufmann and Lustfeld, 2001).

The main difference with respect to the closed case is the dependence of the c measure μ_{Fc} of the flow on the coordinate time r. The survival probability decays in time t as $e^{-\kappa t}$, independent of the $\mathbf{x}$ coordinate. It is thus natural to associate the coordinate time r with t so that μ_{Fc} decays as $e^{-\kappa r}$. Therefore, Eq. (53) has to be replaced by

$$\rho_{Fc}(\mathbf{x}, r) = A_c\rho_c(\mathbf{x})e^{-\kappa r}, \tag{60}$$

where ρ_{Fc} is the density of the flow's c measure, and ρ_c is the density of the true-time map c measure μ_c. This latter is the measure we used in the main part of this paper. The density $\rho_c(\mathbf{x})$ is independent of r, as seen in Eq. (60), and thus it can be thought of as remaining constant from the previous collision ($r = 0$) until the collision at $\mathbf{x}$ [$r = t_{\rm coll}(\mathbf{x})$; see Fig. 10]. This constant value is proportional to $\rho_{Fc}(\mathbf{x}, r = 0)$. The proportionality factor A_c follows from $\int d\mu_{Fc} = 1$ as

$$\int \rho_{Fc}(\mathbf{x}, r) dr d\mathbf{x} = \iint_0^{t_{\rm coll}(\mathbf{x})} A_c\rho_c(\mathbf{x})e^{-\kappa r} dr d\mathbf{x} = A_c \int \rho_c(\mathbf{x})\frac{1}{\kappa}(1 - e^{-\kappa t_{\rm coll}(\mathbf{x})}) d\mathbf{x} = 1. \tag{61}$$

This yields

$$A_c = \frac{\kappa}{1 - \langle e^{-\kappa t_{\rm coll}}\rangle_c}, \tag{62}$$

which tends to $1/\langle t_{\rm coll}\rangle$ for $\kappa \to 0$ as in Eq. (55). The map and flow c measure μ_{Fc} and μ_c are related as

$$d\mu_{Fc} = A_c e^{-\kappa r} dr d\mu_c. \tag{63}$$

This is the generalization to open systems of Eq. (56). In contrast to the case of the closed billiard, the relation between the flow and the true-time map is not given by $\langle t_{\rm coll}\rangle$ (or $\langle t_{\rm coll}\rangle_c$) alone, but includes an explicit dependence on κ and the coordinate time r. In Appendix B we also connected μ_{Fc} and μ_c to the flow measure *projected* to the billiard's boundary.

C. Exact escape rate formula

We can now obtain an exact formula for the escape rate following the arguments used for closed systems at the end of Sec. III.A. From Eq. (63) one can again introduce the rate of change over coordinate time r as $\mathcal{F}_c = d\mu_{Fc}/dr$ which is, in contrast to Eq. (57), not independent of coordinate time r.

From Fig. 10 and Eq. (60), the true-time density flowing out at $\mathbf{x}$ is given by $\rho_{Fc}(f(\mathbf{x}), r=0) = A_c\rho_c(f(\mathbf{x}))$. Therefore the fraction of trajectories that escapes through leak I in time $\langle t_{\rm coll}\rangle_c$ is $\int_0^{\langle t_{\rm coll}\rangle_c} \mathcal{F}_c(f(I))dr$, with $f(I)$ = "escape" as given in Eq. (20). In view of Eqs. (62) and (63), Eq. (58) turns into

$$\int_0^{\langle t_{\rm coll}\rangle_c} \mathcal{F}_c(f(I))dr = \mu_c(f(I))\frac{1-e^{-\kappa\langle t_{\rm coll}\rangle_c}}{1-\langle e^{-\kappa t_{\rm coll}}\rangle_c} = 1-e^{-\kappa\langle t_{\rm coll}\rangle_c}. \tag{64}$$

Here in the last equality we used again the fact that for the c measure the fraction of trajectories escaping up to time t is $1-\exp(-\kappa t)$. Since the escape happens immediately [i.e., $t_{\rm coll}(\text{escape}) = 0$ and thus $\mu_c(f(I)) = \mu_c(I)$], we obtain an implicit relation for κ as

$$\langle e^{-\kappa t_{\rm coll}}\rangle_c = 1-\mu_c(I). \tag{65}$$

This formula, which is a new result and will be derived more formally in Sec. III.D, establishes a relation between the average of an expression containing κ times the collision time and the measure of the leak, both averages taken with respect to the c measure of the true-time map. It is thus a generalization of the Pianigiani-Yorke formula (32), valid for usual maps, which is recovered from Eq. (65) in the limit of $t_{\rm coll} \equiv 1$. It is an exact expression, the culmination of different approximations of κ discussed previously, as summarized in Table III.

It is worth applying the cumulant expansion to the left-hand side of Eq. (65):

$$\ln(\langle e^{-\kappa t_{\rm coll}}\rangle_c) = \sum_{r=1}^{\infty}\frac{(-\kappa)^r}{r!}C_r(t_{\rm coll}) = \ln[1-\mu_c(I)], \tag{66}$$

where $C_r(y)$ are the cumulants of y [$C_1 = \langle y\rangle_c$, $C_2 = \sigma_c^2(y)$, etc.]. Keeping only the first term of the expansion, we find a first order approximation κ_1 of the escape rate as

$$\ln[1-\mu_c(I)] = -\kappa_1\langle t_{\rm coll}\rangle_c.$$

This is the improved escape rate formula (31), obtained in Sec. II as a generalization (based on the theory of transient chaos) from the naive estimate (23).

We estimate the deviation between κ_1 and κ by including the second term of expansion (66). For the second order approximant κ_2, a quadratic equation is obtained:

$$\ln[1-\mu_c(I)] = -\kappa_2\langle t_{\rm coll}\rangle_c + \frac{\kappa_2^2}{2}\sigma^2_{t_{{\rm coll},c}},$$

TABLE III. Summary of the escape rate formulas for strongly chaotic systems with a leak I. The measures are $\mu(I) = \int_I \rho_\mu(\mathbf{x})d\mathbf{x}$ and $\mu_c(I) = \int_I \rho_c(\mathbf{x})d\mathbf{x}$. The averages $\langle\cdots\rangle$ and $\langle\cdots\rangle_c$ correspond to averages μ and μ_c, respectively. The corresponding formulas for systems with *partial* leaks are given in Eqs. (47), (49), and (71).

Escape rate formula	κ	Equation
Sabine's estimate	$\frac{\mu(I)}{\langle t_{\rm coll}\rangle}$	(13)
Naive (Eyring) estimate (κ^*)	$-\frac{\ln[1-\mu(I)]}{\langle t_{\rm coll}\rangle}$	(23)
Improved estimate (κ_1)	$-\frac{\ln[1-\mu_c(I)]}{\langle t_{\rm coll}\rangle_c}$	(31)
Exact expression	$\langle e^{-\kappa t_{\rm coll}}\rangle_c = 1-\mu_c(I)$	(65)

where $\sigma^2_{t_{{\rm coll},c}}$ is the second cumulant of the collision time distribution $t_{\rm coll}(\mathbf{x})$ taken with respect to the c measure μ_c. This yields the explicit form for κ_2:

$$\kappa_2 = \{\langle t_{\rm coll}\rangle_c - \sqrt{\langle t_{\rm coll}\rangle_c^2 + 2\sigma^2_{t_{{\rm coll},c}}\ln[1-\mu_c(I)]}\}/\sigma^2_{t_{{\rm coll},c}} \approx \kappa_1\left(1+\frac{\kappa_1}{2}\frac{\sigma^2_{t_{{\rm coll},c}}}{\langle t_{\rm coll}\rangle_c}\right), \tag{67}$$

where the approximation is valid for small variance $\sigma_{t_{{\rm coll},c}}$ of collision times. In a similar spirit, corrections due to the uneven distribution of $t_{\rm coll}$ have also been obtained by Mortessagne, Legrand, and Sornette (1992); see also Joyce (1975).

The approximation $\kappa_2 \approx \kappa_1$ is valid for

$$\frac{\sigma^2_{t_{{\rm coll},c}}}{\langle t_{\rm coll}\rangle_c^2}\ln[1-\mu_c(I)] \ll 1. \tag{68}$$

Our numerical simulations (see Appendix B) yield independent estimations for κ and $\kappa_{1,2}$. In our typical configuration (see Fig. 5), the agreement between κ_1 and κ_2 was on the order of 0.6% and between κ_2 and κ of 0.06% (below the precision of the results reported in Table II). From Eq. (68) we see that there are two effects that can make κ_1 a good approximation of κ: (a) small leak $\mu_c(I) \ll 1$, and (b) $\sigma_{t_{{\rm coll},c}}/\langle t_{\rm coll}\rangle_c \ll 1$. The latter corresponds to a small variance of the collision time distribution and is the limit under which the true-time map reduces to a usual map [and Eq. (32) is recovered]. Note, however, that the naive estimate κ^*, Eq. (23), does not follow in any order of the cumulant expansion. As previously noted by Joyce (1975, 1978), κ^* coincides with κ only under the physically unrealistic conditions that (i) the distribution in the room is uniform $\rho_c = \rho_\mu$, e.g., nonspecular collisions immediately randomize the trajectories or absorption is uniformly distributed, and (ii) $t_{\rm coll}$ is constant. If only condition (i) is satisfied, Eqs. (65) and (67) could be applied using μ instead of μ_c. Joyce also pointed out that an analog of Eq. (67) was published by Kuttruff in the 1970s. The κ^* estimate (23) is thus the result of a not fully consistent argumentation: it intends to correct for the finite size of the leak, but fully forgets about changing the measure to the c measure, a correction of comparable magnitude. The naive estimate κ^* was also obtained by Bunimovich and Dettmann (2007) as the first term of an expansion in the leak size.

Partial leaks.—We are now in a position to heuristically generalize Eq. (65) for systems with partial leaks $R \neq 0$ discussed in Sec. II D. The key observation is that the left- and right-hand sides of Eq. (65) can be interpreted as *global* and *local* quantities, respectively. The global quantity in the partial leak case remains unchanged: in one *iteration* of the true-time map the c density at position $\mathbf{x}$ decays as $e^{-\tilde\kappa t_{\rm coll}(\mathbf{x})}$, and the global estimation of the proportion $\mathcal{S}$ of the remaining energy after a time $t_{\rm coll}$ is obtained simply as the average of this factor over the full phase space Ω:

$$\mathcal{S} = \int_\Omega \tilde\rho_c(\mathbf{x})e^{-\tilde\kappa t_{\rm coll}(\mathbf{x})}d\mathbf{x} = \langle e^{-\tilde\kappa t_{\rm coll}}\rangle_{\tilde c}. \tag{69}$$

We denote the c density of problems with partial leaks as $\tilde\rho_c$, and index $\tilde c$ refers to such c densities. The same quantity is

obtained in a local approach by considering the proportion of trajectories not crossing the leak in one iteration of the true-time map. In the full leak case this is $1-\int_I \rho_c(\mathbf{x})d\mathbf{x} = 1-\mu_c(I)$ which appears on the right-hand side of Eq. (65). When the leak is partially reflecting, the portion $\int_I R(\mathbf{x})\tilde{\rho}_c(\mathbf{x})d\mathbf{x}$ of the leak's measure enhances the number of survivors. The full proportion $\mathcal{S}$ is

$$\begin{aligned}\mathcal{S} &= 1-\int_I \tilde{\rho}_c(\mathbf{x})d\mathbf{x} + \int_I R(\mathbf{x})\tilde{\rho}_c(\mathbf{x})d\mathbf{x} \\ &= 1-\int_I [1-R(\mathbf{x})]\tilde{\rho}_c(\mathbf{x})d\mathbf{x} = \langle R(\mathbf{x})\rangle_{\tilde{c}},\end{aligned} \tag{70}$$

where we used the fact that the last integral [which is exactly $\mathfrak{m}_c(I)$ of Eq. (48)] can be written as an integral over the full phase space $\int_\Omega [1-R(\mathbf{x})]\tilde{\rho}_c(\mathbf{x})d\mathbf{x}$, since outside the leak $R\equiv 1$, and we used the normalization $\int_\Omega \tilde{\rho}_c(\mathbf{x})d\mathbf{x}=1$. This means that the remaining energy portion is the full phase-space average of the reflection coefficient $\langle R\rangle_{\tilde{c}}$. Equating the global (69) and local (70) expressions we obtain

$$\langle e^{-\tilde{\kappa}t_{\rm coll}}\rangle_{\tilde{c}} = \langle R\rangle_{\tilde{c}}. \tag{71}$$

This is a general exact relationship for the energy escape rate $\tilde{\kappa}$ that applies to all cases and is one of our main new results. In Sec. III.D we provide a derivation of this expression based on Perron-Frobenius operators. Equation (71) goes over into Eq. (65) for full leaks, i.e., for $R=0$ inside the leaks.

Finally it should be noted that the value of our escape rate relations (65) and (71), just like that of the Pianigiani-Yorke formula (32), is conceptual. They do not provide an efficient way for determining the escape rate (that is well handled numerically); rather they illustrate how the escape rate of the flow follows from properties of the true-time map.

D. Operators for true-time maps with partial leaks

Consider an invertible open map $\mathbf{f}$. Its escape rate γ is known to appear as the largest eigenvalue of an operator, the Perron-Frobenius operator. This operator is defined (Tél, 1987; Lai and Tél, 2011) by the iteration scheme of a density function ρ:

$$e^{-\gamma}\rho_{n+1}(\mathbf{x}') = \frac{\rho_n(\mathbf{x})}{|\mathcal{J}(\mathbf{x})|_{\mathbf{x}\in\mathbf{f}^{-1}(\mathbf{x}')}}, \tag{72}$$

where $\mathcal{J}(\mathbf{x})$ is the Jacobian at point $\mathbf{x}$. By considering the right-hand side to be the result of an operator acting on function ρ, the left-hand side shows that $e^{-\gamma}$ is an eigenvalue (in the space of positive ρs, the largest eigenvalue) of this operator. Equation (72) expresses that the total probability in a small region at step n is the same as in the image of that region under map $\mathbf{f}$, when taking into account a factor e^{γ} for compensating the escape. The escape rate follows from the requirement that the integral of ρ_n over a fixed phase-space region containing the chaotic saddle remains finite in the limit $n\to\infty$. The limit distribution ρ_∞ is then the density ρ_c of the conditionally invariant measure concentrated on the unstable manifold of the chaotic saddle. This is the well-known picture for open maps (Tél, 1987; Lai and Tél, 2011).

As a generalization of this idea, in a true-time problem where the distribution of collision times $t_{\rm coll}(\mathbf{x}')$ is known, the continuous-time escape rate κ is determined by the iteration scheme

$$e^{-\kappa t_{\rm coll}(\mathbf{x}')}\rho_{n+1}(\mathbf{x}') = \frac{\rho_n(\mathbf{x})}{|\mathcal{J}(\mathbf{x})|_{\mathbf{x}\in\mathbf{f}^{-1}(\mathbf{x}')}}. \tag{73}$$

In this equation the true-time property is incorporated on the left-hand side in the multiplicative factor containing the escape rate, consistent with our convention for $t_{\rm coll}$ in Eq. (18). This is a higher-dimensional extension of the true-time formalism used for one-dimensional maps by Kaufmann and Lustfeld (2001) and, in a slightly different context, by Gaspard (1996, 1998).

The escape rate κ again can be considered as an eigenvalue, and its value follows from the requirement that the integral of ρ_n over a fixed phase-space region containing the chaotic saddle remains finite in the limit $n\to\infty$. The limit distribution ρ_∞ is the density ρ_c of the conditionally invariant measure of the true-time map. Equation (73) is consistent with the properties of the flow and map measures in billiards discussed in Sec. III.B. A nonzero stationary c density of the map can exist only if we compensate the exponential loss of the densities in time t (and coordinate r). This can be achieved by applying an instantaneous "kick" to the flow density in the form of a multiplicative factor $K(\mathbf{x},\mathbf{x}')>1$ applied when the billiard wall is reached at $(\mathbf{x}, r=t_{\rm coll}(\mathbf{x}))\equiv(\mathbf{x}', r=0)$. The flow density right after the collision can then be written as

$$\begin{aligned}\rho_{Fc}(\mathbf{x}', r=0) &= A_c\rho_c(\mathbf{x}') = K(\mathbf{x},\mathbf{x}')\rho_{Fc}(\mathbf{x}, r=t_{\rm coll}(\mathbf{x})) \\ &= A_c K(\mathbf{x},\mathbf{x}')\rho_c(\mathbf{x})e^{-\kappa t_{\rm coll}(\mathbf{x})}.\end{aligned}$$

This is consistent with Eq. (73) applied to the limit distribution of billiards ($J\equiv 1$) if $K(\mathbf{x},\mathbf{x}') = e^{\kappa[t_{\rm coll}(\mathbf{x})+t_{\rm coll}(\mathbf{x}')]}$.

The problem of maps with partial leaks can be treated as a further generalization. Since the dynamics of trajectories is then closed, we write the map as $\mathbf{f}_{\rm closed}$. The energy escape rate $\tilde{\kappa}$ for partial leaks follows from an iteration scheme in which the reflection coefficient $R(\mathbf{x})$ also appears, in a similar spirit as in Tanner's work on ray dynamics with transmission and reflection in periodically driven problems (Tanner, 2009; Chappell *et al.*, 2013; Chappell and Tanner, 2013). In our notation, R shows up on the right-hand side since there is an immediate loss of density wherever R is different from unity. If collision times are also taken into account, we find

$$e^{-\tilde{\kappa}t_{\rm coll}(\mathbf{x}')}\tilde{\rho}_{n+1}(\mathbf{x}') = \frac{R(\mathbf{x})\tilde{\rho}_n(\mathbf{x})}{|\mathcal{J}(\mathbf{x})|_{\mathbf{x}\in\mathbf{f}^{-1}_{\rm closed}(\mathbf{x}')}}. \tag{74}$$

The limit distribution $\tilde{\rho}_\infty$ is the density $\tilde{\rho}_c$ of the conditionally invariant measure in the true-time map of the partially leaking system. (One might also have leaks in a naturally open system, in which case the open map $\mathbf{f}$ should be used in the relation above.) Full leaks can also be seen as partial leaks with $R(\mathbf{x})=0$ for $\mathbf{x}\in I$. For traditional maps with leaks, $t_{\rm coll}(\mathbf{x})=1$, Eq. (74) yields the escape rate $\tilde{\gamma}$ of such maps: $\tilde{\kappa}\mapsto\tilde{\gamma}$. It is interesting to see from Eqs. (73) and (74) that in closed systems ($R\equiv 1$, $\kappa=0$) the Perron-Frobenius operator coincides with the classical form (59). There is then no essential difference between the true-time and the map picture due to the simple proportionality of the flow's and the map's measure as expressed by Eq. (53).

The operator formalism for true-time maps with partial leaks developed above is a new result of our paper. It unifies and generalizes all previous approaches. In fact, Eq. (74) suggests that the physically rather different phenomena of collision times and of reflection (without taking into account collision times) are described by essentially the same mathematical mechanism: the density $\tilde{\rho}(\mathbf{x})$ in Eq. (74) should be multiplied by a function of the phase-space coordinates $\mathbf{x}$. As a consequence, the inclusion of the collision time distribution has effects on the iteration similar to those of a reflection coefficient larger than unity. We note that Eq. (74) is a particular case of the generalized operators considered in the mathematical literature [see, e.g., Faure, Roy, and Sjoestrand (2008)], augmented here with a well-defined physical interpretation.

It is now straightforward to obtain an exact relation for $\tilde{\kappa}$. Consider the c density $\tilde{\rho}_c(\mathbf{x})$ of a system with full or partial leaks, i.e., the limit distribution of Eq. (74). By integrating both sides over the full phase space, we obtain

$$\begin{aligned}\langle e^{-\tilde{\kappa}t_{\rm coll}}\rangle_{\tilde{c}} &\equiv \int_\Omega d\mathbf{x}' e^{-\tilde{\kappa}t_{\rm coll}(\mathbf{x}')}\tilde{\rho}_c(\mathbf{x}') \\ &= \int_\Omega d\mathbf{x}' \frac{R(\mathbf{x})\tilde{\rho}_c(\mathbf{x})}{|\mathcal{J}(\mathbf{x})|_{\mathbf{x}\in \mathbf{f}^{-1}_{\rm closed}(\mathbf{x}')}} \\ &= \int_\Omega d\mathbf{x} R(\mathbf{x})\tilde{\rho}_c(\mathbf{x}) = \langle R\rangle_{\tilde{c}}, \end{aligned} \tag{75}$$

where we used $|\mathcal{J}(\mathbf{x})| = |d\mathbf{x}'|/|d\mathbf{x}|$, and $f_{\rm closed}(\Omega) = \Omega$. This provides a proof of our exact formula (71).[8] Although Eqs. (71) and (75) are identical, it is worth emphasizing that Eq. (71) was obtained from a qualitative argument based on properties of billiard dynamics. Since Eqs. (73) and (74) are valid for any true-time map, the derivation presented here shows that Eq. (75) is not restricted to billiards; it holds for leaky systems in general.

E. Examples in leaky baker maps

In order to illustrate our formalism in simple examples, we consider area-preserving baker maps. This is motivated not only by the possibility of an analytic treatment, but also by the fact that several previous publications (Nonnenmacher and Zworski, 2005; Keating *et al.*, 2006; Novaes *et al.*, 2009; Pedrosa *et al.*, 2009, 2012; Ermann *et al.*, 2012) use leaky versions of these maps to investigate quantum systems (see Sec. VI.E.2).

[8]Consider defining the collision time as a function of the initial coordinate $\mathbf{f}^{-1}(\mathbf{x})$ as $\hat{t}_{\rm coll}(\mathbf{f}^{-1}(\mathbf{x})) = t_{\rm coll}(\mathbf{x})$, or $\hat{t}_{\rm coll}((\mathbf{x})) = t_{\rm coll}(\mathbf{f}(\mathbf{x}))$. It is then natural to shift the factor $e^{-\kappa\hat{t}_{\rm coll}(\mathbf{x})}$ to the right-hand side of Eq. (74), and the same argument that led to Eq. (75) leads to $\langle Re^{\kappa\hat{t}_{\rm coll}}\rangle_{\hat{c}} = 1$. For the full leak case, Eq. (71) becomes $\langle e^{\kappa\hat{t}_{\rm coll}}\rangle_{\hat{c}} = 1 + \mu_c(I)$, as shown by Altmann, Portela, and Tél (2013). The distance from $\mathbf{f}^{-1}(\mathbf{x})$ to $\mathbf{x}$ [i.e., $t_{\rm coll}(\mathbf{x})$] is the same as from $\mathbf{x}$ to $\mathbf{f}^{-1}(\mathbf{x})$. The latter distance is obtained along a trajectory that starts at $(s, -p)$ and ends at $\mathbf{f}(s, -p)$. By introducing the operator $A(\mathbf{x}) = A(s, p) = (s, -p)$, this distance is $\hat{t}_{\rm coll}(A(\mathbf{x}))$. We thus find the simple relation $\hat{t}_{\rm coll}(\mathbf{x}) = t_{\rm coll}(A(\mathbf{x}))$ and, since $\mathbf{f}^{-1} = A\mathbf{f}A$ and $A^2 = 1$, $t_{\rm coll}(\mathbf{f}(\mathbf{x})) = t_{\rm coll}(A(\mathbf{x}))$ and $t_{\rm coll}(A(\mathbf{f}^{-1}(\mathbf{x}))) = t_{\rm coll}(\mathbf{x})$.

First we consider the triadic area-preserving baker map defined on the unit square $(x, y) \in [0, 1] \times [0, 1]$:

$$\begin{aligned}(x_{n+1}, y_{n+1}) &= \left(\tfrac{1}{3}x_n, 3y_n\right), && \text{for } y_n \le 1/3, \\ (x_{n+1}, y_{n+1}) &= \left[\tfrac{1}{3}(x_n + 1), 3y_n - 1\right], && \text{for } 1/3 \le y_n < 2/3, \\ (x_{n+1}, y_{n+1}) &= \left[\tfrac{2}{3}(x_n + 2), 3y_n - 2\right], && \text{for } y_n \ge 2/3, \end{aligned} \tag{76}$$

with a simple choice of the leak: I is a band of height $1/3$ in the expanding (y) direction in the middle of the square. In this model there are no partial leaks present. The collision times take on two values only: $t_{\rm coll} = \tau_1$ if the point is mapped into the column $x < 1/3$, and $t_{\rm coll} = \tau_2$ if the particle is mapped into the column $x > 2/3$.

We start from a constant distribution $\rho_0 \equiv 1$ on the unit square. Since the Jacobian is unity, Eq. (73) tells us that the measure (under ρ_0) of the lower band $y < 1/3$ is mapped on the column $x < 1/3$ with the measure on it multiplied by $e^{\kappa\tau_1}$. Similarly, the measure of the right column $2/3 < x < 1$ will be $e^{\kappa\tau_2}/3$. The measure from the midband is not mapped anywhere because it is in the leak.

This construction extends to finer scales in a self-similar manner due to the simple choice of the leak. The measure converges to the c measure, which therefore has to remain (conditionally) invariant under the above iteration. The value of the escape rate therefore follows by prescribing the invariance of the c measure. In this case it is sufficient to consider the measure projected on the x axis because the density is constant along y. By construction, this measure is originally 1, and after one step it is the sum of the two values just determined, and thus

$$e^{\kappa\tau_1} + e^{\kappa\tau_2} = 3. \tag{77}$$

This is an (irrational) equation for the escape rate κ. The validity of the new equation (65) can be easily verified:

$$\langle e^{-\kappa t_{\rm coll}}\rangle_c = e^{-\kappa\tau_1}\frac{e^{\kappa\tau_1}}{3} + e^{-\kappa\tau_2}\frac{e^{\kappa\tau_2}}{3} = 2/3,$$

which corresponds to $1 - \mu_c(I)$ since the leak has height $1/3$ and ρ_c is independent of y.

In the limit of traditional maps, $\tau_1 = \tau_2 = 1$, Eq. (77) yields $\kappa \to \gamma = \ln(3/2)$. Since the stretching rate is 3 everywhere in the phase space, the maps average Lyapunov exponent is $\bar{\lambda} = \ln 3$. The Kantz-Grassberger formula (29) then yields $D_1^{(1)}(I) = \ln 2/\ln 3$, i.e., the unstable manifold of this leaky baker map carries the structure of the classical triadic Cantor set.

As a more complex example, consider the dyadic baker map

$$\begin{aligned}(x_{n+1}, y_{n+1}) &= (\tfrac{1}{2}x_n, 2y_n), && \text{for } y_n \le 0.5, \\ (x_{n+1}, y_{n+1}) &= \left(1 - \frac{(1 - x_n)}{2}, 1 - 2(1 - y_n)\right), && \text{for } y_n > 0.5, \end{aligned} \tag{78}$$

with collision times taking on again two values only: $t_{\rm coll} = \tau_1$ if for the image point $x' < 1/2$, and τ_2 otherwise, but with partial leaks. These leaks are introduced with reflection coefficients $R_1, \ldots, R_4$ on four horizontal strips of height $1/4$, as Fig. 11 illustrates.

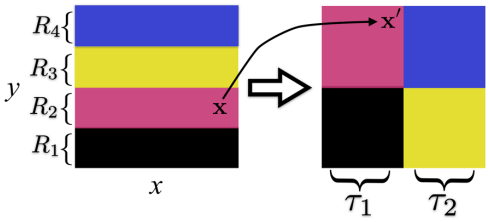

FIG. 11 (color online). Illustration of the dynamics of a dyadic true-time area-preserving baker map with partial leaks. The right square is obtained by applying baker map (78) to the left panel.

We again consider $\rho_0 \equiv 1$. After one iteration one finds that four different c densities appear in the four quadrants of the unit square. The next iteration refines the picture, but one feature remains: the c measure coarse grained on these four quadrants has four different densities. The values on the four rectangles change as iteration goes on, but the four-value structure remains unchanged.

In order to find an analytic expression for the energy escape rate, it proves to be sufficient to deal with the coarse-grained c density $\tilde{\rho}_c(y)$ projected on the expanding (y) axis. As follows from above, after a large number of iterations, this c density is piecewise constant and has a jump at $y = 1/2$. We therefore assume its form as

$$\tilde{\rho}_c(y) = \begin{cases} 2 - c, & \text{for } 0 < y < 0.5, \\ c, & \text{for } 0.5 \geq y \leq 1, \end{cases} \tag{79}$$

which fulfills normalization $\int_0^1 \tilde{\rho}_c(y)dy = 1$ for any c. The values of c and $\tilde{\kappa}$ follow from the requirement that this projected measure remains invariant after one more time step.

The lowest horizontal strip of height $1/4$ [and of c measure $(2 - c)/4$] is mapped, in view of Eq. (74), on the bottom left quarter of the square with a new measure $\exp(\tilde{\kappa}\tau_1)R_1(2 - c)/4$ (note that the Jacobian is unity). The second horizontal strip is mapped on the top left quarter with c measure $\exp(\tilde{\kappa}\tau_1)R_2(2 - c)/4$. The third and fourth strips come into the remaining quarters with weights $\exp(\tilde{\kappa}\tau_2)R_3c/4$ and $\exp(\tilde{\kappa}\tau_2)R_4c/4$, respectively (the last one representing the top right quarter).

The criterion of the invariance of the projected measure is that the total c measure in the two bottom (top) quarters is the same as the integral of Eq. (79) over $0 < y \leq 1/2$ ($1/2 < y \leq 1$). Thus, we find two equations

$$\begin{aligned} 1 - \frac{c}{2} &= \frac{1}{4}[e^{\tilde{\kappa}\tau_1}R_1(2 - c) + e^{\tilde{\kappa}\tau_2}R_3c], \\ \frac{c}{2} &= \frac{1}{4}[e^{\tilde{\kappa}\tau_1}R_2(2 - c) + e^{\tilde{\kappa}\tau_2}R_4c]. \end{aligned} \tag{80}$$

After rearrangement, we obtain

$$4 - 2e^{\tilde{\kappa}\tau_1}R_1 - 2e^{\tilde{\kappa}\tau_2}R_4 + e^{\tilde{\kappa}(\tau_1+\tau_2)}(R_1R_4 - R_2R_3) = 0 \tag{81}$$

and

$$c = \frac{4 - 2e^{\tilde{\kappa}\tau_1}R_1}{2 - e^{\tilde{\kappa}\tau_1}R_1 + e^{\tilde{\kappa}\tau_2}R_3} = \frac{2e^{\tilde{\kappa}\tau_1}R_2}{2 - e^{\tilde{\kappa}\tau_2}R_4 + e^{\tilde{\kappa}\tau_1}R_2}. \tag{82}$$

Equation (81) is an implicit equation for the escape rate, while Eq. (82) provides the value of c determining the jump in the c measure (79) projected onto the y axis. We verified that $\tilde{\kappa}$ obtained from such implicit relations agrees with direct numerical simulations of the baker map including the intensity J_n and real time t_n.

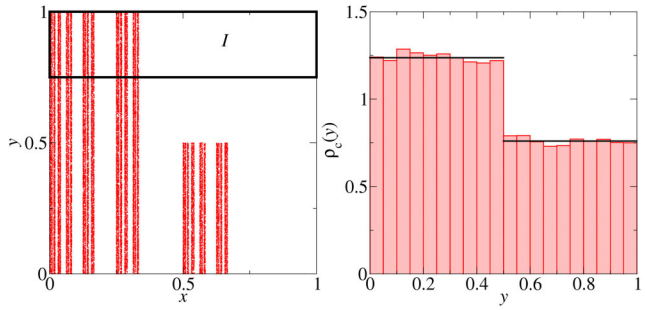

FIG. 12 (color online). Numerical results for the dyadic baker map with a full leak I over the uppermost strip of height $1/4$: $R_4 = 0$, $R_1 = R_2 = R_3 = 1$, and $\tau_1 = \tau_2 = 1$. Left panel: Unstable manifold obtained as the end point of particles surviving up to $n = 30$ iterations. Right panel: Distribution of the c density projected on the y axis $\rho_c(y)$. The straight lines are the analytical results $2 - c = \sqrt{5} - 1$ for $y < 0.5$ and $c = 3 - \sqrt{5}$ for $y > 0.5$.

To have more analytic insight, now we focus on the particular case of $\tau_1 = \tau_2 = 1$ (map with partial leaks). Equation (81) leads then to a quadratic expression for escape rate $\tilde{\gamma}$:

$$4 - 2(R_1 + R_4)e^{\tilde{\gamma}} + (R_1R_4 - R_2R_3)e^{2\tilde{\gamma}} = 0. \tag{83}$$

As a simple particular case, we assume that there is a full leak over the uppermost horizontal band and no partial leak anywhere: $R_4 = 0$, $R_1 = R_2 = R_3 = 1$. From Eqs. (82) and (83) we obtain $e^{\gamma} = \sqrt{5} - 1$, $c = 3 - \sqrt{5}$. Since the average Lyapunov exponent in this uniform baker map is $\bar{\lambda} = \ln 2$, the stable manifold's information dimension is, in view of Eqs. (27) and (29),

$$D_1^{(s)} = 2 - \frac{\ln(\sqrt{5} - 1)}{\ln 2},$$

clearly below 2. The numerically generated unstable manifold of this map can be seen in the left panel of Fig. 12 and confirms the fractal property. The right panel shows the projected c measure which clearly exhibits a jump at $y = 1/2$. The plateau values agree well with the theoretical predictions.

Had we taken the leak with $R_1 = 0$ ($R_2 = R_3 = R_4 = 1$), the same result would have been obtained. The situation is different, however, for $R_2 = 0$ or $R_3 = 0$. In the first case, we see from Eq. (82) that $c = 0$, implying a vanishing c measure for the entire upper half square. The escape rate is then $\gamma = \ln 2$ which implies $D_1^{(s)} = 1$. Fractality is then lost, and the stable and unstable manifolds are one dimensional. The dynamics is fully leaked, there is no chaos, and a single unstable fixed point, the one at (0, 0), governs the escape dynamics (hence $\gamma = \bar{\lambda}$). For $R_3 = 0$, $c = 2$, the c measure vanishes in the bottom half square, and the situation is otherwise the same. These observations again illustrate that the location of a leak of the same area is very important, and even chaos can be lost if they do not overlap with a period-1 orbit.

Now we consider the more general case of a partial leak of arbitrary reflection coefficient over the uppermost strip $R_4 \leq 1$ ($R_1 = R_2 = R_3 = 1$). The solution of Eqs. (82) and (83) leads to

$$e^{\tilde{\gamma}} = 2 - c, \qquad c = \frac{R_4 - 3 \pm \sqrt{R_4^2 - 2R_4 + 5}}{R_4 - 1}.$$

We took here the + root because for the − root the density $2 - c$ for $y \in [0, 0.5]$ would be negative. Using the result above and Eq. (83) with $R_1 = R_2 = R_3 = 1$ it is not difficult to confirm the validity of Eq. (71) for this partial leak case. As expected, for $R_4 \to 1$ we obtain $c = 2 - c = 1$ and $\tilde{\gamma} = 0$.

IV. IMPLICATIONS IN STRONGLY CHAOTIC SYSTEMS

A. Dependence of the escape rate on the leak

The main message of Sec. II is that for systems with finite leaks the naive theory based on the closed dynamics differs from the correct theory based on open systems. One of the most striking and best studied effects arising due to this difference is the dependence of the escape rate on the position of a fixed-size leak (Paar and Pavin, 1997; Schneider, Tél, and Neufeld, 2002; Altmann, da Silva, and Caldas, 2004; Bunimovich and Dettmann, 2007; Afraimovich and Bunimovich, 2010; Bunimovich and Yurchenko, 2011; Demers and Wright, 2011). This result is shown in Fig. 13 for the cardioid billiard with a leak $I = [s_l - \Delta s, s_l + \Delta s] \times [p_l - \Delta p, p_l + \Delta p]$ with fixed size $\Delta s = 0.1$, $\Delta p = 0.2$, $p_l = 0$, and different positions s_l. Physically this type of leak, illustrated in Figs. 13(a) and 13(b), could be realized in optical systems by replacing the perfect mirror boundaries in the region $[s_l - \Delta s, s_l + \Delta s]$ by dielectric material with refraction index $n = 1/\sin(\Delta p)$. The results in Fig. 13(c) confirm the nontrivial dependence of κ on s_l, which can take values both smaller and larger than the naive estimation $\kappa^* = -\ln(1 - \Delta s \Delta p)/\langle t_{\text{coll}} \rangle$ given by Eq. (23). The theory developed in Sec. II.B tells us that κ depends on $\mu_c(I)$ and $\langle t_{\text{coll}} \rangle_c$ through the improved escape rate formula [Eq. (31)]. Figures 13(d) and 13(e) show that both factors $\mu_c(I)$ and $\langle t_{\text{coll}} \rangle_c$ contribute to $\kappa \neq \kappa^*$ but the variation of $\mu_c(I)$ is the stronger factor in the dependence of κ on s_l (at least for this size of the leak). The results also indicate that the improved escape rate formula [Eq. (31)] provides an excellent approximation of the numerical results [and to Eq. (65)] in this example.

Apparently the first to report the dependence of the maps escape rate γ on leak position were Paar and Pavin (1997). The most pronounced effect shown for the doubling map (see Fig. 14) was the relationship between small values of γ and positions of the leak around short periodic orbits of the system [see also Altmann, da Silva, and Caldas (2004) and Bunimovich and Yurchenko (2011)]. This effect is less pronounced but also visible in Fig. 13, where local minima of the κ vs s_l curve are obtained when the leak is placed around the lowest periodic orbits of the billiard: the horizontal orbit at $(s = 0, p = 0) \mapsto (s = -1, p = 0)$ and the vertical orbit $(s = -0.5, p = 0) \mapsto (s = 0.5, p = 0)$.

An intuitive explanation of these results is found by looking at the images and preimages of leak I (Paar and Pavin, 1997; Buljan and Paar, 2001). The surviving trajectories at iteration n correspond to all trajectories that are not in any of

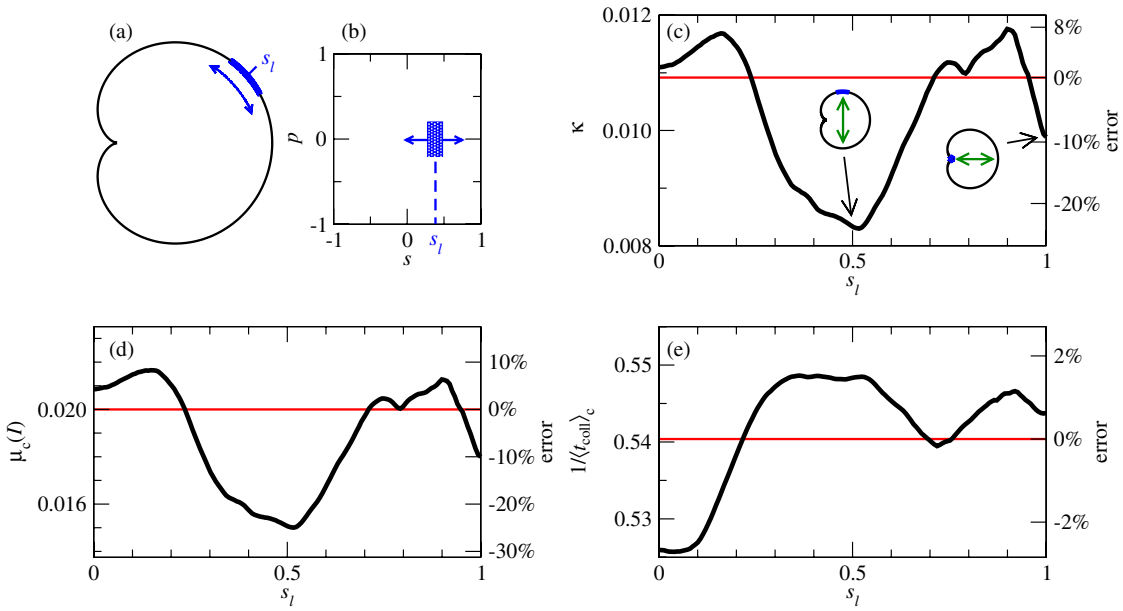

FIG. 13 (color online). Dependence of the escape rate on the position of the leak. (a) Cardioid billiard with a leak centered at some position s_l with $p_l = 0$. (b) Phase-space representation showing the leak $I = [s_l - \Delta s, s_l + \Delta s] \times [p_l - \Delta p, p_l + \Delta p]$ with $\Delta p = 0.2$, $\Delta s = 0.1$, $p_l = 0$, and $s_l \in [0, 1]$. (c) The escape rate κ obtained from numerical simulations such as the ones in Fig. 1. (d) The c measure of the leak $\mu_c(I)$ and (e) the inverse of the mean collision time. Results in (d) and (e) were calculated from $\rho_c(s, p)$ as described in Appendix B. Using these values to compute κ through Eq. (31) leads to results indistinguishable from those of (c). The estimates based on the closed billiard theory of Sec. II.A are shown as horizontal lines and correspond to the following: in (c) the naive estimate κ^* given by Eq. (23), in (d) $\mu(I) = \Delta s \Delta p$, and in (e) $\langle t_{\text{coll}} \rangle$ given by Eq. (14). The y axis on the right edges of (c)–(e) indicates the relative deviation between these values and the actual data.

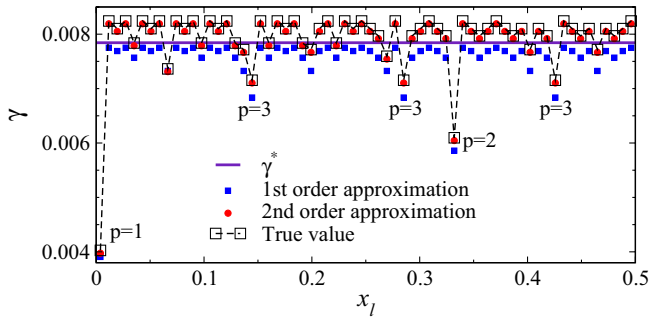

FIG. 14 (color online). Dependence of the escape rate γ on the location of the leak in the strongly chaotic doubling map $x_{n+1} = 2x_n (\mathrm{mod}\, 1)$. Leaks have $\mu(I) = 2^{-7}$ and are placed in nonoverlapping positions starting at $x = 0$ (Markov partitions). The periods p of the shortest unstable periodic orbits are marked at the positions x of leaks containing these orbits. The approximations to the true γ (squares) correspond to $\gamma^* = -\ln[1 - \mu(I)]$ as in Eq. (23) (horizontal line), Eq. (84) (squares, first order), and the corrected results obtained by Georgiou, Dettmann, and Altmann (2012) (circles, second order). Data by O. Georgiou.

the n preimages of I. Now, if preimages overlap repeatedly, there are more surviving trajectories for increasing n, and therefore the escape rate is smaller. The overlap between the leak and its images (or preimages) is obviously increased when the leak is around periodic orbits. We already learned in Sec. II.B that the escape rate can be calculated in terms of the periodic orbits inside the leak through Eq. (35). In this formalism, orbits with low period play an important role, with weights inversely proportional to their instability. If periodic orbits with low period (in particular, those with small expansion rates) are in the leak, they appear in the sum (35) and reduce γ.

This qualitative argument has been rigorously extended for different classes of strongly chaotic systems, such as 1D expanding linear maps (Keller and Liverani, 2009; Afraimovich and Bunimovich, 2010; Bakhtin and Bunimovich, 2011; Bunimovich and Yurchenko, 2011; Bunimovich, 2012; Ferguson and Pollicott, 2012). An important feature in these approaches is that all systems investigated admit a Markov partition and the holes are chosen to coincide with one element of the partition. For small leak sizes, a fractal dependence of the escape rate γ has been observed (Bunimovich and Yurchenko, 2011; Knight *et al.*, 2012) [see also Altmann and Endler (2010)]. As noticed by Bakhtin and Bunimovich (2011) and Bunimovich and Yurchenko (2011), the position dependence of γ might be so strong that there are cases in which a hole 2 times *larger* than another one can have a *smaller* escape rate. These results can also be understood in the exact expansions developed and applied to strongly chaotic billiards with finite but small leaks in Bunimovich and Dettmann (2007) and Dettmann (2013).

Beyond the Markovian approach, an alternative explanation based on recurrence times and Kac's lemma appears in Altmann, da Silva, and Caldas (2004). While a great number of analytical results can be obtained in 1D Markov systems, the results shown above in the cardioid billiard (area-preserving true-time map) appear to show a smoother dependence on position.

We mention that strong dependences are observed also by varying other parameters of the leaks such as the *orientation* of (asymmetric) leaks, as observed for Hamiltonian systems in Schneider, Tél, and Neufeld (2002). Interestingly, similarly complicated even fractal dependences with the position of the leak have also been observed in the diffusion coefficient (Klages, 2007; Knight *et al.*, 2012). Exponential decay and leaks with different shapes were investigated in detail in the periodic Lorentz gas in Demers, Wright, and Young (2010).

Complementary to the position dependence of κ, the dependence on the leak size is illustrated in Fig. 15 (Schneider, Tél, and Neufeld, 2002; Altmann, da Silva, and Caldas, 2004; Bunimovich and Dettmann, 2007). We change the size of the leak $I = [s_l - \Delta s, s_l + \Delta s] \times [p_l - \Delta p, p_l + \Delta p]$ by changing $\Delta p = \Delta s$ at a fixed $s_l = 0.4$, $p_l = 0$, as illustrated in Figs. 15(a) and 15(b). The dependence of κ on Δs depicted in Fig. 15(c) follows roughly the dependence of κ^* [straight diagonal line in (c)] but a nontrivial behavior is observed apart from this trend. Again, both the measure $\mu_c(I)$ shown in Fig. 15(d) and the mean collision time $\langle t_{\mathrm{coll}} \rangle_c$ shown in Fig. 15(e) are clearly different from the closed-system prediction (straight lines). The oscillations in $\mu_c(I)$ are stronger than the ones in $\langle t_{\mathrm{coll}} \rangle_c$ (at least for the leak sizes considered here) and provide the strongest contribution to $\kappa \neq \kappa^*$. In 1D piecewise-linear chaotic maps it was shown that the main properties (escape rate, entropy, fractal dimensions) of the leaky map vary nonsmoothly with the leak size (as the devil's staircase) (Życzkowski and Bollt, 1999; Lai, Życzkowski, and Grebogi, 1999; Demers and Wright, 2011) and position (Georgiou, Dettmann, and Altmann, 2012). Note that in view of the dependence of κ on the leak position discussed above, one can easily find situations in which larger leaks have smaller escape rates not only in the case of Markov leaks.

One particularly important limit is the case of vanishingly small leaks $\Delta s, \Delta p \to 0$. This is the traditional limit mathematicians are interested in (e.g., in the context of Poincaré recurrences) (Haydn, Lacroix, and Vaienti, 2005). It is interesting to see what happens with the position dependence of γ in the limit $\mu(I) \to 0$. For the case of the doubling map with Markov leaks, the escape rate γ depends only on the periodic orbit of the lowest period p inside the leak and is given in leading order by [see, e.g., Keller and Liverani (2009) and Bunimovich (2012)[

$$\gamma = \mu(I)(1 - 2^{-p}), \tag{84}$$

for arbitrary small $\mu(I)$. In this limit almost every leak position will have $p \to \infty$ so that Sabine's result is recovered in μ—almost every case. Indeed also the results in Figs. 15(c)–15(e) show that all quantities converge to the closed system's prediction (straight lines) in this limit. The dashed line in Fig. 15(c) shows that the relative difference $(\kappa - \kappa^*)/\kappa^*$ is of the order of 10% for $\mu(I) \approx 0.1$ but that it also consistently decays for small Δs. Altogether these convergences are physically relevant, particular manifestations of the more general convergence $\rho_c(s, p) \to \rho_\mu(s, p)$ for $\mu(I) \to 0$, discussed in Sec. II.B. For finite but small leaks, an approximation which improves Eq. (84) was obtained by Georgiou, Dettmann, and Altmann (2012) for maps with complete symbolic dynamics; see Fig. 14. It considers not only the period p but also the full symbolic dynamics of the periodic

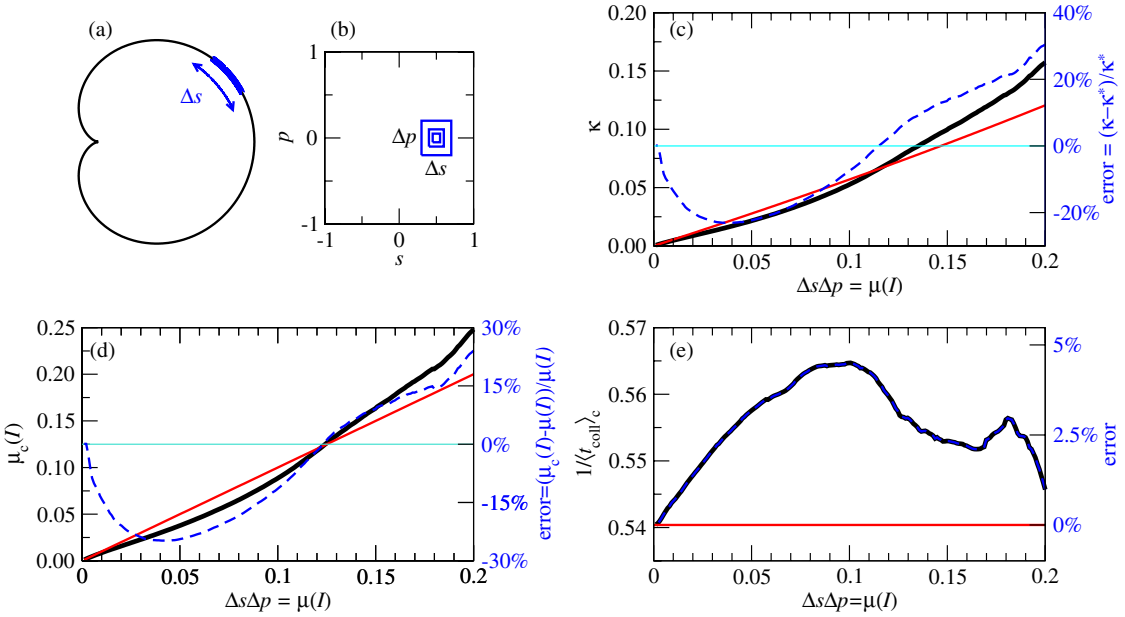

FIG. 15 (color online). Dependence of the escape rate on the size $\Delta s\Delta p$ of the leak. (a) Cardioid billiard with a leak centered at $s_l = 0.4$, $p_l = 0$ and variable size. (b) Phase-space representation showing the leak $I = [s_l - \Delta s, s_l + \Delta s] \times [-\Delta p, +\Delta p]$, with $\Delta p = \Delta s \in [0, 1/\sqrt{5}]$. (c) Escape rate κ as a function of $\Delta s\Delta p$. The improved estimate (31) again provides a good approximation to the numerical results. (d) The c measure of the leak $\mu_c(I)$, and (e) the inverse of the mean collision time. Results from (d) and (e) were calculated from $\rho_c(s, p)$ as described in Appendix B. Bold lines: numerical results. Thin lines: estimates based on the closed billiard theory of Sec. II.A: in (c) the naive estimate κ^* given by Eq. (23), in (d) $\mu(I) = \Delta s\Delta p$, and in (e) $\langle t_{\rm coll}\rangle$ given by Eq. (14). Dashed lines: relative deviation between thin and thick lines; see the y axis at the right edge of (c) and (d).

orbits inside I and shows that the average of γ taken over all (Markovian) leak positions is larger than $\mu(I)$ (and γ^*), contrary to what Eq. (84) suggests. An alternative approach which leads to an optimal expansion of κ versus the leak size was developed by Bunimovich and Dettmann (2007) and applied to billiards. See also Bunimovich and Webb (2012) and Cristadoro, Knight, and Degli Esposti (2012) for recent alternative approaches.

B. Multiple leaks and basins of escape

The idea of introducing more than one leak into the system is very natural in numerous circumstances (Bleher *et al.*, 1988). Quantum systems often have more than one leak due to input, output, transmission, reflection, or antennas, and multiple leaks in chaotic systems have also been considered (Buljan and Paar, 2001; Bunimovich and Dettmann, 2005, 2007; Portela *et al.*, 2007; Dettmann and Georgiou, 2011b). The results of Sec. IV.A show that the c measure depends sensitively on the position of the leak. As a consequence, the results for multiple leaks are not only different from those obtained in the closed-system approximation, but also cannot be easily obtained from the results for each leak alone. For instance, with two leaks I_1 and I_2, the escape rate is, in general, different from the sum of the single leak case:

$$\kappa(I_1 + I_2) \neq \kappa(I_1) + \kappa(I_2). \tag{85}$$

This result is not surprising in view of the nontrivial dependence of κ on the leak size, reported in Fig. 15, in which case it was clear that doubling the leak size does not imply doubling κ. Indeed, the difference reported in Eq. (85) has been understood in terms of the overlap of the preimages of the two leaks (Buljan and Paar, 2001; Pikovsky and Popovich, 2003) and has been developed more systematically by Bunimovich and Dettmann. They found that $\kappa(I_1 + I_2)$ can be expressed as $\kappa(I_1) + \kappa(I_2)$ plus a series of correlation terms (with decreasing importance) (Bunimovich and Dettmann, 2007).

In contrast to the escape rate, the dimensions of the invariant sets of the system opened with multiple leaks can be estimated from the dimensions of the invariant sets with single leaks. Consider the case of two leaks I_1 and I_2. The saddle (or the manifolds) obtained for the case in which I_1 and I_2 are simultaneously opened corresponds to the intersection of the saddle (manifold) when only I_1 is opened with the saddle (manifold) obtained when only I_2 is opened. Very generally, fractal dimensions $D(I_1 + I_2)$ of the intersection are given by (Falconer, 1985)

$$D(I_1 + I_2) = D(I_1) + D(I_2) - D_{\rm embedding},$$

where $D(I_1)$ $[D(I_2)]$ is the dimension of the set obtained when only I_1 (I_2) is opened and $D_{\rm embedding}$ is the dimension of the embedding space. For full leaks, the dimension and the escape rate are related to the Lyapunov exponent through Eq. (29). The argument above can trivially be extended to more then two leaks. It is not valid, however, in cases when the saddles of the two leaks are trivially connected to each other (e.g., $I_2 \subset I_1$ or I_2 is an image of I_1).

The interesting phenomenology of multiple leaks is better illustrated through an example. We consider the cardioid billiard with two leaks I_1 and I_2 of the same size $\mu(I_1) = \mu(I_2) = 0.04$ but at different positions, as depicted in Fig. 16. We first consider the effect of each of these leaks separately. Following the procedures described in Fig. 13,

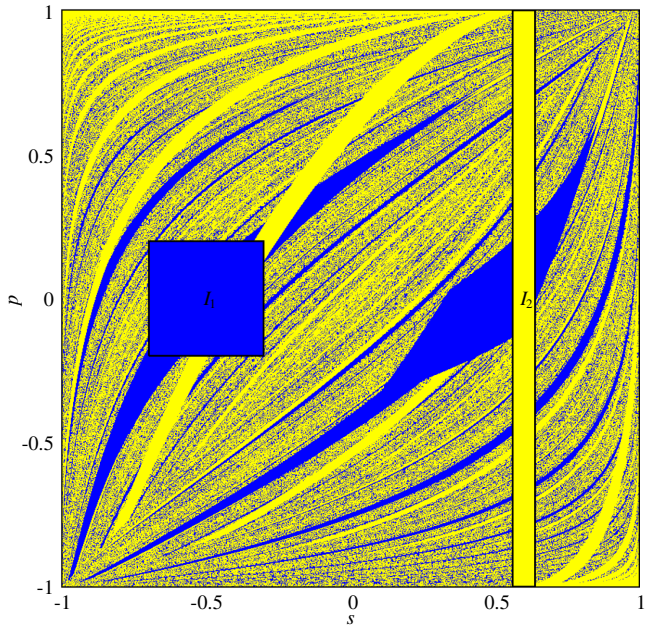

FIG. 16 (color online). Escape basins for two leaks in the cardioid billiard. Leak I_1 is centered at $s_l = -0.5$, $p_l = 0$ with $\Delta s = \Delta p = 0.2$, and I_2 at $s_l = 0.6$, $p_l = 0$ with $\Delta s = 0.04$, and no restriction in the collision angle is applied (i.e., $\Delta p = 1$). Both leaks have the same area in the phase space; nevertheless, 41% of the trajectories escape through leak I_1 (dark region) while 59% of the trajectories escape through leak I_2 (light region) when both leaks are open. Different characteristic values obtained for this system are reported in Table IV.

we obtain the results reported in the first two columns of Table IV.

We now consider the case when both leaks are simultaneously open. The result reported in Table IV confirms inequality (85). Similarly, we compute $\mu_c(I_i)$, the c measure for both leaks open calculated at I_i. The mean collision time is not defined with respect to a given leak as it depends on ρ_c in the whole phase space, hence the identical values in Table IV. A natural question is that of the nature of the sets of initial conditions which escape through each I_i, i.e., of the properties of the escape basins B_i, as the ones depicted in Fig. 16. The border between the two escape regions contains the stable manifold of the chaotic saddle (Lai and Tél, 2011). Note that the total area of the basins corresponds to the amount of initial conditions that escape through each leak, while $\mu_c(I_1)$ and $\mu_c(I_2)$ are proportional to the rate of escape through each leak for large times. Note that the escape rate should be independent of the leak through which the particle flux is monitored when both leaks are opened simultaneously. The obtained κ values are indeed the same within the numerical precision (three columns on the right). Apart from the standard c measure (in μ_c and $\langle t_{\rm coll}\rangle_c$), which considers normalization in the full phase space, we have also computed the c measure restricted to the set of points $(\mathbf{x})$ which escape through leak I_j. These results appear in the last two rows of Table IV and carry a superscript $\dagger, j$. In addition, it is interesting to note that all values are consistent with those obtained from $\kappa \simeq -\ln(1-\mu_c)/\langle t_{\rm coll}\rangle_c$ with $\mu_c^{\dagger,j}(I_j)$, $\langle t_{\rm coll}\rangle_c^{\dagger,j}$.

It was shown by Bunimovich and Yurchenko (2011) that it is possible to construct examples in which arbitrarily small escape rates are achieved even in the presence of leaks of arbitrarily large sizes. This surprising claim can be understood intuitively from the results of this section. Starting from a system with an arbitrarily small leak, consider expanding the leak in such a way that the new leak also contains many images (and/or preimages) of the original leak. This new leak can take an arbitrarily large proportion of the phase space without affecting the saddle and thus the escape dynamics which is by construction slow.

C. Emission

The most natural observable quantity in the configuration space of leaking systems is the emission of trajectories through the leak. Here we provide a representative configuration in which emission plays an important role and connect the observed quantities to our theoretical formulation.

Consider that detectors are placed around a circle far away from the cardioid billiard, as usually considered in optical microcavities. We introduce a leak on the right-hand side of the cardioid billiard with $s_l = 0$, $p_l = 0$, $\Delta s = 0.5$, and $\Delta p = 0.2$. The detectors collect the intensity of light emitted through the leak under different polar angles Φ measured

TABLE IV. Measurements in the system depicted in Fig. 16. The superscripts $\dagger, j$ in the last two rows indicate that the c measure was restricted to the set of points x which escape through leak I_j. The κ's in the three last columns are consistent with each other and with the values obtained from $\kappa_1 = -\ln(1-\mu_c)/\langle t_{\rm coll}\rangle_c$ with $\mu_c^{\dagger,j}(I_j)$, $\langle t_{\rm coll}\rangle_c^{\dagger,j}$ (the values in the last two rows of these columns). Obviously, $\mu_c^{\dagger,j} = \mu_c$ whenever only I_j is open ($I_j = \{I_1, I_2, I_1 + I_2\}$, compare rows 5 and 6 to 7 and 8). For the computation procedures; see Fig. 42 [for the $\dagger, j$ cases the set $S(t^*)$ was divided into two subsets according to the leak through which trajectories escape]. Error bars are of order 5 in the last digit.

Leaks open during experiment:	Only I_1	Only I_2		Both I_1 and I_2	
Measurement ($\downarrow$) applied in leak $I_j = (\rightarrow)$	I_1	I_2	$I_1 + I_2$	I_1	I_2
$\mu(I_j)$	0.04	0.04	0.08	0.04	0.04
κ	0.016 07	0.023 60	0.037 76	0.037 80	0.037 73
$\mu_c(I_j)$	0.028 56	0.043 32	0.066 97	0.027 66	0.039 31
$\langle t_{\rm coll}\rangle_c$	1.805 9	1.879 9	1.842 4	1.842 4	1.842 4
$\mu_c^{\dagger,j}(I_j)$	0.028 56	0.043 32	0.066 97	0.069 99	0.065 00
$\langle t_{\rm coll}\rangle_c^{\dagger,j}$	1.805 9	1.879 9	1.842 4	1.927 3	1.786 9

from the center of the billiard. Numerically, we distribute a large number of trajectories with an initial density $\rho_0(\mathbf{x})$ in the phase space and record the emission angle Φ of escaped trajectories in the configuration space. The proportion of trajectories escaping in a small interval around Φ is measured. For short times, the distributions are very irregular and depend strongly on the initial distribution $\rho_0(\mathbf{x})$ of the trajectories inside the cavity. After a transient period of the time $\rho(\mathbf{x}, t) \to \rho_c(\mathbf{x})$, the total intensity decays exponentially and the shape of the spatial distribution remains the same. Figure 17 shows the spatial distribution as a function of Φ, the so-called far-field emission. A multipeaked nonuniform emission is observed. The spatial density of light rays for $t \gg 1$ is shown in Fig. 18.

For long times, the emission is fully described by the c density $\rho_c(\mathbf{x})$ inside the leak ($\mathbf{x} \in I$). For instance, the emission angle Φ is a geometrical function of $\mathbf{x} = (s, p)$ in the leak, $\Phi = \phi(\mathbf{x})$, and the far-field intensity $\varrho(\Phi)$ is

$$\varrho(\Phi) \sim \int_I \rho_c(\mathbf{x})\delta(\Phi - \phi(\mathbf{x}))d\mathbf{x}. \tag{86}$$

Figure 19 shows $\rho_c(\mathbf{x})$ in I for our example. The leak placed only on the right side of the billiard $s \in [-0.5, 0.5]$ and the nonuniform distribution of $\rho_c(\mathbf{x})$ are responsible for the peaked and nonuniform emission in Figs. 17 and 18. The filamentary structure of $\rho_c(\mathbf{x})$ inside I seen in Fig. 19 reflects the filamentary pattern of the unstable manifold of the chaotic saddle, as discussed in Sec. II.B. After performing the projection by $\rho_c(s, p)$ as indicated in Eq. (86), these filaments give rise to the zigzagged far-field emission shown in Fig. 17. In Sec. VI.D we see that similar emission properties can be experimentally observed in lasing microcavities, in which case the factor $1 - R(\mathbf{x})$ has to also be included in Eq. (86) in order to account for the partial reflection-transmission property of the leak (see also Sec. II D).

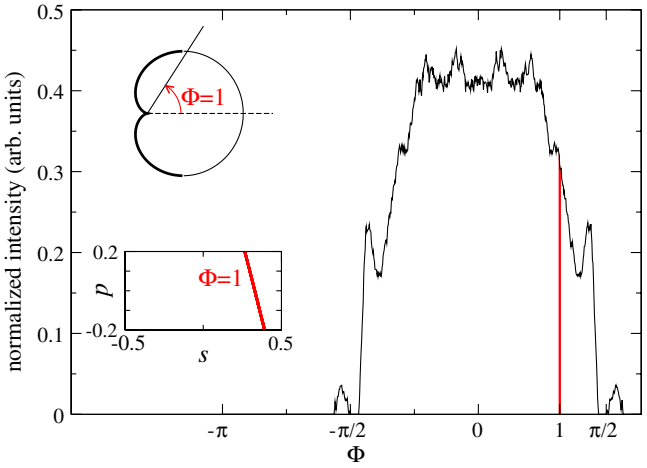

FIG. 17 (color online). Far-field emission for the cardioid billiard with a leak I centered at $(s_I, p_I) = (0, 0)$, with $\Delta s = 0.5$ and $\Delta p = 0.2$. The far-field intensity distribution is computed by collecting the number of trajectories emitted in the asymptotic direction given by the angle Φ (upper inset), measured over the time interval $(t_0, \ldots, \infty)$ with $t_0 \gg 1$. The lower inset displays the leak with the phase-space positions corresponding to a fixed emission angle Φ (gray curve). The initial density was uniform in the full phase space $\rho_0(\mathbf{x}) = \rho_\mu(\mathbf{x})$, and 1000 bins in $\Phi \in [-\pi, \pi]$ were used.

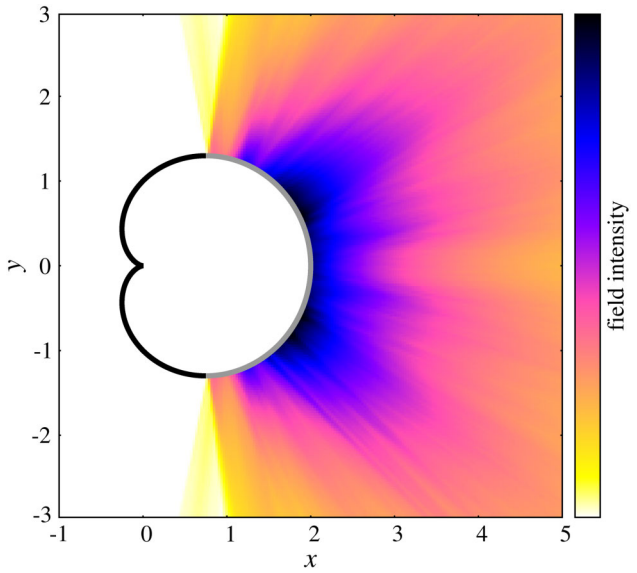

FIG. 18 (color online). Emission from the cardioid billiard described in Fig. 17 over the full configuration space. The color code indicates the density of trajectories outside the billiard at large times $t > 50$. Figure 17 is obtained by summing up all the intensities in a given direction. 10^8 initial conditions were used and data are presented on a grid of 200×200.

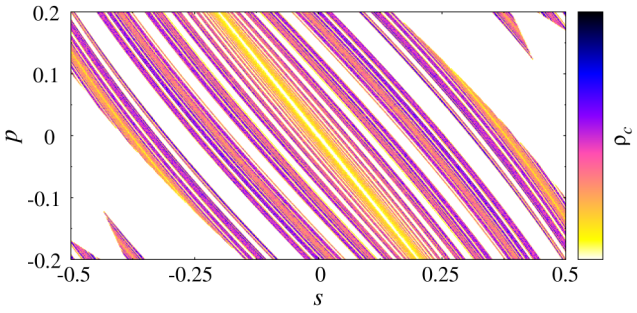

FIG. 19 (color online). Invariant density $\rho_c(s, p)$ inside the leak of Figs. 17 and 18. The emission patterns are ultimately determined by $\rho_c(s, p)$, e.g., the zero density around $(s, p) = (\pm 0.5, 0)$ leads to the zero emission around $\phi = \pm\pi/2$ in Fig. 17.

V. EXTENSION TO WEAKLY CHAOTIC SYSTEMS

A. Closed-system phase space

So far we have focused on the case of strongly chaotic systems and used the cardioid billiard to illustrate the theory. While these results apply to a broad class of (Hamiltonian and dissipative) systems, there is an evident need to expand them to the larger class of weakly chaotic systems. For instance, in closed Hamiltonian systems stable periodic orbits and, around them, quasiperiodic Kolmogorov-Arnold-Moser (KAM) tori form regions of regular motion in the phase space. These regions coexist with regions of chaotic motion. The situation is illustrated in Fig. 20 for the limaçon billiard (19) with $\varepsilon = 0.46$. Such mixed-phase-space systems are generic among all Hamiltonian systems and we focus on this type of nonlinearity. This is the typical case for billiards whose boundaries are defined by arbitrary (smooth) curves. Famous examples are

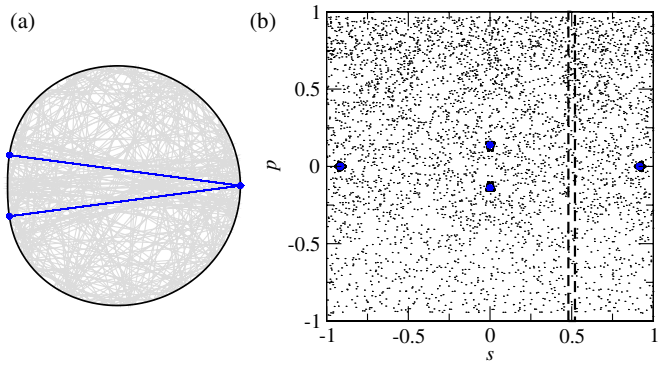

FIG. 20 (color online). Limaçon billiard defined by Eq. (19) with $\varepsilon = 0.46$. (a) Configuration space and (b) phase space of the closed billiard. The trajectory (V-shaped curve and •) is a stable period-4 orbit around which a KAM island exists. A chaotic trajectory is shown as gray lines in (a) and as black dots in (b). The dashed line in (b) indicates the leak used in Figs. 21 and 22.

the limaçon (Robnik, 1983) billiard for any $\varepsilon \neq 1$ in Eq. (19) and the annular billiard (Saito *et al.*, 1982).

The arguments above emphasize that the closed system is not ergodic: the phase space is divided in multiple independent components. One can imagine that the dynamics inside any chaotic component are described by the theory above. In reality, the situation is more involved because KAM tori are sticky surfaces that can be thought to affect trajectories in the surrounding chaotic component. Because of the smoothness of the dynamics, the local finite-time Lyapunov exponent close to the border of the KAM islands approaches zero (the Lyapunov exponent of the tori). A trajectory in the chaotic region that comes near some KAM surface wanders close to that surface for a long time before leaving it and showing intermittent bursts of chaos. This effect is called *stickiness* and the dynamics is said to be weakly chaotic (references are given Sec. V.B). Stickiness is typical in nonhyperbolic dynamical systems and can be thought of as a consequence of the vanishing local Lyapunov exponent in the sticky region. The independence of this effect from nonergodicity becomes evident by noting that even zero measure sets can lead to stickiness and weak chaos (e.g., the bouncing ball orbits discussed below).

When a leak is introduced in a mixed-phase-space system, only the ergodic components that intersect the leak will be affected. Here we focus on leaks placed in chaotic components and, accordingly, the estimations of the measure of the leak $\mu(I)$ has to be normalized by the measure of the chaotic sea $\mu(\Omega_{\text{chaos}})$. This usually involves estimating the measure of the regions of regular motion $\mu(\Omega_{\text{regular}})$ and subtracting from $\mu(\Omega) \equiv 1$ because typically $\mu(\Omega) = \mu(\Omega_{\text{chaos}}) + \mu(\Omega_{\text{regular}})$. Beyond this trivial correction accounting for the nonergodicity of the system, weak chaos and stickiness is manifested in the survival probability $P(t)$.

B. Decay of the survival probability in open systems

The most important effect of the presence of sticky regions on the survival probability $P(t)$ is that it modifies the asymptotic decay from exponential to power law $P(t) \sim t^{-z}$, where z is the algebraic decay exponent related to the properties of chaotic regions close to regular ones. This power-law scaling of $P(t)$ can be related to other observables such as Poincaré recurrences (Chirikov and Shepelyansky, 1984; Zaslavsky, 2002) (as in Sec. II.C), long-term correlations (Karney, 1983; Chirikov and Shepelyansky, 1984, 1999), $1/f$ spectrum (Geisel, Zacherl, and Radons, 1987), Lyapunov exponents (Kantz and Grassberger, 1987; Artuso and Manchein, 2009), and anomalous transport (Karney, 1983; Geisel, Zacherl, and Radons, 1988). The value $z = 2$ can be obtained analytically in leaking billiards with bouncing balls or marginally unstable (parabolic) periodic orbits (Gaspard and Dorfman, 1995; Altmann *et al.*, 2008), such as the Sinai (Bauer and Bertsch, 1990; Legrand and Sornette, 1990a; Fendrik and Sánchez, 1995; Kokshenev and Nemes, 2000), the stadium (Vivaldi, Casati, and Guarneri, 1983; Dumont and Brumer, 1992; Alt *et al.*, 1996; Armstead, Hunt, and Ott, 2004; Nagler *et al.*, 2007; Dettmann and Georgiou, 2009), the mushroom (Altmann, Motter, and Kantz, 2005; Tanaka and Shudo, 2006; Miyaguchi, 2007; Dettmann and Georgiou, 2011a), and other billiards (Fendrik and Wisniacki, 1997; Altmann *et al.*, 2008), and also for area-preserving maps with sharply divided phase space (Fendrik and Wisniacki, 1997; Altmann, Motter, and Kantz, 2006; Akaishi and Shudo, 2009). Even a single marginally unstable point in an area-preserving map can lead to stickiness (Artuso and Prampolini, 1998), allowing for a direct connection to one-dimensional (Pommeau-Manneville–type) intermittent maps (Artuso, Cavallasca, and Cristadoro, 2008). Stickiness also appears in higher-dimensional Hamiltonian systems (Ding, Bountis, and Ott, 1990; Fendrik and Sánchez, 1995; Altmann and Kantz, 2007). In area-preserving maps different stickiness scenarios can be distinguished (Zaslavsky, 2002, 2005), but there are examples of billiards with divided phase space for which stickiness is absent (Bunimovich, 2008). For the generic KAM scenario strong fluctuations are observed due to the presence of *Cantori* (Meiss, 1992) acting as a partial barrier to the transport of particles. The universality of z in the KAM scenario is an old problem that has not been completely solved despite different approaches and substantial advance in the last 30 years (Chirikov and Shepelyansky, 1984, 1999, 2002; Meiss and Ott, 1985, 1986; Weiss, Hufnagel, and Ketzmerick, 2002; Cristadoro and Ketzmerick, 2008; Venegeroles, 2009). The most recent results (Cristadoro and Ketzmerick, 2008) indicate the universal exponent to be $z \approx 1.57$.

Even if for long times the decay is expected to be power law due to the tori, there are interesting preasymptotic regimes of $P(t)$ for systems with mixed phase space. For very short times $t < t_s$, initial-condition and system-dependent fluctuations are typical and may play a predominant role in specific applications (Dumont and Brumer, 1992; Dietz, Friedrich *et al.*, 2006; Tanaka and Shudo, 2006; Grete and Markus, 2007; Altmann and Tél, 2008). Furthermore, when the leak is far away from any KAM tori and the chaotic component is large,[9] typical trajectories will exit before having the chance of approaching the KAM islands. These

[9]This situation is important in high-dimensional systems for which the measure of the regular regions decreases (but is still different from zero).

trajectories will experience an effective hyperbolic system and render an intermediate-time exponential decay as reported in different systems (Jung, Tél, and Ziemniak, 1993; Gaspard and Dorfman, 1995; Alt *et al.*, 1996; Kokshenev and Nemes, 2000; Zaslavsky, 2002; Altmann and Tél, 2008; Dettmann and Georgiou, 2009, 2011a).

Based on the different decay regimes discussed above, we can write the survival probability as (Altmann and Tél, 2008)

$$P(t) \approx \begin{cases} \text{irregular}, & \text{for } 0 < t < t_s, \\ ae^{-\kappa t}, & \text{for } t_s < t < t_z, \\ ae^{-\kappa t} + b(\kappa t)^{-z}, & \text{for } t_z < t, \end{cases} \tag{87}$$

where t_z corresponds to the time needed for the first trajectories to approach the sticky region, a/b is proportional to the ratio of the measure of the chaotic and of the regular components of the phase space, and t_s, t_z depend on the initial condition $\rho_0(\mathbf{x})$. Even if trajectories are started in the sticky region (see Sec. V.C), both power-law and exponential regimes are seen because for large chaotic components $ae^{-\kappa} \gg b\kappa^{-z}$. These regimes are clearly observable in the example of the limaçon billiard as Fig. 21 illustrates.

An actual crossover time t_{cross} between the exponential and the algebraic decay can be defined as (Altmann and Tél, 2008; Akaishi and Shudo, 2009)

$$ae^{-\kappa t_{\text{cross}}} = b(\kappa t_{\text{cross}})^{-z}, \tag{88}$$

which is the time when the contributions from the hyperbolic and the nonhyperbolic components are of *equal* importance.

We can easily estimate the dependence of the crossover time on the size of the leak $\mu(I)$ assuming that the ratio b/a depends at most weakly on κ for small $\mu(I)$. From Eq. (88) we obtain that (Altmann and Tél, 2008)

$$t_{\text{cross}} \sim 1/\kappa \sim 1/\mu(I). \tag{89}$$

A logarithmic correction to this relation was found by Akaishi and Shudo (2009) as $t_{\text{cross}} \sim 1/\mu(I) - [\log(\mu(I)) + 1]/\mu(I)$. For exact calculations and simulations in specific systems see also Kokshenev and Nemes (2000), Dettmann and Georgiou (2009, 2012), and Altmann, Leitao, and Lopes (2012). Taking this correction into account, after the usual rescaling of time $t \mapsto t\kappa$ and in the limit $\mu(I) \to 0$, we find that in the rescaled units $\kappa \to 1$ and $t_{\text{cross}} \to \infty$, i.e., the exponential decay always *dominates* $P(t)$. This provides an example of precise statements for infinitely small leaks that mask an interesting dynamical phenomenon (the power law) because for any finite leak a transition to power-law decay exists. Instead, here we do not apply any rescaling and discuss the dependence of the intermediate-time regimes in Eq. (87) on leak size and other parameters. Alternatively, one could take a different rescaling of time, e.g., $t \mapsto t\mu(I)/\log\mu(I)$, that would not suppress the crossover.

C. Dependence on the initial distribution

The connection between escape time in open systems and recurrence time in closed systems described in Sec. II.C remains valid for weakly chaotic systems as well. In particular, the intermediate-time decay of $P(t)$ in Eq. (87) appears in the (cumulative) distribution $P_r(T)$ of the Poincaré recurrence times T: $P_r(T) \sim P(t)_{t=T}$. With initial condition $\rho_r(\mathbf{x})$ (in the image of leak I taken with respect to $\mathbf{f}_{\text{closed}}$ as in Sec. II.C) the entire distributions coincide $P_r(T) = P(t)_{t=T}$. In area-preserving cases ρ_r is a uniform distribution over the image $\mathbf{f}_{\text{closed}}(I)$ of the leak.

The power-law exponent shows an important dependence on the initial condition $\rho_0(\mathbf{x})$. In fact, z in Eq. (87) characterizes "scattering" cases, i.e., situations in which the support of $\rho_0(\mathbf{x})$ is far away from KAM surfaces. For $\rho_0(\mathbf{x})$ inside the sticky region, arbitrarily close to KAM islands, the escape process—called a *transient chaos* situation (Pikovsky, 1992)—can be shown to be characterized by a survival probability P_{tr} for which

$$P_{\text{tr}}(t) \sim t^{-z_{\text{tr}}}, \quad \text{for large } t, \tag{90}$$

with a different decay exponent z_{tr}. As shown by Pikovsky (1992) and Meiss (1997) and explained below, z_{tr} is smaller than z with unit difference

$$z_{\text{tr}} = z - 1. \tag{91}$$

The impact of such a slower decay of the survival probability can be clearly seen in Fig. 21 since the support of ρ_r remains far away from KAM islands, but this is not the case for ρ_μ.

The similarity between a properly opened up dynamics and the Poincaré recurrences in the closed system can be used to explain the difference between the algebraic decay exponents z and z_r (Altmann, Motter, and Kantz, 2006). Consider first initial conditions touching the sticky region, the case of transient chaos, and examine the time a trajectory takes to escape to a region far away from the sticky region. The survival probability distribution $P_{\text{tr}}(\tau)$ is proportional to the natural measure $\mu(\tau)$ of the region of the phase space to which the trajectories stick for a time longer than τ. Because of ergodicity, we can write

$$P_{\text{tr}}(\tau) \sim \mu(\tau) = \frac{t_\tau}{t_{\text{total}}}, \tag{92}$$

where t_τ is the total time spent in the sticky regions (in events with recurrences time $T > \tau$) within the total observation time t_{total}; see Fig. 8.

For the recurrence problem with a single trajectory of length t_{total} initialized far away from the sticky region, the cumulative probability $P_r(\tau)$ to find recurrence times T larger than τ can be expressed as

$$P_r(\tau) = \frac{N_\tau}{N} \sim P(\tau), \tag{93}$$

where N_τ is the number of recurrences with recurrence times larger than τ and N is the total number of recurrences observed in the time interval t_{total}. The right-hand side expresses the above mentioned connection between recurrence and escape times. Since the total observation time can be estimated as N times the mean recurrence time $\bar{T}$ [Eq. (40)], we have $t_{\text{total}} \sim N\bar{T}$. Similarly, the total time t_τ spent inside the sticky region is approximately the number N_τ of recurrences with times longer than τ multiplied by τ: $t_\tau \sim N_\tau\tau$. As $\bar{T}$ is a constant, independent of τ, these allow us to write

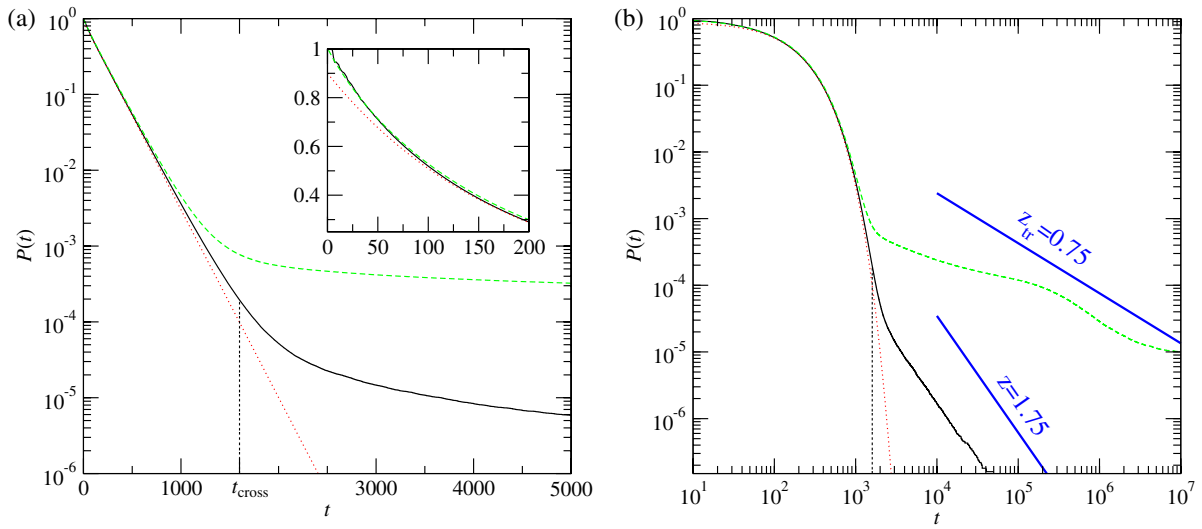

FIG. 21 (color online). Survival probability $P(t)$ inside the limaçon billiard depicted in Fig. 20 with a leak I centered around $s_l = 0.5$, $p_l = 0$ with $\Delta s = 0.05$, $\Delta p = 1$. Two different initial ensembles $\rho_0(\mathbf{x})$ are taken: $\rho_r(\mathbf{x})$ on the image of I (continuous lines), and $\rho_\mu(\mathbf{x})$ uniform in the chaotic component (the regions outside KAM tori) of the closed billiard (dashed lines). The exponential curve (dotted lines) fits $P(t)$ between times $1/\kappa$ and $2/\kappa$. (a) Log-linear representation; inset: magnification for short times. (b) Log-log representation. $P(t)$ decays with intermediate escape rate $\kappa \approx 0.0057(3)$, and with a power law $P(t) \sim t^{-z}$ for $t > t_{\text{cross}} \approx 1600$ [see Eq. (87)]. Straight lines with scalings $z = 1.75$ and $z_{tr} = 0.75$ are shown for comparison.

$$P(\tau) \sim \frac{N_\tau}{N} \sim \frac{t_\tau/\tau}{t_{\text{total}}/\bar{T}} = \frac{t_\tau \bar{T}}{t_{\text{total}}\tau} \sim \frac{P_{\text{tr}}(\tau)}{\tau}, \tag{94}$$

from which the shift of algebraic decay exponent by 1, Eq. (91), immediately follows from the asymptotics of Eqs. (87) and (90).

D. Hyperbolic and nonhyperbolic components of chaotic saddles

A theory based on invariant sets has to consider that in this case the chaotic saddle responsible for transient cases encircles KAM tori; moreover, it comes arbitrarily close to the tori (Lau, Finn, and Ott, 1991; Christiansen and Grassberger, 1993). The survival probability in Eq. (87) suggests that the invariant sets governing the temporal decay of weakly chaotic systems can be divided in hyperbolic and nonhyperbolic components (Jung, Tél, and Ziemniak, 1993; Fendrik, Rivas, and Sánchez, 1994). The intermediate-time ($t_s < t < t_z$) exponential decay is the manifestation of the hyperbolic component of the chaotic saddle, and the power-law decay, becoming observable for long times $t > t_{\text{cross}}$, of the nonhyperbolic component.

In Fig. 22 we show numerical approximations of the chaotic saddle and its unstable manifold in the hyperbolic and nonhyperbolic regimes. We employed the same procedures as used before for the case of strongly chaotic systems (see Appendix C), but varied the effective time t^* used in the simulation. For intermediate values of t^* the exponential decay dominates $P(t)$ in Eq. (87), and the obtained saddle and its unstable manifolds are disjoint from the region containing the KAM island and show the structure typical of hyperbolic systems. For large times $t^* > t_{\text{cross}}$ the asymptotic dynamics is governed by the nonhyperbolic regions, and the saddle and unstable manifold concentrate around the islands.

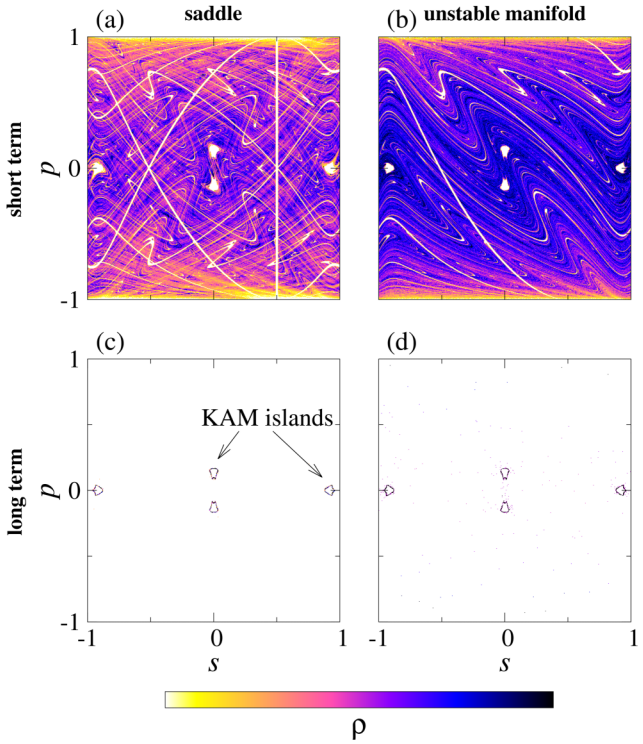

FIG. 22 (color online). (a), (c) Chaotic saddles and (b), (d) the corresponding unstable manifolds computed at different times t^* for the leaky billiard in Fig. 20. The color code indicates the phase-space density $\rho(s, p)$ and is valid for all panels. (a), (b) For short times $t^* \approx 1/\kappa \approx 175 < t_{\text{cross}} \approx 1600$ the hyperbolic component of the saddle is dominant and ρ exhibits the characteristic fractal or filamentary patterns (compare with Fig. 6). (c), (d) For long times $t^* \approx 2t_{\text{cross}}$ the nonhyperbolic component is dominant and the densities stick to the KAM islands responsible for the power-law decay in Eq. (87). See Sec. C for details on the simulation.

We assumed, as in Sec. II.B, that a single chaotic saddle exists. An interesting and nontrivial example that violates this assumption was reported by Dettmann and Georgiou (2011b) in the stadium billiard with two full leaks I_i at the boundary: I_1 in the flat and I_2 in the circular component of the billiard's boundary. With only one of these leaks, $P(t) \sim t^{-2}$ as reviewed in Sec. V.B. Consider now the survival probability $P_i^j(t)$ of particles that start in leak i and leave through leak j ($i = j$ corresponds to a reflection survival probability and $i \neq j$ to a transmission survival probability). From the four $P_i^j(t)$ in the example above, only $P_1^1(t)$ shows the expected power-law tail. $P_1^2(t)$, $P_2^1(t)$, and $P_2^2(t)$ decay exponentially. This surprising result is a consequence of the sticky region due to the parallel walls in the stadium billiard, which cannot be approached from all positions of the phase space if a leak is placed along these parallel walls. More generally, this example shows that the ergodicity of the closed system is not automatically transferred to the leaky system.

An interesting effect beyond the results of this paper was reported by Custódio and Beims (2011): the shape of the leak (rounded, squared, etc.) introduced at the border of the billiard can modify the dynamics of the billiard (e.g., create sticky or chaotic motion). Similarly, openness in optical systems can lead to a modification of the dynamics of the reflected rays due to nonspecular reflection close to the angle of total internal reflection (Schomerus and Hentschel, 2006; Altmann, Del Magno, and Hentschel, 2008; Song *et al.*, 2010). Here we consider only leaks for which the trajectory either escapes or is reflected as in the closed system.

Finally, we discuss further examples which go beyond the setup considered in this section. In integrable cases, leaks (or recurrence regions) in billiards (Bauer and Bertsch, 1990; Vicentini and Kokshenev, 2001; Bunimovich and Dettmann, 2005) and maps (Buric *et al.*, 2003) lead to a power-law decay of $P(t)$ with $z = 1$. This is due to stickiness caused by families of marginally unstable periodic orbits (e.g., parallel walls) and is consistent with Eq. (91) since there is no chaotic region and hence all initial conditions are close to sticky regions. Leaks placed inside regular islands will lead to similar observations. Leaks (or recurrence regions) centered in periodic orbits have been considered by Hu *et al.* (2004). For leaks centered at the border of regular and chaotic regions, a weighted sum of exponential and power-law escapes was found by Buric *et al.* (2003). A similar composition was also reported by Vicentini and Kokshenev (2001) and Kokshenev and Vicentini (2003) for the case of leaking polygonal billiards, which are neither integrable nor chaotic. Dettmann and Leonel (2012) and Leonel and Dettmann (2012) reported a decay of survival probability with a stretched exponential $P(t) \sim \exp(-\alpha t^{\beta})$ when a leak is introduced in the open bouncer model (vibrating billiard), which exhibits mixed phase space and Fermi acceleration in the closed version.

VI. APPLICATIONS

We now present different applications for which the results of the previous sections are relevant to understand the specific phenomena and observations. Accordingly, the models discussed intend to capture the essential dynamical aspects of the system but do not intend to describe all details of a given experimental configuration. The extent to which dynamical systems provide an appropriate description of reality has been the subject of discussion in the context of wave dynamics for a long time. For instance, in acoustics the dynamical-systems description corresponds to the ray approach, which has been repeatedly debated (Joyce, 1975) but systematically used nevertheless. Two recent advances that confirm the validity of the ray picture are (i) the derivation of Sabine's law in the wave picture (Legrand and Sornette, 1991b; Dennis, 2010), and (ii) the recognition of the relevance of classical periodic orbits in room acoustics (Berry, 2010). Similar considerations involving ray and wave pictures apply to the quantum and optics applications below, while the astronomy, fluids, and plasma applications also have simplifying assumptions and regimes of validity of their own.

A. Planetary astronomy

Chaotic systems with leaks might play a role in one of the most traditional problem of celestial mechanics, the three-body problem (three masses interacting through gravitational forces). This has been noted in Bleher *et al.* (1988) and explored in detail for particular cases in Nagler (2002, 2004, 2005). The most natural leakage mechanism corresponds to collisions of the finite-size celestial bodies, a realistic possibility even in our Solar System (Laskar and Gastineau, 2009).

The simplest case discussed by Nagler (2004) corresponds to two main bodies with equal mass M moving along the same circle around their center of mass, and a test body of mass $m \ll M$ (circular restricted three-body problem). In the corotating reference frame centered at the center of mass, this problem can be described by a four-dimensional time-independent system. By using the conservation of energy and employing a suitable Poincaré surface of section, one can reduce the dynamics to a two-dimensional discrete-time problem, as the billiard systems considered here. For a fixed energy, confined trajectories coexist with trajectories that escape to infinity. The system is nonintegrable, with regular and chaotic trajectories coexisting in the phase space.

Leakage is introduced by considering that the masses of the two main bodies are not concentrated in a point and therefore collisions occur whenever the pointlike test particle approaches one of the bodies to a distance $r < R$, where R is the radius of the main bodies (the velocity can be arbitrary). The size of the leak in the configuration space is proportional to the radius R of the main bodies, and the position of the leak is given by the positions of the main bodies, which is fixed in the corotating frame. This situation corresponds to the problem of systems with more than one coexisting leak discussed in Sec. IV.B. In fact, at a given energy, particles can also go to infinity; therefore here there are two leaks in an otherwise open system. Figure 23 illustrates how the basin of escape to infinity and the basin of collision with each of the main bodies varies as a function of the leak size R. The typical fractal-like structures observed in Fig. 16 are clearly seen and coexist with smooth boundaries (Nagler, 2004). Nagler (2005) extended this analysis to the case of different masses and different circular orbits for the main bodies.

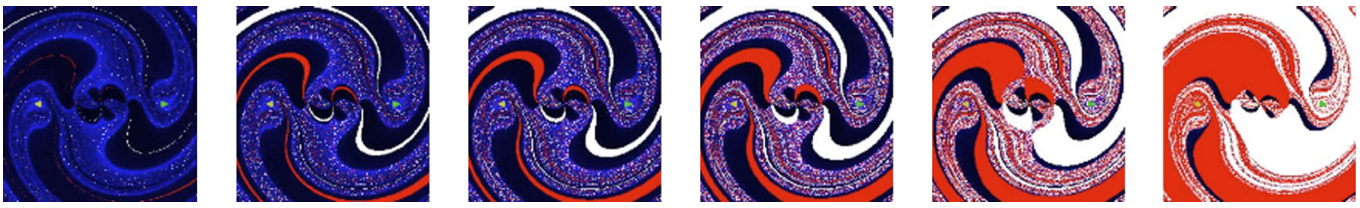

FIG. 23 (color online). The configuration space of the small body in the restricted three-body problem in a frame corotating with the main bodies. This section of the phase space is obtained at a fixed energy under the condition that the particle's velocity toward the origin vanishes, and the angular velocity is negative. The colors correspond to trajectories colliding with main body 1 (white), colliding with main body 2 (gray), and escape to infinity (dark to light, from short to long escape times). From left to right the diameter of the two main bodies is increased, which corresponds to increasing the size of the leaks (not visible in this section) and the collision probability. From Nagler, 2004.

B. Hydrodynamical flows

The advection of tracer particles in hydrodynamical flows represents an important application of dynamical system's theory. Since molecular diffusion is typically negligible on the relevant time and length scales, the equation of motion for an idealized particle of zero size and zero mass expresses the fact that the particle velocity $\dot{\mathbf{r}}$ coincides, at any instant of time, with the flow velocity $\mathbf{u}(\mathbf{r}, t)$. The velocity field is assumed to be known and the advective dynamics is thus described by

$$\dot{\mathbf{r}}(t) = \mathbf{u}[\mathbf{r}(t), t]. \tag{95}$$

The solution to this differential equation is the path $\mathbf{r}(t)$ of the particle.

Chaos is typical in two-dimensional time-dependent flows and in any kind of three-dimensional flows, leading to the phenomenon of *chaotic advection* (Aref, 1984). Indeed, the main physical mechanism for fluid stirring is advection, whose efficiency can be greatly enhanced by chaotic dynamics. The spreading of pollutants on large scales is also dominated by advection. Potential applications of chaotic advection thus range from laboratory investigations of fluid dynamics to the study of large-scale environmental flows, and these aspects are well reviewed in the literature (Ottino, 1989; Aref and Naschie, 1995; Lai and Tél, 2011).

The existence of a leak in a flow implies a sink for fluid elements. In such cases the amount of fluid in a finite container is decreasing in time, and this leads to a qualitative change of the dynamics sooner or later. Here we focus on a less evident, but physically more appealing, realization of leaking dynamics, which is related to advected particles and to the first arrival to certain regions of the flow. The problem of reactions in fluid flows provides an interesting example. Reactive particles have typically no considerable influence on flow; therefore the velocity field remains the same $\mathbf{u}(\mathbf{r}, t)$ as without reactions. The reactive dynamics, represented, e.g., by a temporal change of certain particle properties, is thus superimposed on the advection problem (95). The change might happen upon entering a region of the flow. The most important examples of activities in flows involve chemical (e.g., $A + B \rightarrow C + D$) and biological (e.g., $A + B \rightarrow 2A$) reactions. The combination of reaction and advection provides a realistic model for a plethora of applications (Tél *et al.*, 2005; Neufeld and Hernández-Garcia, 2009). Next we discuss two particular problems in which leaking is introduced in a closed hydrodynamical flow by allowing particles to enter or also react in preassigned fluid regions (that play the role of leaks).

1. Spreading of pollutants in the environment

Imagine that a pollutant is released in an observation region within a water basin. A typical problem in the prevention of environmental pollution is to determine which coastal region the pollutant will be advected to so that one can estimate which parts are most likely to be affected by the pollution release. This is one particular example of the general problem of partitioning the initial conditions in an observation region of a closed flow according to the first arrival of advected particles to predetermined subregions of interest. The boundary between the different partitions typically shows fractal patterns that correspond to the *stable manifold* of the chaotic saddle formed by tracers that never reach any of the target regions. The target regions act as leaks for the dynamics of the tracers [following Eq. (95)], but not for the velocity field $\mathbf{u}(\mathbf{r}, t)$.

Figure 24 shows an example in a square-shaped wind-driven lake of 4 km^2. The boundaries are vertical walls of height 2 m, and below this depth the lake has a pyramidal form with the deepest point at a depth of 2.5 m in the middle. The water flow is generated by wind stress. A similar problem was studied by Károlyi *et al.* (2010) by applying a shallow-water approximation in which layers of different depths are assumed to move in a synchronized manner. In Fig. 24 the flow is obtained from a numerical solution of the hydrodynamical equations in three dimensions (Cioffi, Gallerano, and Napoli, 2005). A wind of strength 12 m/s changes periodically in time, with a period of $T = 8$ h. It blows from the southwest (lower left corner) for $T/2$, changes abruptly to the southeast, and after an interval of length $T/2$ it changes back again, etc.

The region of observation is the full lake area outside narrow bands along the coasts. Layers at different depths are investigated. Each point in a layer is colored according to which of the coastal bands (of width 100 m and height 2 m) along the four vertical walls at the shores will be reached by the tracer first (the vertical coordinate of the first arrival is not recorded). The results in Fig. 24 indicate a strong height dependence. In the uppermost layer, pollutants released in the lake are most dangerous for the northern shore (Szanyi, 2012). The western shore is somewhat less polluted than the eastern one. The southern coast is hardly affected. This is consistent with the fact that the average wind direction is southerly, and particles are thus

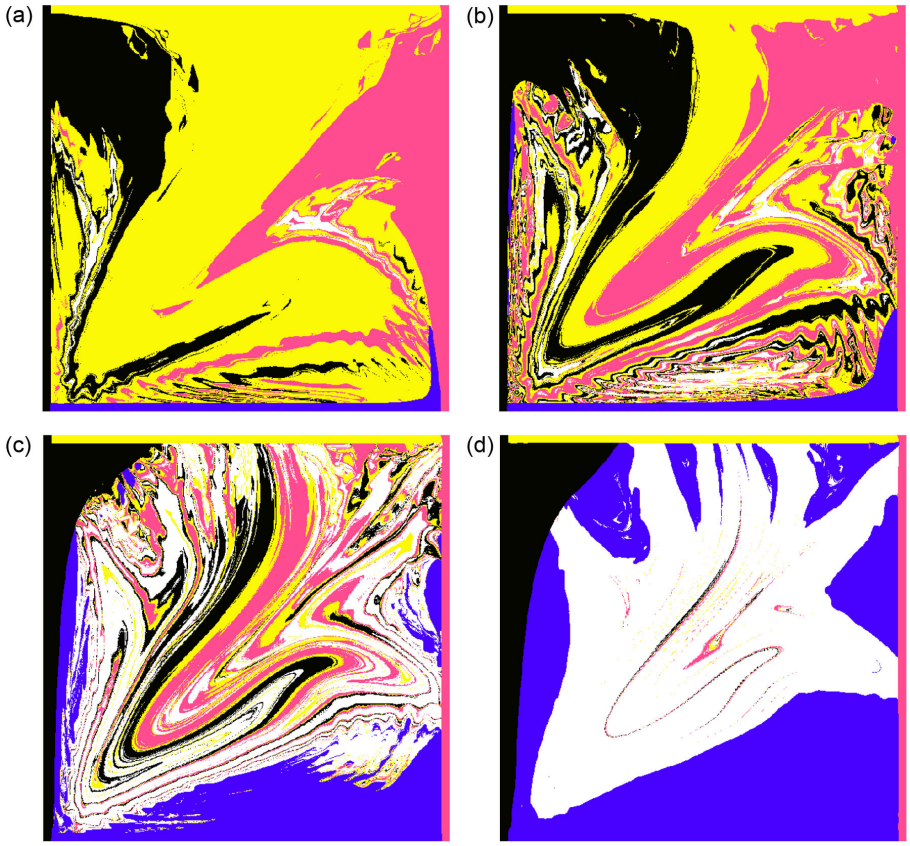

FIG. 24 (color online). Spreading of pollutants in a model of a wind-driven lake. The wind field is periodic with period T. Positions x, y are colored according to which of the four coastal regions (bands along the boundaries, also colored) a tracer starting with initial condition x, y [at time $t = 0$ (mod$T$)] is advected to. Tracers that do not reach any of the bands along the shores over 60 h of observation are colored white. (a)–(d) represent layers at depths 0.7, 1.0, 1.3, and 1.6 m. Picture by S. Szanyi.

pushed mainly northward. Considerable deviations from this pattern occur when going to deeper and deeper layers. The pollution of the northern coast is becoming less and less strong, while the southern one becomes heavily polluted. This is due to the development of an overturning circulation that has an overall southward component in the deeper regions. The hazard for the four shores thus strongly depends on the level in which pollution is released. The boundaries between different colors contain the stable manifold of a three-dimensional chaotic saddle residing in the region of observation. The main result obtained from this example is that a two-dimensional shallow-water approximation might lead to an oversimplification of the three-dimensional flow and also of the advection patterns since the observed height dependence in the pollutant distribution cannot appear then.

2. Reactivity in flows, resetting

Perhaps the simplest model of reactions is provided by what was invented and called by Pierrehumbert (Ngan and Pierrehumbert, 2000) as the *resetting mechanism*. Whenever a tracer enters a preselected region of the flow, a given property of the tracer such as concentration (or color) is reset to a value associated with that region, regardless of its previous value (Neufeld, Haynes, and Picard, 2000; Matyas and Gaspard, 2005). This mimics a situation where dye is introduced by diffusion from a solid surface and is maintained at the saturation concentration in a diffusive boundary layer. An atmospheric example of the resetting mechanism is provided by the dynamics of water vapor. Water vapor is removed from an air parcel whenever it enters a region where the local humidity is lower than that of the parcel. Its humidity is then reset to this lower value and the difference is rained out. When a parcel of low humidity comes into a humid region (typically close to the Earth's surface), its water vapor content is reset to a high value. The water vapor distribution in the atmosphere is similar indeed to the ones obtained from resetting models (Pierrehumbert, Brogniez, and Roca, 2007). As in the example of Sec. VI.B.1, the leaking mechanism always refers to the particles of a given type (color), and not to the fluid, as fluid is never lost from the system.

In two-dimensional incompressible flows $\boldsymbol{\nabla} \cdot \mathbf{u} = 0$, and the advective dynamics (95) is area preserving. The resetting problem provides thus a close analog of a leaky 2D billiard. Chaotic advection in closed flows is characterized by space-filling chaos, and correspondingly by space-filling stable and unstable manifolds. Nonhyperbolic regions might also exist around KAM tori. The resetting mechanism reveals the foliations of the dynamics, in a similar spirit as a leak, because in both cases a particle can be considered to be lost after entering a preselected region. The advective dynamics with the leak is typically transiently chaotic. Particles never escaping the complement of the leak(s), both forward and backward in time, form a chaotic saddle. The manifolds of this saddle are

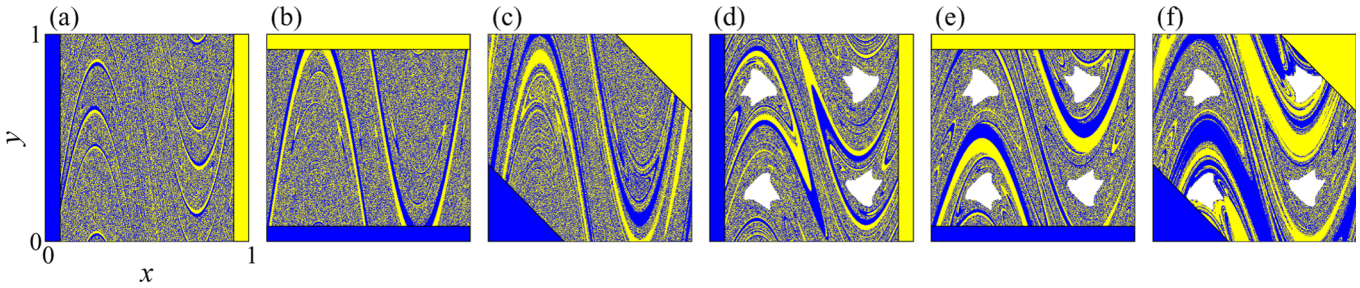

FIG. 25 (color online). Tracer distributions with resetting in a closed time-periodic flow. The particles' color (concentration) is set to dark and light at two resetting bands with total area 0.14 placed (a), (d) vertically, (b), (e) horizontally, and (c), (f) as a triangle at the corners. In the full phase space the two colors come arbitrarily close to each other along a filamentary pattern. In (a)–(c) the bands foliate a strongly chaotic flow, while in (d)–(f) the fluid flow is slower and KAM islands (white) appear outside the resetting regions. Data by G. Drótos.

subsets of the closed system's manifolds since the advective dynamics outside the leak is exactly the same as in the closed system.

With two or more resetting regions, tracers of different concentrations or different colors come close to each other along fractal-like boundaries. An example is shown in Fig. 25 where the flow is chosen as the alternating sinusoidal shear flow model (Pierrehumbert, 1994). The dark (light) dots are obtained as initial conditions of trajectories reaching the dark (light) region when iterated *backward* in time. Particles close to the boundary have long lifetimes outside the resetting regions and therefore they come close to the saddle in the time-reversed dynamics. The boundaries trace thus out here the *unstable* manifold of the chaotic saddle. The resetting pattern is a fingerprint of the chaotic saddle underlying the leaking advection dynamics, where the leak is the union of the resetting regions. Figures 25(a)–25(c) show that resetting regions of the same area lead to different patterns and also to different average lifetimes in full agreement with what we saw for strongly chaotic billiards in Sec. IV. Figures 25(d) and 25(e) represent a case where the average fluid velocity is smaller and four elliptic islands appear with a nonhyperbolic component of the chaotic saddle around the outermost KAM tori.

Resetting-like methods have been applied to visualizing the foliations of three-dimensional model flows (Tuval *et al.*, 2004) and they also have applications in geophysics (Schneider, Fernández, and Hernández-Garcia, 2000; Schneider, Schmalzl, and Tél, 2007).

C. Magnetic confinement of plasma

The research on plasma confinement devices in the last 60 years has been driven by the expectation of designing controlled fusion reactors. One of the best studied and most promising strategies is to use magnetic confinement machines with toroidal shape as illustrated in Fig. 26. These machines are called tokamaks. Here we describe the dynamics in lowest order approximation only, when the charged particles follow the magnetic field lines while being within the tokamak (Wesson, 1987). A chaotic layer at the border of the plasma is long known to enhance the confinement of particles to the core. This enhancement is accomplished by controlling plasma wall interactions in the tokamak (Engelhardt and Feneberg, 1978). Chaos is present whenever the ideal toroidal symmetry is broken, which can be achieved by generating weak electric currents along the toroidal vessel via the so-called *ergodic magnetic limiters* shown in Fig. 26 (left). In any specific tokamak the wall is fixed and the efforts to control plasma wall interactions concentrate on manipulating the magnetic structure at the plasma edge (Schmitz, 2012).

Here we are interested in the dynamics of the magnetic field lines and of the charged particles. These lines are divergence free and thus correspond to trajectories of volume preserving flows. They can therefore be described by time-dependent Hamiltonian systems where, for the tokamak geometry, the toroidal angle Φ of the trajectories corresponds to the time variable of the flow and slices of them can be described by area-preserving maps (Morrison, 2000).

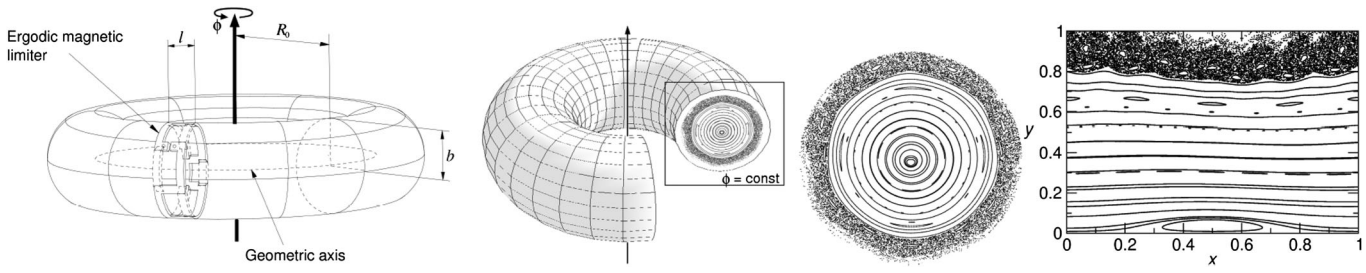

FIG. 26. Construction of an area-preserving map of the magnetic field lines in a tokamak. From left to right: main geometrical parameters of a tokamak with an ergodic magnetic limiter, a torus in which the magnetic field lines are confined, and the surface of a section at fixed toroidal angle Φ used to construct the discrete-time map. Black dots on this map represent field line trajectories with many iterates confined to the torus. They correspond to long-lived charged particles. Trajectories are shown both in polar $(\mathfrak{r}, \theta)$ and in rectangular coordinates $(x = \theta/2\pi, y = \mathfrak{r}/b)$.

Figure 26 illustrates the steps that map the magnetic field line dynamics into a discrete map between two successive intersections with the Poincaré surface of section with fixed toroidal angle Φ; see Portela, Caldas, and Viana (2008) for a recent review. Iterations in these maps correspond to toroidal turns and are thus proportional to the magnetic field line length. The connection to systems with leaks is established by noting that the evolution of the particles is interrupted at the vessel's wall and at any obstacle inside the tokamak chamber, like probes and antennas. Here we concentrate on the main loss of particles in tokamaks, which is due to collisions with the chamber's wall located at $y = 1$. Although being ideally mainly confined to the torus, the magnetic field extends outside the tokamak wall as well. The chaos in the field lines is thus not limited to $y \leq 1$. For the charged particles, it is therefore essential to consider a modified map in which the wall acts as a leak of the field line map. Since the wall can be considered to not affect the magnetic field lines, the particle map is identical to the field line map but is restricted to $y \leq 1$. Even if the position of the leak in a map is fixed at $y = 1$, it can effectively be controlled by changing other control parameters of the map. For instance, in Fig. 26 this could be achieved by choosing a different wall position (parameter b) or current in the ergodic magnetic limiter.

The asymptotic particle dynamics of the leaky system is governed by a chaotic saddle and its manifolds. Figure 27 shows an approximation of the corresponding invariant sets for the so-called Ullmann-Caldas map (Ullmann and Caldas, 2000), based on the manifolds of a single fixed point embedded into the chaotic saddle (Portela *et al.*, 2007. From the results of Sec. IV we conclude that for more general situations the invariant sets depend sensitively on the particular choice of the leak. Viana *et al.* (2011) provided a detailed review of the role of the chaotic saddle and fractal structures in plasma confinement devices. We emphasize that the chaotic saddle is nonhyperbolic due to the presence of KAM islands, as discussed in Sec. V.

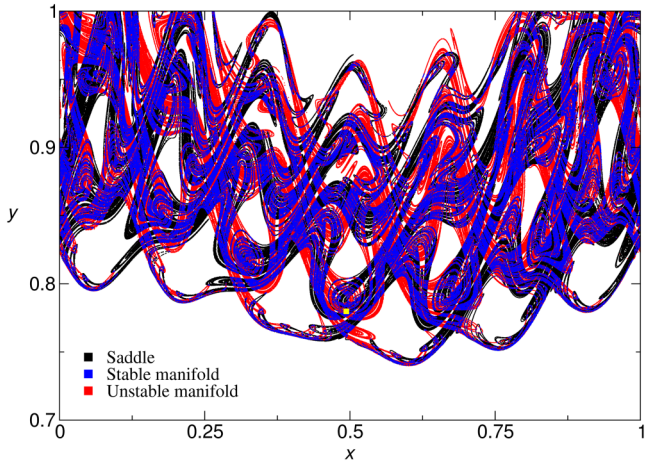

FIG. 27 (color online). The saddle, stable, and unstable manifolds in the Ullmann-Caldas tokamak map. The coordinates x, y are as in Fig. 26. The (stable) unstable manifold was obtained as the 80th (pre-)image of a small ball of initial conditions around the unstable periodic point indicated as a small square at $\sim(0.49, 0.78)$. The intersection of both manifolds approximates the chaotic saddle for the leaky particle dynamics. The intersection of the manifolds with the line $y = 1$ can be considered as "footprints" on the wall. From Portela *et al.*, 2007.

Experimental signatures of the invariant sets of the leaking dynamics appear in the heat flux into the tokamak's wall (Evans, Moyer, and Monat, 2002; da Silva *et al.*, 2002; Wingen *et al.*, 2007; Viana *et al.*, 2011). It was noticed that the heat flux is not uniform in the poloidal angle (proportional to x in Fig. 26) (Shen *et al.*, 1989; Takamura *et al.*, 1989). Apart from the dispersion caused by collisional effects (Schelin *et al.*, 2011), the charged particles leave the system closely following the unstable manifold of the chaotic saddle of the leaky system and are deposited at the positions where this manifold intersects the wall. Such lines survive for a long time and reach deeper inside the torus (hot plasma) (Abdullaev, Eich, and Finken, 2001). Note that the plasma current in the Φ direction implies that particles with different electrical charge follow the magnetic field lines in opposite directions. Recalling that time corresponds to the length of the magnetic field lines, we see that this implies that while the positively charged particles escape following the unstable manifold,

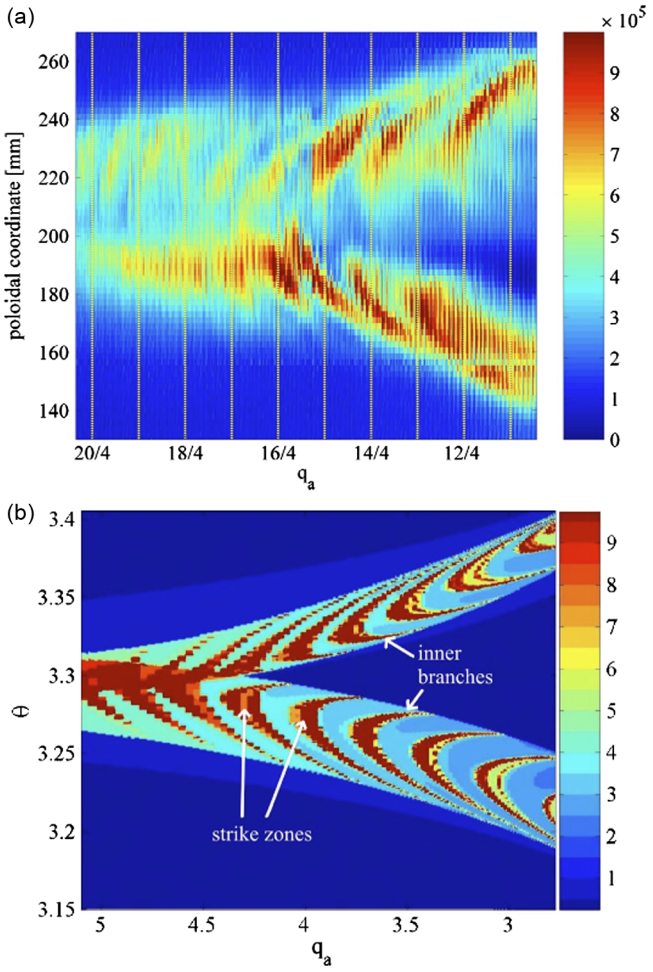

FIG. 28 (color online). Comparison between experimental and numerical results for the heat flux pattern in tokamaks. Upper panel: Experimental measurements of the heat flux (color scale) through different poloidal coordinates (proportional to x in Fig. 26) shown for different edge safety factors q_a. Lower panel: Numerical simulations indicating the length (in toroidal turns) of the field lines that hit the tokamak wall vs q_a. From Wingen *et al.*, 2007.

the negatively charged particles follow the stable manifold of the same chaotic saddle. Altogether, this reasoning predicts that the heat flux at the wall should be enhanced at the position of the intersection of these manifolds with the wall and thus be proportional to the length of the magnetic field lines within the tokamak. Figure 28 shows experimental and numerical results that confirm this prediction. In the upper panel the concentration of the heat flux in specific poloidal angles is shown for different edge safety factors q_a, a control parameter that is inversely proportional to the plasma current. In the lower panel we observe that the same patterns are observed in the length of the field lines.

Here, again, similar to the advection and resetting problem, we have a chance to see a direct fingerprint of transient chaos in the configuration space, since the phase space and the configuration space coincide in both cases.

D. Optical microcavities

Optical microcavities are used in applications ranging from dynamic filters in optical communications to quantum electrodynamics [see Vahala (2003) for a review]. Here we focus on the case of optical microcavities used as lasers. Besides the practical applications, these cavities allow for fundamental scientific investigations (e.g., in quantum chaos) in systems in which only partial leaks are present. An example of an optical microcavity is given in Fig. 29 from Shinohara *et al.* (2010, 2011), a system used here to illustrate the achievements of the last 15 years of intense research (Nöckel and Stone, 1997; Lee *et al.*, 2004; Schwefel *et al.*, 2004; Ryu *et al.*, 2006; Tanaka *et al.*, 2007; Wiersig and Hentschel, 2008; Altmann, 2009; Dettmann and Georgiou, 2009; Yan *et al.*, 2009; Harayama and Shinohara, 2011).

The connection to leaking chaotic systems is based on the observation that the shape of the microlaser matters: while the regular trajectories present in spherical and circular shaped cavities provide the good confinement necessary for lasing (high-Q modes), deformation of these geometries leading to chaotic dynamics (Mekis *et al.*, 1995; Nöckel and Stone, 1997) can add to the good confinement of other desired properties such as the directionality of the emission (Nöckel and Stone, 1997; Gmachl *et al.*, 1998; Liu and Lai, 2002; Schwefel *et al.*, 2004; Lebental *et al.*, 2007; Tanaka *et al.*, 2007; Wiersig and Hentschel, 2008; Dettmann and Howard, 2009; Song *et al.*, 2009; Yan *et al.*, 2009). Even if these systems are often far from the limit of vanishing wavelength (geometrical optics), the so-called ray-wave correspondence applies in a surprisingly large number of cases; see Harayama and Shinohara (2011) for a recent review. A description based on rays makes robust numerical simulations possible and provides intuitive interpretations of experimental observations that can be directly connected to orbits and the geometry of the corresponding billiard.

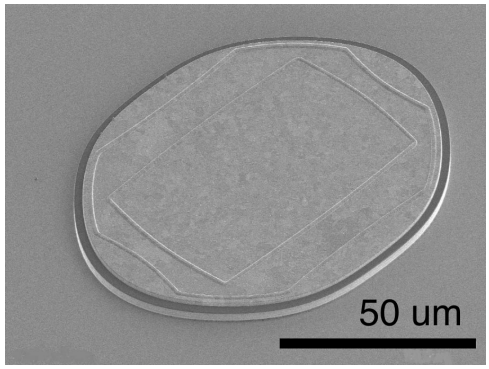

FIG. 29. Scanning electron microscope image of a microlaser with deformed-disk shape. From Shinohara *et al.*, 2010.

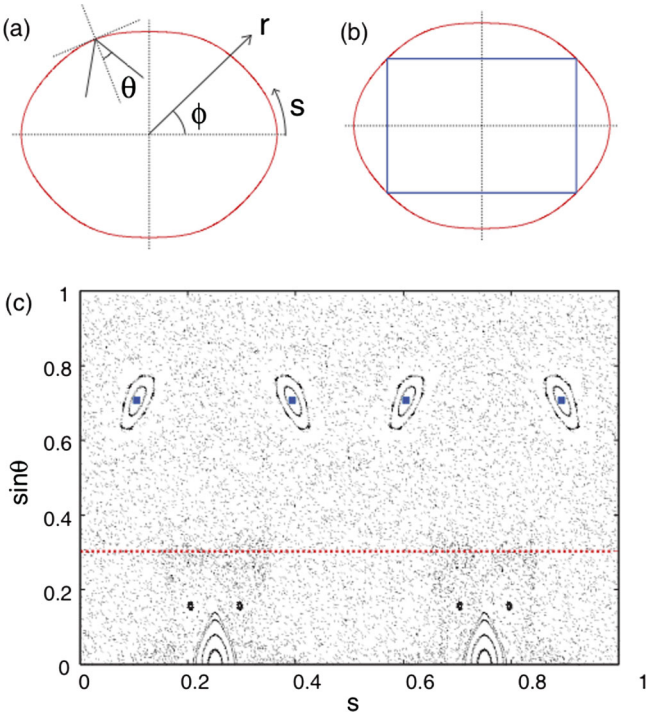

FIG. 30 (color online). Ray model of the microlaser depicted in Fig. 29. (a) Definitions of the coordinates. (b) A stable periodic orbit. (c) Phase space of the closed billiard. The upper edge of the partial leak is indicated by the dashed (horizontal) line in (c). From Shinohara *et al.*, 2011.

The ray model in optical cavities is equivalent to the dynamics in closed billiards with partial leaks. Figure 30 shows the phase space of the system used by Shinohara *et al.* (2010, 2011). As mentioned in Secs. I.E and II D, the partial leak has a natural physical origin in the collisions inside the cavity (with refractive index $n_{\text{in}} > n_{\text{out}} \equiv 1$). Rays with angles smaller than the critical angle of total internal reflection [$p < p_c = \sin\theta_c = 1/n_{\text{in}}$, dashed line in Fig. 30(c)] are partially transmitted (with angles given by Snell's law) and partially reflected. The intensities of the reflected and transmitted rays are given by Fresnel's law (Nöckel and Stone, 1997; Lee *et al.*, 2004; Schwefel *et al.*, 2004; Ryu *et al.*, 2006; Tanaka *et al.*, 2007; Altmann, 2009; Harayama and Shinohara, 2011). For rays with $p > p_c$ no transmission takes place.

Interestingly, limaçon shaped microlasers such as the ones used in the main part of this review have also been used in experiments and simulations (Wiersig and Hentschel, 2008; Shinohara *et al.*, 2009; Song *et al.*, 2009; Yan *et al.*, 2009). An important additional aspect of lasing cavities is the gain medium that continuously pumps energy into the system enhancing the intensity of long-living trajectories (a precise modeling of this effect is beyond our scope). For corrections

to the ray model due to wave effects, see Schomerus and Hentschel (2006) and Altmann, Del Magno, and Hentschel (2008).

The main relevant observable is the far-field emission intensity, as computed in Fig. 17 (see also Sec. IV.C). A comparison between experimental results and ray-dynamics simulations is presented in Fig. 31. The agreement is remarkable, in particular, if one takes into account that the system is far from the formal semiclassical limit of small wavelength; see Shinohara *et al.* (2010, 2011) and Redding *et al.* (2012) for further evidence of the robustness of ray results. The important and somehow surprising aspect of the emission in Fig. 31 is the concentration of the emission in specific directions, even if the leak lies in a region where the closed system is more or less uniformly chaotic.

The specific directions of emission have been explained using the unstable manifold of a single unstable periodic orbit close to the border of the leak region, first by Schwefel *et al.* (2004). Another important theoretical development was the proposal of the existence of a so-called quasistationary energy distribution in the classical ray dynamics; see Lee *et al.* (2004) and Ryu *et al.* (2006). As noticed by Altmann (2009), and better explained in Secs. II D and III, these two important concepts can more generally be expressed, respectively, as the unstable manifold of the chaotic saddle (which aligns with the unstable manifold of specific periodic orbits) and the c measure distributed along it. In as much as the ray model provides a good description of the laser, these two key concepts of the theory of dynamical systems have direct observable consequences for the far-field emission of lasing microcavities. Here the results of Sec. V have to be taken into account because microlasing cavities are typically not strongly chaotic (Liu and Lai, 2002). The main effect of weak chaos is that the long-living modes (high-Q factors) are usually concentrated inside KAM islands and regions of regular motion. It remains to be seen to what extent the effect of weak chaos described in Sec. V can be detected experimentally.

Recent developments show links to many other results discussed in this review. For instance, while dielectric microcavities have leaks restricted in the p direction, recent experiments use waveguides that restrict the leak also in the other direction. Additional leaks are constructed around positions s_l that showed to be efficient in *channeling* the rays out of the cavity (Redding *et al.*, 2012; Song *et al.*, 2012). Such coexistence of different leaks was discussed in Sec. IV.B. Another example is the periodic-orbit formula for the resonance spectrum of dielectric cavities proposed by Bogomolny, Dubertrand, and Schmit (2008) and experimentally verified in regular (Bittner *et al.*, 2010) and chaotic (Bittner *et al.*, 2012) systems. The main novelty in this formula is the incorporation of partial leakage as a multiplicative term proportional to the product of the reflection coefficients at collisions along periodic orbits, in a similar manner as the reflection coefficient appears in the operator (74).

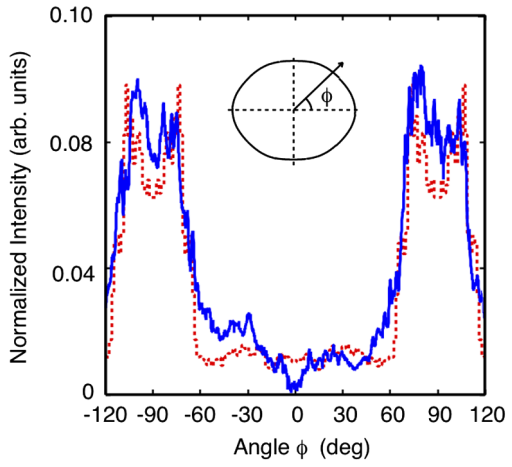

FIG. 31 (color online). Far-field emission observed experimentally (solid line) and predicted by the ray model (dashed line). From Shinohara *et al.*, 2011.

E. Quantum and wave chaos in systems with leaks

The quantum and wave analogs of classically chaotic systems with leaks appear in theoretical analyses, controlled experiments, and real-world systems. Quantum mechanically, the major differences to closed systems originate from the non-Hermitian Hamilton operator (nonunitarian scattering matrix). The intrinsic openness of any quantum mechanical experiment, highlighted in a quote from the early 1990s in Sec. I, has already been fully discussed (Stockmann, 1999). Still, an important question influencing the research in quantum and wave chaos in the last decade was the effect of openness on results known for closed systems. A driving force are experiments in quantum dots, microwaves, optics, acoustics, etc. These more recent developments appear in essays on open quantum systems: Kuhl, Stöckmann, and Weaver (2005) reviewed spectral and scattering properties with a focus on classical waves (microwaves and sound waves); Fyodorov, Savin, and Sommers (2005) used a formalism based on correlation and distribution functions that goes beyond random matrices; Rotter (2009) used a Feshbach projection operator formalism to non-Hermitian Hamiltonian operators; Nonnenmacher (2011) reviewed the mathematical results and methods of semiclassical theories of wave operators in scattering systems; and Novaes (2012) gave an overview of the properties and recent research on the eigenstates of leaky quantum-chaotic maps.

The results of these review papers are to a great extent valid for scattering systems in general, with the main distinction being between, as they call, "weak and strong absorption" (coupling to the environment). Throughout we distinguished leaking from genuinely open systems based on the key elements: (i) the possibility of comparing the results to a closed-system and (ii) the control over properties of the leak (see Sec. I.A). These two elements affect spectral properties, which were recently observed in experiments (Barthélemy, Legrand, and Mortessagne, 2005; Dietz, Heine *et al.*, 2006; Xeridat *et al.*, 2009) and fully analyzed theoretically (Savin, Legrand, and Mortessagne, 2006; Poli *et al.*, 2009). Point (i) is used, for instance, when the universal distribution of nearest neighbor levels observed in strongly chaotic closed systems (Stockmann, 1999) is compared to the results obtained in leaking systems (Poli, Luna-Acosta, and Stöckmann, 2012). Point (ii) is related to the importance of the localization of the leak or perturbation in the phase space,

a recent observation that was summarized by Savin, Legrand, and Mortessagne as

> Open wave-chaotic systems in the presence of energy losses (absorption) are nowadays under intense experimental and theoretical investigations.... Most of the works concern the case of uniform absorption which is responsible for homogeneous broadening $\Gamma_{\rm hom}$ of all the modes (resonance states). However, in some experimentally relevant situations... one should take into account also localized-in-space losses which lead to an inhomogeneous part $\Gamma_{\rm inh}$ of the widths which varies from mode to mode (Savin, Legrand, and Mortessagne, 2006).

The use of antennas and measurement devices typically fulfills properties (i) and (ii) mentioned above.

Next we focus on three measurable properties of quantum systems which can be directly connected to classical properties and the main results of this paper.

1. Loschmidt echo (fidelity)

The absence of well-defined trajectories in quantum mechanics makes it difficult to precisely define chaos (Berry, 1987), a concept usually based on the exponential instability of classical trajectories under small perturbations of initial conditions (one positive Lyapunov exponent). The effects of classical chaos in quantum and wave systems can be observed following an idea by Peres (1984), who proposed to compare the evolution of a wave packet with its evolution in a perturbed Hamiltonian. A central concept here is the Loschmidt echo, also known as fidelity. It is defined as the overlap between two quantum states: the first state is obtained from an initial state $|\Phi\rangle$ in the course of its evolution up to time t under a Hamiltonian H, and the second state results from the same initial state by evolving up to the same time with a perturbed Hamiltonian H'. The measure of this overlap is

$$M(t) = |\langle\Phi|e^{iH't/\hbar}e^{-iHt/\hbar}|\Phi\rangle|^2,$$

where $\hbar$ is Planck's constant. This quantity can also be interpreted as the overlap of the initial state and the state obtained by first propagating this state up to time t with H, and then backward in time, up to $-t$ under H'. $M(t)$ equals unity at $t = 0$ and typically decays in time.

The term *Loschmidt echo* refers to the debates in the 19th century about the irreversibility of thermodynamical systems and the foundations of statistical mechanics (in which Loschmidt participated). Similar echo concepts are important in classical systems (Eckhardt, 2003), with applications in sensing techniques (Taddese *et al.*, 2010), and have recently been extended to relativistic quantum systems (Sadurní and Seligman, 2008). The term fidelity is used mainly in the field of quantum information. The overlap $M(t)$ is known to quantify the robustness of systems to perturbations and has nowadays numerous applications in quantum information, statistical physics, and quantum chaos (Gorin, Prosen, and Seligman, 2006).

The first and most natural investigations in quantum chaos considered global perturbations (e.g., $H' = H + \varepsilon V$ with V acting globally). Global perturbations affect all (or a dominant part of) the phase space accessible to the quantum particle in the course of its time evolution. It was shown that the decay of $M(t)$ with t has a variety of regimes, many of them reflecting classical properties of the closed system (e.g., Lyapunov exponents). See Gorin, Prosen, and Seligman (2006) and Jacquod and Petitjean (2009) for reviews, and García-Mata and Wisniacki (2011) for limitations of the Lyapunov regime.

More recently, experimental realizations in billiards (Höhmann, Kuhl, and Stöckmann, 2008) emphasized the importance of the case of quantum mechanically local perturbations (Goussev and Richter, 2007; Goussev *et al.*, 2008; Ares and Wisniacki, 2009; Köber *et al.*, 2011). Next we review recent results on local perturbations that show that in this case the decay of $M(t)$ has an important regime dominated by properties of the corresponding classical system with leak (e.g., the escape rate).

Figure 32 illustrates the concept of local perturbations on the example of a chaotic billiard. The perturbation consists of a deformation of width w localized in a region $\tilde{B}_1$ of the boundary. The rest of the boundary B_0 is unaffected by the perturbation. Three trajectories starting from the same location $\mathbf{r}_0$ (and reaching point $\mathbf{r}$ afterward) are shown. The two nearby trajectories S_1 and $\bar{S}_1$ marked by continuous and dashed lines correspond, respectively, to an evolution with the unperturbed and perturbed Hamiltonians. In a semiclassical approximation, the action difference between these trajectories should be determined. The third trajectory (S_0) hits the boundary only at B_0. For this case the perturbed and unperturbed trajectories coincide; hence the action difference of this pair is zero.

The quantum mechanical implementation and interpretation of the Loschmidt echo with a localized perturbation is illustrated in Fig. 33. The evolution of a wave packet is shown in the original billiard up to time t. At this time the perturbation along the boundary is introduced, and the dynamics is followed in the time-reversed evolution up to the same time. Gray shading represents the probability distribution. The initial Gaussian wave packet appears thus as a dot in the upper left panel. The arrow in this panel marks the momentum direction of the wave packet. The lower left panel shows that the original form is only partially recovered after the full process, and the overlap is thus incomplete $M(t) < 1$.

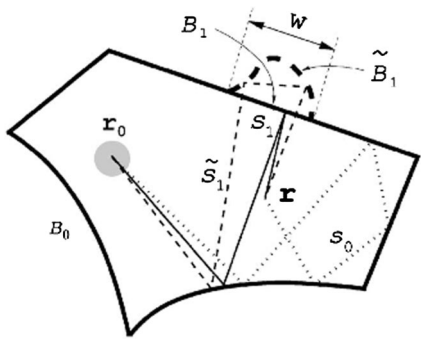

FIG. 32. Schematic diagram of a billiard with a local perturbation $\tilde{B}_1$ along its boundary and three classical trajectories between $\mathbf{r}_0$ and $\mathbf{r}$. From Goussev and Richter, 2007.

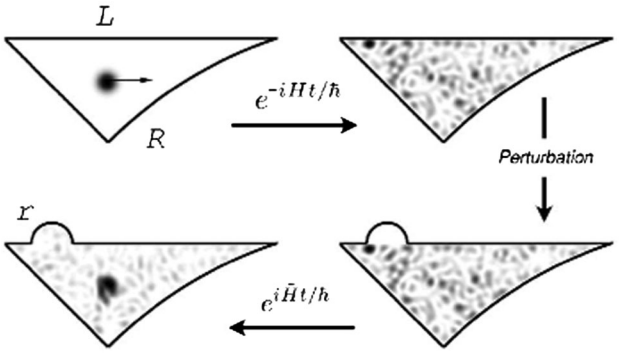

FIG. 33. Forward-time wave packet evolution in an unperturbed diamond billiard up to time t corresponding to about $10\langle t_{\rm coll}\rangle$, followed by the time-reversed evolution in the perturbed billiard. The width of the localized perturbation is $w = 60$, 15% of the length L of the horizontal edge, and the de Broglie wavelength is $\lambda = 4.8$ in the same units. From Goussev and Richter, 2007.

Goussev and Richter (2007) considered a classically weak but quantum mechanically strong perturbation in a region of the boundary of a strongly chaotic billiard. More precisely, the length w and depth r of the perturbed boundary should be much smaller than the length of the billiard boundary, and the perturbation is considered quantum mechanically strong if w and r are much larger than the de Broglie wavelength λ. Their main result is that in such cases there is a long time interval for which the Loschmidt echo decays as

$$M(t) \sim \exp(-2\kappa t), \tag{96}$$

where κ is the classical escape rate of the billiard with a leak I extending precisely through the perturbation region of length w along the original boundary. The time interval over which decay (96) is valid extends from the mean collision time (flight time) $\langle t_{\rm coll}\rangle$ to a saturation time $t_s = -1/(2\kappa)\ln M_\infty$, where $M_\infty = \lambda\sigma/(2\pi A)$, with σ as the wave packet size at $t = 0$, and A as the area of the billiard (Gutiérrez and Goussev, 2009). Note that t_s can be even larger than the Heisenberg time $t_H \sim 1/\hbar$. This result is obtained by showing that, in this regime, the main contribution to $M(t)$ is due to trajectories that do not collide with the perturbation region (collisions there would radically change the dynamics of the trajectories). In our formulation, this means that such trajectories start from the stable manifold of the saddle characterizing the billiard with this leak. Figure 34 shows results of numerical simulations in the billiard depicted in Fig. 33. The quantity $M(t)$ is plotted for different depths r, and its decay is governed by the classical escape rate κ of the billiard with a leak of length w, independent of the value of r. Time is normalized by the classical mean collision time $\langle t_{\rm coll}\rangle$.

These results have been refined and generalized to perturbations which are quantum mechanically not necessarily strong. The decay of $M(t)$ then remains exponential, but the decay rate is a factor α times the classical escape rate:

$$M(t) \sim \exp(-\alpha\kappa t). \tag{97}$$

For pistonlike perturbations, semiclassical expressions have been derived for the coefficient α (Goussev *et al.*, 2008). As a function of the perturbation strength, α turns out to be an oscillatory function converging to 2 for large perturbations.

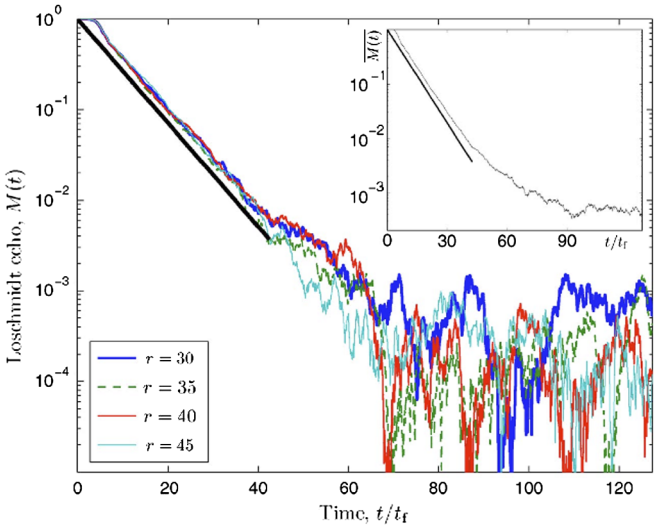

FIG. 34 (color online). The decay of $M(t)$ in the diamond billiard of Fig. 33 for four different values of depth r at $w = 60$. Time is scaled with $\langle t_{\rm coll}\rangle \equiv t_f$ as given in Eq. (14). The solid straight line corresponds to $\exp(-2\kappa t)$ with the escape rate given by Eq. (9), Sabine's result. The inset presents the decay of $\bar{M}(t)$, the Loschmidt echo averaged over several values of r. From Goussev and Richter, 2007.

These results were confirmed in recent experiments in microwave cavities (Köber *et al.*, 2011). The correspondence between the Helmholtz equation (describing 2D microwave cavities) and the Schrödinger equation makes microwave cavities a unique tool for the experimental investigation of quantum chaos (Richter, 1999; Stockmann, 1999), including the exploration of the effect of classical trajectories in chaotic systems with leaks (Dembowski *et al.*, 2004). Figure 35 shows the configuration used by Köber *et al.* (2011) for the experimental investigation of Loschmidt echo decays. For not very strong perturbations, good agreement was found with the semiclassical coefficient α in Eq. (97). On the experimental side, the investigation of the strong perturbation case remains a challenge since the signals are then expected to be rather weak.

Altogether these results on Loschmidt echoes show that there is increasing recent interest in systems with leaks, not only in applications but also on the side of fundamental properties of quantum chaos. In the semiclassical limit such systems reflect the properties of the underlying classical systems, including semiclassical corrections to the classical

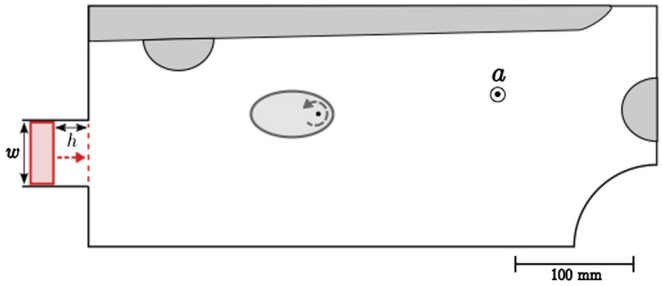

FIG. 35 (color online). Geometry of the chaotic billiard used in the experiments of Köber *et al.* (2011). The local perturbation is pistonlike, of width w and of depth h. The measuring antenna is placed at location a. The rotatable ellipsis is used to perform ensemble averages, and the additional elements are introduced to reduce the influence of bouncing balls. From Köber *et al.*, 2011.

escape rate (Sieber and Richter, 2001; Waltner *et al.*, 2008; Gutiérrez *et al.*, 2009).

2. Fractal distribution of eigenstates

Another signature of chaos in open quantum systems is provided by the fractality of certain invariant sets of the corresponding classical systems. The eigenstates of the quantum system turn out to be distributed along the manifolds of the classical chaotic saddle[10] discussed in Sec. II.B (Casati, Maspero, and Shepelyanski, 1999a). Open quantum systems are characterized by nonunitary evolution operators having a set of right and left decaying nonorthogonal eigenfunctions. The left and right eigenstates of the nonunitary propagator concentrate in the limit of $\hbar \to 0$ on the stable and unstable manifolds of the chaotic saddle, respectively (Keating *et al.*, 2006). This affects the statistical properties of energy levels (e.g., Weyl's law discussed next).

Classical maps can be quantized (Berry *et al.*, 1979). Quantized area-preserving baker maps with leaks (often called open baker maps in the quantum chaos community) nicely exemplify the results mentioned above and can be directly related to the findings reported in Sec. III.E. Keating *et al.* (2006) studied the ternary baker map (76) with a leak, exactly as in Sec. III.E. Figure 36 shows their results: the long-lived (right) eigenstates concentrate in the semiclassical limit on the unstable manifold (horizontal filaments parallel to the q axis). Correspondingly, the momentum representation of any long-lived right eigenstate is supported on a Cantor set which is the projection of the unstable manifold on the momentum (p) axis. This is apparent in Fig. 37, which also shows a magnification that reveals the self-similar character of this distribution.

In another study, Pedrosa *et al.* (2009) considered the quantized version of the binary baker map (78) with leaks as stripes along the $p \equiv x$ axis, centered at $q_l \equiv y_l$ and of width Δq. In the classical version, they found a similar strong dependence of the escape rate on the leak position q_l (for any fixed finite Δq), as discussed in Sec. IV.A. The influence of the shortest periodic orbit falling into the leak was also noticed. Looking for a quantum mechanical analog of this, they determined the distribution of eigenvalues of the quantum evolution operator in the complex plane, as shown in Fig. 38. Since the map is open, moduli are less than 1, and the eigenvalues fall thus all inside the unit circle. For a leak with smaller escape rate, the distribution of eigenvalues is found to be dense at the outer ring, while the distribution is characterized by an increase of density near the origin for a case with faster escape. The strong dependence of the classical escape rate on the position of the leak is thus found to be reflected in the eigenvalue distribution of the quantum evolution operator.

Weyl's law states that in closed systems the number $N(k)$ of energy levels with wave number smaller than k grows as

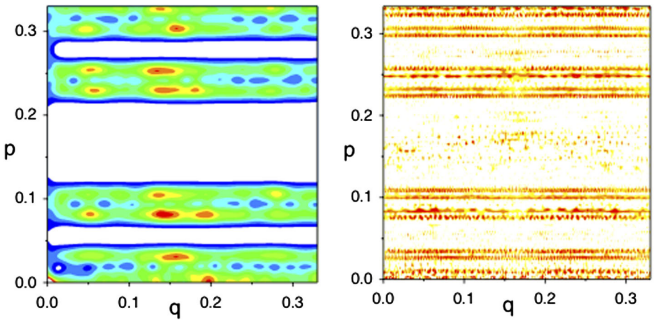

FIG. 36 (color online). Representations of the long-lived right eigenstates in the leaky ternary baker map. The classical map is described by Eq. (76) but the variables are $p \equiv x$ and $q \equiv y$. The scale of $\hbar$ is 0.0005. Because of symmetry, here only one-ninth of the phase space is shown, outside the leak (a central vertical strip of area one-third). Left panel: The average of the so-called Husimi function. Right panel: The corresponding Wigner function average. From Keating *et al.*, 2006.

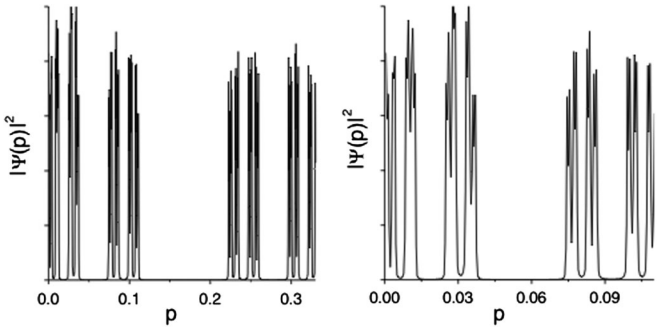

FIG. 37. Probability density of the leaky ternary baker map in momentum space from right eigenstates averaged over the longest-lived states. The magnification (right panel) illustrates the self-similar Cantor set character. From Keating *et al.*, 2006.

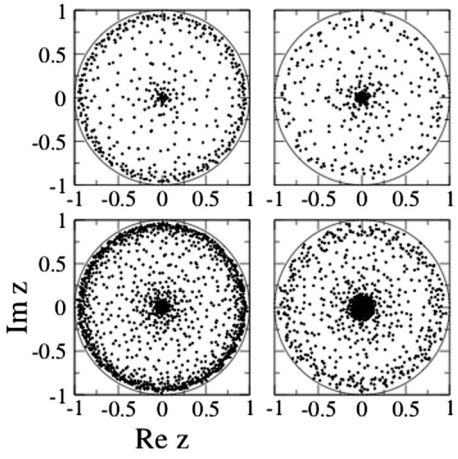

FIG. 38. Eigenvalues of the leaky binary baker map in the complex plane. In the upper panels the dimension of the Hilbert space is $N = 602$, while in the lower ones $N = 2048$. In the left (right) column $q_l = 0.3$ ($q_l = 0.5$) with classical escape rate $\gamma = 0.090$ ($\gamma = 0.165$). $\Delta q = 0.1$, $\Delta p = 0.5$ in all cases. From Pedrosa *et al.*, 2009.

[10]In spite of the fact that repellers (i.e., unstable sets with only expanding directions) cannot exist at all in Hamiltonian systems, this misleading term is often also used in the quantum literature to refer to the chaotic saddle (Lu, Sridhar, and Zworski, 2003b; Novaes *et al.*, 2009; Pedrosa *et al.*, 2009; Ramilowski *et al.*, 2009; Eberspächer, Main, and Wunner, 2010).

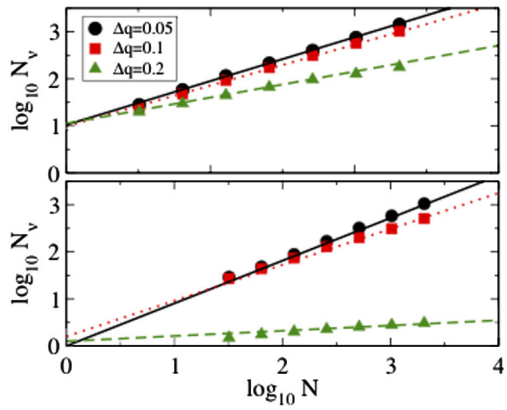

FIG. 39 (color online). Logarithmic plot of the fraction of eigenstates N_ν for $\nu > 0.3$ as a function of the dimension N of the Hilbert space in the leaky binary baker map. Lines correspond to the prediction of the fractal Weyl law. The different slopes reflect the sensitivity of the classical saddle to the position (q_l, p_l) and size $(\Delta q, \Delta p)$ of the leak. In the upper (lower) panel $q_l = 0.3$ ($q_l = 0.5$), and circles correspond to $\Delta q = 0.05$, squares to $\Delta q = 0.1$, and triangles to $\Delta q = 0.2$ ($p_l = 0$, $\Delta p = 0.5$ in all cases). From Pedrosa *et al.*, 2009.

$$N(k) \sim k^{\beta_W}, \tag{98}$$

where the exponent β_W is an integer proportional to the dimension of the system (e.g., for d-dimensional symplectic maps $\beta_W = d/2$). In open chaotic maps the number $N(k)$ of resonances with wave numbers of real part smaller than k scales with an exponent (Lu, Sridhar, and Zworski, 2003):

$$\beta_W = \frac{D_0}{2} = D_0^{(1)}, \tag{99}$$

where D_0 is the fractal dimension of the underlying classical chaotic saddle, and $D_0^{(1)} = D_0^{(2)}$ is the partial box-counting dimension [see Eq. (28)]. Equation (99) shows that the original Weyl law is converted into a *fractal Weyl law* (Lu, Sridhar, and Zworski, 2003; Schomerus and Tworzydło, 2004; Nonnenmacher and Zworski, 2005; Shepelyansky, 2008; Wiersig and Main, 2008; Ramilowski *et al.*, 2009; Eberspächer, Main, and Wunner, 2010; Ermann and Shepelyansky, 2010; Kopp and Schomerus, 2010; Spina, Garcia-Mata, and Saraceno, 2010; Nonnenmacher, 2011; Novaes, 2012; Pedrosa *et al.*, 2012; Körber *et al.*, 2013). An investigation of this property was also carried out (Pedrosa *et al.*, 2009). As Fig. 39 shows, they determined the fraction of eigenvalues N_ν with modulus $\nu > 0.3$ as a function of the Hilbert's space dimension N for different leaks. The prediction of the fractal Weyl law for this case is $\log N_\nu \sim D_0^{(1)} \log N$, which is fulfilled for all graphs. An experimental investigation of fractal Weyl's law on open microwave cavities was recently reported by Potzuweit *et al.* (2012). It confirms a noninteger scaling of Eq. (98) and discusses the origin of potential deviations from the classical prediction.

3. Survival probability and quantum Poincaré recurrences

In Sec. II.C we related the escape of trajectories in systems with leaks to the problem of Poincaré recurrences. In the same spirit, Casati, Maspero, and Shepelyansky (1999b) used the quantum survival probability $P_q(t)$ to investigate what they define as quantum Poincaré recurrences. This is performed introducing absorbing boundary conditions (the leak) in quantized area-preserving maps in the weakly chaotic regime. The quantum decay $P_q(t)$ is identical to the classical decay $P_q(t) = P(t)$ up to a time $t_q \sim \sqrt{1/\hbar}$. This time is larger than the Ehrenfest time $t_E \sim \ln(1/\hbar)$ (Casati, Maspero, and Shepelyansky, 1997); see also Schomerus and Tworzydło (2004) and Waltner *et al.* (2008) for important effects on the t_E time scale. For times longer than the Heisenberg time $t > t_H \sim 1/\hbar$, one finds $P_q(t) \sim 1/t$. This is valid up to a maximum time $t_{\max} \sim \exp(1/\hbar)$ after which an exponential decay sets in, whose rate is, however, different from the classical escape rate.

The origin of the new quantum decay regimes can be understood following (Wimberger, Krug, and Buchleitner, 2002, see also references therein) and writing

$$P_q(t) = \sum_j \omega_j \exp(-\Gamma_j t), \tag{100}$$

where $\Gamma_j > 0$ is the decay rate of the eigenstates $|\psi_j\rangle$ and ω_j is the expansion coefficient $\omega_j = |\langle\varphi_0|\psi_j\rangle|^2$ for the initial state $|\varphi_0\rangle$. The asymptotic exponential decay corresponds to the smallest Γ_j with $\omega_j \neq 0$. In a mixed phase space this longest living state is localized in the center of a KAM island and has $\omega_j \neq 0$ due to chaotic tunneling. KAM islands (or sticky regions) are not the only source of power-law decays in $P_q(T)$, which can be originated through genuine quantum effects such as the quantum mechanical (or dynamical) localization of states due to chaos (Stockmann, 1999). In particular, even classical systems showing exponential tails in $P(t)$ have power-law tails in $P_q(t)$ (Alt *et al.*, 1995, 1996; Fendrik and Wisniacki, 1997; Casati, Maspero, and Shepelyansky, 1999b). The full description of $P_q(t)$ has to consider the effect of the localization of many states, not only in the chaotic and regular components of the phase space but also at the hierarchical border of the KAM islands (Ketzmerick *et al.*, 2000). In general, P_q depends both on the distribution of the decay rates [Γ's in Eq. (100)] and on the initial condition (ω_j), as seen from Eq. (100) and emphasized by Wimberger, Krug, and Buchleitner (2002). The existence of regimes of power-law decay is generic, but exponents different from $P_q(t) \sim 1/t$ are also typically found (Skipetrov and van Tiggelen, 2006). Altogether, the decay of $P_q(t)$ and the previously mentioned Loschmidt echo (fidelity) decay show that the classical decay is still observed in quantum systems, but quantum effects dominate the large and asymptotic behavior. These quantum effects are unfortunately not easy to detect in experiments [for more discussions on the time when $P_q(t)$ deviates from $P(t)$, see Savin and Sokolov (1997) and Puhlmann *et al.* (2005)].

The most detailed experiments of the survival probability are on atom-optics billiards as reported by Friedman *et al.* (2001) and Kaplan *et al.* (2001). In these experiments the survival probabilities of atoms inside cavities were measured for different boundaries and leak positions. The connection to classical billiards becomes evident when comparing the escape from integrable (circular) and strongly chaotic billiards

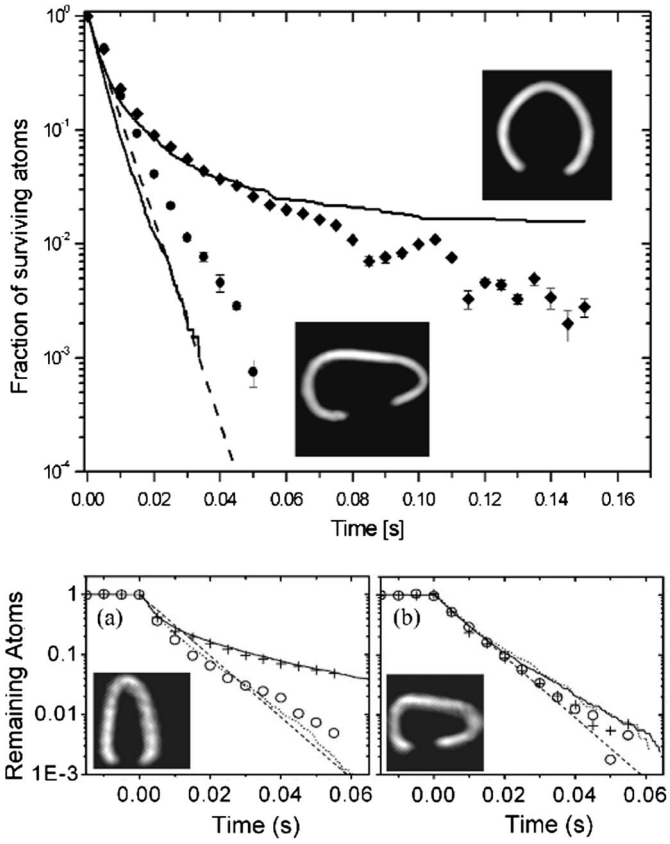

FIG. 40. Survival probability of ultracold rubidium atoms confined by an optical potential. Upper panel: Diamonds (circles) correspond to the experimental results for a circular (stadium) billiard with a leak at the bottom, as shown in the upper (lower) insets. Lower panels: Different potentials along the boundary of the stadium billiard, with two different positions (a) and (b) of the leak. In both panels results with harder (∘) and softer (+) billiard walls are shown. Full and dotted lines correspond to numerical simulations and the dashed lines indicate Sabine prediction $\kappa = \mu(I)/\langle t_{\rm coll}\rangle$, Eq. (13). From Friedman *et al.*, 2001 and Kaplan *et al.*, 2001.

(tilted stadium billiard[11]). The measurements shown in the upper panel of Fig. 40 confirm that a much faster (exponential-like) decay is observed for the chaotic case than for the integrable one. A subsequent study (Kaplan *et al.*, 2001) considered the effect of soft walls along the boundaries of the (tilted) stadium billiard, which generically lead to the creation of KAM islands. The lower panels of Fig. 40 show the experimental survival probabilities. They confirm a slower decay for soft walls, which was shown to be related to the stickiness of trajectories around the islands (see Sec. V.B). A strong dependence on the leak position is also found. If the leak corresponds to a region of the phase space that fully contains the island(s), no stickiness effect can be observed [see Fig. 40, lower panel].

VII. SUMMARY AND OUTLOOK

There are many different configurations in which a leak is introduced in a chaotic system, but in all cases the simplest theoretical approaches rely on the same principle: the properties of the leaky system can be compared to the properties of the closed system. Simple estimates based on this principle led to Sabine's law for acoustical reverberation at the end of the 19th century and, more than a century later, were used to explain the emission patterns of microlasers [see, e.g., Lebental *et al.* (2007)] and the survival probability of cold atoms (Friedman *et al.*, 2001; Kaplan *et al.*, 2001). Here we presented a transient chaos based theory of the problem of leaky systems that goes beyond the closed-system approximation (see Sec. II.A) and leads to a proper treatment of finite leaks (see Sec. II.B and Table III), partial reflection (see Secs. II D and III), and weak chaos (see Sec. V).

Another aim of this review has been to illustrate the abundance of applications of leaky systems (see Secs. I and VI). In the regimes in which dynamical-system models apply, the results reviewed show that all important quantities of the transient chaos theory of leaky systems (see Secs. II.B, III.D, and IV) have direct consequences to experiments and applications of contemporary physics research:

- The *escape rate* (see Sec. III.C) dominates some regimes of the Loschmidt echo (see Sec. VI.E.1) and was directly measured in cold-atom experiments (see Sec. VI.E.3).
- The *chaotic saddle and its invariant manifolds* (see Sec. II.B) leave direct fingerprints on astronomical problems (see Sec. VI.A), hydrodynamical flows (see Sec. VI.B), magnetic field lines inside tokamaks (see Sec. VI.C), optical microcavities (see Sec. VI.D), and the distribution of eigenstates in quantum systems (see Sec. VI.E.2). Many of these examples include weakly chaotic systems, where the observations often become easy to interpret in view of the division of the chaotic saddle in hyperbolic and nonhyperbolic components (see Sec. V.D).
- The *stickiness* due to the nonhyperbolic component (see Sec. V.B) becomes observable in transport properties (see Sec. V.D) and in quantum systems (see Sec. VI.E.3).
- The dependence on *leak position, size, and shape* (see Sec. IV.A) is clearly observable in hydrodynamical problems (see Sec. VI.B), in optical microcavities (see Sec. VI.D), and in quantum experiments (see Sec. VI.E.3).
- *Basins of escape* (see Sec. IV.B), shaped by an underlying chaotic saddle, prove to be concepts usefully applicable to the three-body problem (see Sec. VI.A), in asymmetric transport (see Sec. V.D), and in the plasma problem (see Sec. VI.C).
- Far-field *emission* (see Sec. IV.C) and *partial reflection* (see Sec. II D) play a crucial role in experiments on optical microcavities (see Sec. VI.D) and in room acoustics (see Sec. I.B).

Our review also contains new results. They mainly arise within the framework of our operator description of true-time maps with partial leaks (see Sec. III). The general formula (71) relates averages taken with the c measure to the energy escape rate $\langle e^{-\tilde{\kappa} t_{\rm coll}}\rangle_{\tilde{c}} = \langle R\rangle_{\tilde{c}}$. The idea of a partial reflection or absorption is not incorporated in traditional descriptions of dynamical systems, despite being physically very natural, and

[11]The usual parallel walls of the stadium billiard were tilted in order to avoid the influence of the bouncing ball orbits discussed in Sec. V.B.

also of easy implementation in ray simulations. Here we have shown that reflectivity can be naturally incorporated into the operator formalism that avoids the artificial factorization of the total energy density $\tilde{\rho}$ in ray density ρ and intensity J. More generally, the approach makes superfluous the attaching of *labels* (e.g., intensity or true time) to trajectories that are modified at each collision. Also the numerical procedures (see Appendix B) to estimate the different measures of leaky billiards should be relevant not only for simulations but also in experiments for which data can be collected within a snapshot (as in the S set) or during some time interval (as in the Q set).

The significance of these results is not restricted to billiards or even to Hamiltonian systems; they apply to any true-time map obtained from a Poincaré surface of section. The collision times are then to be replaced by the return times to the Poincaré section. It is a widespread practice to assume that results for maps extend immediately to flows or true-time maps. While this holds for stroboscopic maps of periodically driven systems, autonomous problems, or more generally problems with Poincaré maps, are different. Our results further emphasize the message of Kaufmann and Lustfeld (2001) that the connection between true-time and discrete-time maps in open systems is different from the case of closed systems and often involves surprising nontrivial results (e.g., see Table III).

Finally we discuss unsolved problems and future research directions. First we note that leaky systems are intimately related and provide further motivation to fundamental problems in dynamical systems. In particular, in Hamiltonian systems we mention the understanding of the mechanisms of stickiness in higher dimensions and its connection to Arnold diffusion (Bunimovich, 2008), and a formal treatment of the division of the chaotic saddle in hyperbolic and nonhyperbolic components [see, e.g., Altmann and Tél (2008)]. Among the questions directly related to leaky systems, and in addition to Dettmann (2011), the following general problems claim for further investigations.

- Adapt and extend current results on the sensitivity on the leak position to more generic situations. For instance, the most rigorous mathematical results about the escape rate (see Sec. IV.A) are demonstrated for one-dimensional systems with leaks in Markov partitions. A similarly nongeneric feature is the standard explanation of directional emission in 2D optical microcavities (see Sec. VI.D), which relies on the existence of an unstable periodic orbit close to the leak. There is an evident need for extending these results to generic leak positions and chaotic saddles.
- Find the conditions for the existence of a single chaotic saddle (with a single physically relevant c measure) after a leak is introduced (Collet, Martínez, and Maume-Deschamps, 2000; Demers and Young, 2006). The hypothesis of the existence of a single saddle was used in our theory (see Sec. II.B). To explore the cases in which this is violated (Claus and Gaspard, 2001; Dettmann and Georgiou, 2011b) remains a task for the future.
- Consider novel configurations of leakage such as introducing a temporal dependence or a random choice on the properties of the leak (Bahsoun and Vaienti, 2012; Georgiou, Dettmann, and Altmann, 2012; Nándori and Szász, 2012).
- Explore the implications of partial leak and true time (see Sec. III.D) in operator approaches based on Ulam's method, which have been applied to the usual Perron-Frobenius operator (Kovács and Tél, 1992; Bunimovich and Webb, 2012; Cristadoro, Knight, and Degli Esposti, 2012; Georgiou, Dettmann, and Altmann, 2012) and received renewed interest in relation to the concept of almost invariant sets (Froyland and Pradberg, 2009; Froyland and Stancevic, 2010).
- Recent works suggest that certain nontraditional (e.g., location dependent) boundary conditions in problems of wave chaos can be interpreted as a generalization of leakage (Berry, 2009). It remains to be explored how this can be related to the traditional leakage discussed here.
- Further investigate the connection to transport properties (Kuhl, Stöckmann, and Weaver, 2005; Dettmann and Georgiou, 2011b; Knight *et al.*, 2012) and the effect of stochastic perturbations (Faisst and Eckhardt, 2003; Dettmann and Howard, 2009; Altmann and Endler, 2010; Altmann, Leitao, and Lopes, 2012; Bodai, Altmann, and Endler, 2013).
- Partial leaks: clarify the nature of the spectrum of dimensions of the invariant sets (as mentioned in Sec. II D), and relate these dimensions to the escape rate and to the Lyapunov exponent. Extend the results to noninvertible systems and develop efficient algorithms for the computation of chaos characteristics (e.g., escape rate, dimensions, and Lyapunov exponents). For first results, see Altmann, Portela, and Tél (2013).
- Quantum partial leaks: deepen the connection between quantum systems with absorption and classical dynamical systems with partial leaks. First results already revealed interesting phenomena, such as, e.g., a drastic modification of the fractal Weyl's law (Nonnenmacher and Schenk, 2008; Wiersig and Main, 2008; Schenck, 2009; Novaes, 2012) and changes in the localization of eigenfunctions (Lippolis *et al.*, 2012). Additional interesting developments can be expected in view of the results presented in Sec. II D and Altmann, Portela, and Tél (2013) and Arnoldi, Faure, and Weich (2013).

Besides these general problems, a clear future research line is to adapt the models to make them more realistic to specific applications. This involves including new features in the dynamics, e.g., gain medium in lasing cavities, reactions of particles, or properties of the wave systems [e.g., modified collision laws (Schomerus and Hentschel, 2006; Altmann, Del Magno, and Hentschel, 2008; Song *et al.*, 2010)]. The challenge here is to show how to connect experiments and observations to the theory proposed here. Also important is to show to what extent and to what level of detail the models match the experiments, e.g., to what extent nonhyperbolic properties of chaotic dynamical systems play a role in the experimental results. In turn, these adaptations toward applications bring new problems and inspiration for theoreticians, a virtuous circle illustrated here by the case of partial leaks. We are convinced that the collection of problems that can be

modeled as a leaky chaotic system will keep growing and pushing the research forward also in unforeseeable directions.

ACKNOWLEDGMENTS

The authors thank A. Bäcker, M. V. Berry, C. Dettmann, G. Drótos, O. Georgiou, A. Goussev, Z. Kauffmann, M. Novaes, S. Shinohara, S. Szanyi, S. Wimberger, and D. A. Wisniacki for their valuable contributions, and all the authors who kindly allowed reproduction of their results in Sec. VI. This work was supported by OTKA Grant No. NK100296, the von Humboldt Foundation, and the Fraunhofer Society.

APPENDIX A: PROJECTED MEASURE AND AVERAGES

We now turn to the c measure μ_{Pc} of the dynamics obtained by projecting the flow on the boundary. This describes, in an ensemble of escaping trajectories, the probability of the occurrence of collisions with Birkhoff coordinates $\mathbf{x}$ *irrespective* of the time of collision. Let the corresponding density be denoted as $\rho_{Pc}(\mathbf{x})$, then

$$d\mu_{Pc} = \rho_{Pc}(\mathbf{x})d\mathbf{x}. \tag{A1}$$

The projected measure is obtained by integrating the flow measure $d\mu_{Fc}$ in Eq. (63) over coordinate time up to its maximum $t_{\rm coll}(\mathbf{x})$ (see Fig. 10). This measure can thus be written as

$$\begin{aligned} d\mu_{Pc} &= \int_0^{t_{\rm coll}(\mathbf{x})} d\mu_{Fc} = \int_0^{t_{\rm coll}(\mathbf{x})} A_c e^{-\kappa r} dr d\mu_c \\ &= \frac{1-e^{-\kappa t_{\rm coll}(\mathbf{x})}}{\kappa} A_c d\mu_c. \end{aligned} \tag{A2}$$

The relation between the densities is then

$$\rho_{Pc}(\mathbf{x}) = \rho_c(\mathbf{x}) \frac{1-e^{-\kappa t_{\rm coll}(\mathbf{x})}}{\kappa} A_c \to \rho_\mu(\mathbf{x}) \frac{t_{\rm coll}(\mathbf{x})}{\langle t_{\rm coll}\rangle_\mu}, \tag{A3}$$

where the arrow indicates the limit of closed systems ($\kappa \to 0$). Equivalently,

$$\rho_{Fc}(\mathbf{x}, r) = \rho_{Pc}(\mathbf{x}) \frac{\kappa e^{-\kappa r}}{1-e^{-\kappa t_{\rm coll}(\mathbf{x})}} \to \frac{\rho_{Pc}(\mathbf{x})}{t_{\rm coll}(\mathbf{x})}. \tag{A4}$$

Using these relations, we can write average values in the projected and flow measures as a function of those in the true-time map measure. Particularly interesting is the case of the average collision time. In the flow measure it is obtained as the average of the coordinate time r

$$\begin{aligned} \langle t_{\rm coll}\rangle_{Fc} &= \int d\mathbf{x} \int_0^{t_{\rm coll}(\mathbf{x})} dr r e^{-\kappa r} A_c \rho_c(\mathbf{x}) \\ &= \int d\mathbf{x} \frac{1-e^{-\kappa t_{\rm coll}(\mathbf{x})} - \kappa t_{\rm coll}(\mathbf{x}) e^{-\kappa t_{\rm coll}(\mathbf{x})}}{\kappa^2} A_c \rho_c(\mathbf{x}) \\ &= \frac{1-\langle e^{-\kappa t_{\rm coll}}\rangle_c - \langle \kappa t_{\rm coll} e^{-\kappa t_{\rm coll}}\rangle_c}{\kappa^2} A_c \to \frac{\langle t_{\rm coll}^2\rangle}{2\langle t_{\rm coll}\rangle}. \end{aligned} \tag{A5}$$

In the projected measure the average collision time is obtained from Eq. (A3) as

$$\begin{aligned} \langle t_{\rm coll}\rangle_{Pc} &= \int d\mathbf{x} t_{\rm coll}(\mathbf{x}) \rho_{Pc}(\mathbf{x}) \\ &= A_c \int d\mathbf{x} \frac{t_{\rm coll}(\mathbf{x})(1-e^{-\kappa t_{\rm coll}(\mathbf{x})})}{\kappa} \rho_c(\mathbf{x}) \\ &= \frac{\langle t_{\rm coll}\rangle_c - \langle t_{\rm coll} e^{-\kappa t_{\rm coll}}\rangle_c}{\kappa} A_c \to \frac{\langle t_{\rm coll}^2\rangle}{\langle t_{\rm coll}\rangle} = 2\langle t_{\rm coll}\rangle_F. \end{aligned} \tag{A6}$$

The difference between the average collision time in the projection and in the true-time map is then

$$\begin{aligned} \langle t_{\rm coll}\rangle_{Pc} - \langle t_{\rm coll}\rangle_c &= (\langle t_{\rm coll}\rangle_c \langle e^{-\kappa t_{\rm coll}}\rangle_c - \langle t_{\rm coll} e^{-\kappa t_{\rm coll}(\mathbf{x})}\rangle_c) \\ &\quad \times \frac{A_c}{\kappa} \to \frac{\sigma^2_{t_{\rm coll}}}{\langle t_{\rm coll}\rangle}, \end{aligned} \tag{A7}$$

where $\sigma^2_{t_{\rm coll}}$ is the second cumulant of the distribution of the collisions times in the closed map. The difference between the two averages is thus due to the inhomogeneity of the collision time distribution.

An even simpler relation can be obtained between the averages taken in the true-time map and the projected representation. Rearranging Eq. (A3) and using the fact that ρ_c is normalized, we obtain

$$\int \rho_c(\mathbf{x}) d\mathbf{x} = 1 = \int \rho_{Pc}(\mathbf{x}) \frac{1}{A_c} \frac{\kappa}{1-e^{-\kappa t_{\rm coll}(\mathbf{x})}} d\mathbf{x}, \tag{A8}$$

from which it follows that

$$\frac{1}{1-\langle e^{-\kappa t_{\rm coll}}\rangle_c} = \left\langle \frac{1}{1-e^{-\kappa t_{\rm coll}}} \right\rangle_{Pc}. \tag{A9}$$

For closed systems this relation goes over into

$$\frac{1}{\langle t_{\rm coll}\rangle} = \left\langle \frac{1}{t_{\rm coll}} \right\rangle_P. \tag{A10}$$

APPENDIX B: ALGORITHMS FOR OPEN BILLIARDS

We describe the numerical simulations of open billiards. For the limaçon billiard considered map $\mathbf{f}$ was obtained using the standard geometric techniques (Robnik, 1983; Bäcker and Dullin, 1997): given a collision position $\mathbf{x} = (x, y)$ and velocity $\mathbf{v}$ [correspondingly coordinates (s, p)], the next collision position is obtained as the first intersection of the ray $\mathbf{x} + \mathbf{v}t$ with the billiard boundary. That is achieved by imposing that the point $\mathbf{x} + \mathbf{v}t$ satisfies Eq. (19) of the cardioid, which can be written for $S = 1$ as $(x^2 + y^2 - \varepsilon x)^2 - (x^2 + y^2) = 0$. The smallest solution of the resulting fourth order polynomial in t yields the collision time $t_{\rm coll}(\mathbf{x}')$ and the next collision position $\mathbf{x}' = \mathbf{x} + \mathbf{v}t_{\rm coll}(\mathbf{x}')$.

We search for numerically efficient procedures to compute observable quantities in true-time open maps. In Sec. II.B we learned that asymptotic quantities and invariant properties of the escape process are given by the density $\rho_c(\mathbf{x})$ of the c measure. Next we describe how this density can be approximated in numerical simulations, related to the different representations of invariant measures.

For the billiard, ρ_c is approximated by taking all trajectories in an initial ensemble that survive up to a large time t^*.

Mathematically, $t^* \to \infty$, but in practice, for $t^* > 2/\kappa$ a good approximation of ρ_c is obtained. For true-time maps, we have only the Birkhoff coordinates $\mathbf{x}_n = (s_n, p_n)$ and the time t_n of collisions. It is natural to take for each trajectory surviving up to time t^* the values s_{n^*} and p_{n^*}, where n^* is the smallest n such that $t_{n^*} \geq t^*$. Figure 41 illustrates this procedure. Note that n^* is different for each trajectory and depends on the whole history of each trajectory [through Eq. (18)]. The points $\mathbf{x}^* \equiv (s_{n^*}, p_{n^*})$ obtained through this procedure group together all points that at $t = t^*$ have coordinates $\mathbf{x}^*$ irrespective of their coordinate time r after the last collision (small dots in Fig. 10). Therefore, these points are then sampled according to $\rho_{Pc}(\mathbf{x})$, the projected density [which is insensitive to sliding orbits, see Eq. (A3)]. This means that the average $\langle B\rangle_{Pc}$ of any observable $B(\mathbf{x})$ [e.g., $B(\mathbf{x}) = t_{\rm coll}(\mathbf{x})$] can be numerically obtained as

$$\langle B\rangle_{Pc} \approx \frac{1}{N^*}\sum_{S(t^*)} B(\mathbf{x}^*),$$

where $S(t^*)$ denotes the set of trajectories that survives inside the billiard up to time t^*. Qualitatively speaking, the use of the $\mathbf{x}^*$ coordinates belonging to set $S(t^*)$ corresponds to an instantaneous observation of the system. In a simulation using N initial conditions, let the size of $S(t^*)$ be denoted by N^*. The survival probability can then be estimated as $P(t^*) = N^*/N$. Furthermore, it is possible to use Eq. (A3) and this numerical procedure to efficiently compute the true-time map average value of any observable $B(\mathbf{x})$ as

$$\begin{aligned}\langle B\rangle_c &\equiv \int d\mathbf{x}\rho_c(\mathbf{x})B(\mathbf{x})\\ &= \int d\mathbf{x}\frac{1-\langle e^{-\kappa t_{\rm coll}}\rangle_c}{1-e^{-\kappa t_{\rm coll}(\mathbf{x})}}\rho_{Pc}(\mathbf{x})B(\mathbf{x})\\ &\approx \frac{1}{N^*}\sum_{S(t^*)}\frac{1-\langle e^{-\kappa t_{\rm coll}}\rangle_c}{1-e^{-\kappa t_{\rm coll}(\mathbf{x}^*)}}B(\mathbf{x}^*),\end{aligned} \tag{B1}$$

where the last relation is valid for N^*, $t^* \gg 1$. In particular, with the choice $B(\mathbf{x}) \equiv 1$, one recovers Eq. (A9). Equation (A6) is recovered with the choice $B(\mathbf{x}) = t_{\rm coll}(\mathbf{x}) \times (1 - e^{-\kappa t_{\rm coll}(\mathbf{x})})/\kappa$. Once the value of $\langle e^{-\kappa t_{\rm coll}}\rangle_c$ is known, Eq. (B1) can be directly applied to an arbitrary observable. The measure of the leak $\mu_c(I)$ is computed, e.g., by choosing $B = 1$ for $\mathbf{x} \in I$ and $B = 0$ for $\mathbf{x} \notin I$.

For partial leaks discussed in Sec. II D, Eq. (B1) is generalized to

$$\langle B\rangle_{\tilde c} \approx \frac{1}{J^*}\sum_{S(t^*)} J_{t^*}\frac{1-\langle e^{-\tilde\kappa t_{\rm coll}}\rangle_c}{1-e^{-\tilde\kappa t_{\rm coll}(\mathbf{x}^*)}}B(\mathbf{x}^*), \tag{B2}$$

where J_{t^*} is the intensity of the trajectory over which summation runs, and $J^* = \sum_i^{N^*} J_{t^*}$ is the total intensity of the rays in $S(t^*)$ (i.e., of all trajectories in the system at time t^*), which are all trajectories if $R(\mathbf{x}) \neq 0$. The advantage of this procedure, and of any application using the $S(t^*)$ set, or of projected densities, is that we can have good control on the time $t = t^*$ at which the measures are approximated numerically. This is particularly important for systems with mixed phase space discussed in Sec. V, where a crossover from exponential to power-law decay is observed in $P(t)$.

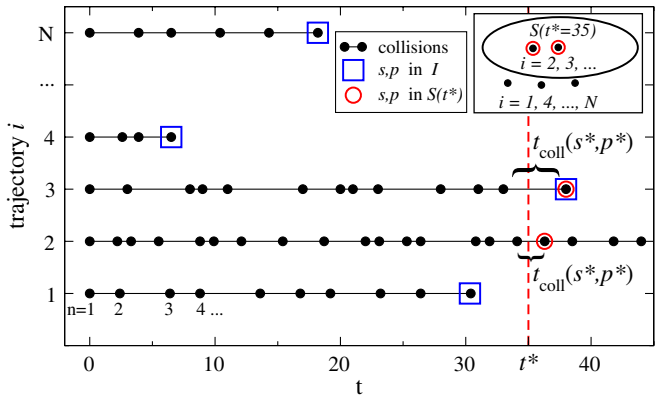

FIG. 41 (color online). Schematic illustration of the numerical procedure to obtain the true-time c measure in open billiards. The time instants of collisions at the boundary are plotted, with black dots, for different trajectories. Trajectories $i = 2$ and $i = 3$ belong to $S(t^* = 35)$ (inset) and have $n^*(i = 2) = 17$ and $n^*(i = 3) = 13$. $S(t^*)$ denotes the set of trajectories that survive inside the billiard up to time t^* at least. Trajectories $i = 1$, 4, N do not belong to $S(t^* = 35)$.

An alternative procedure for generating averages in the true-time map is based on sampling a set of collision points according to the density ρ_c of the map. This is done by collecting in a set $Q(t^*, \Delta t^*)$ all collisions in a time interval $\Delta t^* = [t^*, t^* + \Delta t^*]$ for $\Delta t^* > \max\{t_{\rm coll}(\mathbf{x})\}$ and over all N trajectories. The use of the Q set assumes an observation of the system over an extended time period.

To see how this procedure generates the c measure, first consider q different time instants $t_j^* \in \Delta t^*$, $j = 1, \ldots, q$, and let $S^q(t^*) = \{S(t_j^*)\}_{j=1}^q$. Since ρ_{Pc} is independent of time, points in all $S(t_j^*)$'s and in $S^q(t^*)$ are distributed according to ρ_{Pc}. However, the coordinates $\mathbf{x}^*$ of a single trajectory i will typically appear multiple times in $S^q(t^*)$ because different time instants $t^* \in \Delta t^*$ may have the same n^*. This can be seen by considering two close-by values of t^* in Fig. 41. (For $t_j^* - t_{j+1}^* < \langle t_{\rm coll}\rangle_c$, most trajectories will lead to repeated values of $\mathbf{x}^*$.) For $q \to \infty$, the number of times a given $\mathbf{x}^*$ appears in $S^q(t^*)$ is proportional to $\int_0^{t_{\rm coll}(\mathbf{x}^*)} e^{-\kappa t}dt$.

A point $\mathbf{x}^*$ of a single trajectory is included only once in $Q(t^*, \Delta t^*)$ and possibly many times in $S^q(t^*)$. Therefore, noting that the S set is sampled according to ρ_{Pc}, we find that points in $Q(t^*, \Delta t^*)$ are sampled according to

$$\rho_Q(\mathbf{x}) = \frac{\rho_{Pc}(\mathbf{x})}{A_c\int_0^{t_{\rm coll}(\mathbf{x})} e^{-\kappa t}dt} = \frac{\kappa}{A_c(1-e^{-\kappa t_{\rm coll}(\mathbf{x})})}\rho_{Pc}(\mathbf{x}),$$

where A_c is the normalization constant (62). Comparing to Eq. (A3), we obtain $\rho_Q(\mathbf{x}) \equiv \rho_c(\mathbf{x})$. [Numerically it is efficient to consider the case $Q(t^*) \equiv Q(t^*, \Delta t^* \to \infty)$, i.e., to consider all collisions until escaping the system.] Using this sampling procedure, Eq. (B1) is rewritten as

$$\langle B\rangle_c \approx \frac{1}{N_Q}\sum_{Q(t^*)} B(\mathbf{x}^*), \tag{B3}$$

where $N_Q \gg 1$ is the number of points in the set $Q(t^*)$. The case of partial leak (B2) is in this case simply

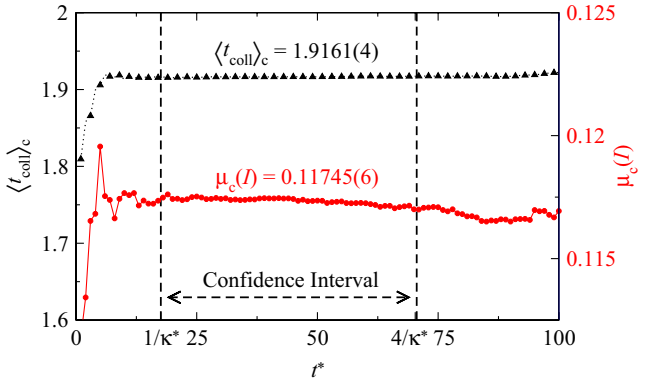

FIG. 42 (color online). Convergence of the numerical estimation of $\mu_c(I)$ and $\langle t_{coll}\rangle_c$. These results were obtained using Eq. (B3) for the cardioid billiard [$\varepsilon = 1$ in Eq. (19)] with the leak as in Fig. 4 using 2.5×10^7 initial conditions uniformly distributed in the full phase space $[-1, 1] \times [-1, 1]$. Short time fluctuations are present during the convergence to the c measure. The results $\mu_c(I) = 0.117\,45 \pm 0.000\,06$ and $\langle t_{coll}\rangle_c = 1.9161 \pm 0.0004$ follow as the mean and the standard deviation of the values obtained for integers t^* in the interval $t^* \in [1/\kappa^*, 4/\kappa^*]$ with the naive estimate $\kappa^* = 0.056\,93$ obtained with Eq. (23) using $\mu(I) = 0.10$ and $\langle t_{coll}\rangle = 3\pi^2/16 = 1.850\,55\ldots$. The Q sets at each time t^* include all collisions for $t > t^*(\Delta t^* = \infty)$. The actual decay rate κ was obtained through a direct fit of $P(t)$ (not shown) and resulted in $\kappa = 0.065\,59 \pm 0.000\,01$. The procedures described here have been used with finite Δt^*'s in all computations throughout.

$$\langle B\rangle_{\tilde{c}} \approx \frac{1}{J_{Q,t^*}} \sum_{Q(t^*)} J_{t^*} B(\mathbf{x}^*), \tag{B4}$$

where J_{Q,t^*} is the sum of the intensities of all collisions in the set Q.

In our simulations we used the set Q for calculating $\mu_c(I)$ and $\langle t_{coll}\rangle_c$, as illustrated in Fig. 42. While the set Q provides better statistics and should typically be used, the results for the set S are conceptually interesting and may find applications in different simulations or experimental applications.

APPENDIX C: COMPUTATION OF INVARIANT MANIFOLDS AND DENSITIES

Numerical approximations of the invariant sets of transiently chaotic maps can be obtained using the sprinkler method (Tél and Gruiz, 2006; Lai and Tél, 2011). The idea is to use initial conditions distributed uniformly in the phase space and keep track of the trajectories that never escape up to a time t^*. Coherent with the notation of Appendix B, t^* corresponds to the transient time needed for the convergence to $\rho_c(\mathbf{x})$. For $t^* \gg 1/\kappa$, the surviving trajectories necessarily start close to the stable manifold of the saddle (at $t = 0$), approach the saddle (at $t \approx t^*/2$), and most of them will be about to leave the system through the unstable manifold of the saddle (at $t = t^*$). The invariant sets are approximated by the position of these surviving trajectories at the times $t_s = \{0, t^*/2, t^*\}$. More precisely, the stable manifold, the chaotic saddle, and the unstable manifolds build the support of densities $\rho(\mathbf{x}, t_s)$ obtained from the position of the trajectories $\mathbf{x}(t_s)$ at the different times $t_s = \{0, t^*/2, t^*\}$, respectively. For $t_s = t^*$ we recover the c density $\rho_c(\mathbf{x})$.

Modifications of the methods above are needed to address true-time maps with partial leaks. In order to address the true-time aspect of the map, the modifications discussed in Appendix B are needed. In the simulations shown we considered an approach based on the Q set, with a fixed $t^* \gg 1/\kappa$ and a finite $\Delta t^* > \max\{t_{coll}(\mathbf{x})\}$. From trajectories surviving up to t^*, the positions $\mathbf{x}$ of all collisions (until escape) in the time interval $t \in [t_s, t_s + \Delta t^*]$ with $t_s = \{0, t^*/2, t^*\}$ generate the densities $\rho(\mathbf{x}, t_s)$. This procedure ensures that the requirement of surviving up to time t^* is satisfied by all considered points. (Note that when initial distributions reach the saddle relatively fast within the chosen interval Δt^*, the initial positions are a better approximation to the stable manifold than the positions in the time interval $t \in [0, \Delta t^*]$.) For the case of partial leaks the same procedure is employed, and the position $\mathbf{x}$ of each collision with $t \in [t_s, t_s + \Delta t^*]$ is counted with a weight given by the intensity $J(t^* + t - t_s)$ (at a given time $t > t^*$, the same intensity is used for the computation of the densities along the saddle, stable, and unstable manifolds). Note that for the case of full leak ($R = 0$) and fixed collision time ($t_{coll} = 1$) the usual definitions are practically recovered. This general procedure was employed to compute Figs. 6 and 9.

APPENDIX D: DIFFERENCE BETWEEN POINCARÉ AND TRUE-TIME MAPS

The distinction between the usual Poincaré map and the true-time map is crucial in all open systems because the c measures in both maps are different (Kaufmann and Lustfeld, 2001). This difference becomes dramatic in the case of billiards with concave borders such as the limaçon billiard considered here, because of the existence of trajectories with $t_{coll}(\mathbf{x}) = 0$ sliding along the boundaries (whispering gallery) characterized by $p \approx \pm 1$. In the Poincaré map, these orbits build one-parameter families (the boundary) of nonhyperbolic trajectories. However, these orbits have little influence on the flow, where time is counted by t and not by the number n of collisions.

The flow of the closed cardioid billiard is proved to be ergodic and strongly mixing (Robnik, 1983; Wojtkowski, 1986), and we expect a well-defined c measure in the leaky case both in the flow and in the true-time map. Figure 43 shows that the usual Poincaré map is not fully (uniformly) hyperbolic due to the sliding trajectories. They convert the long time decay to nonexponential in the leaky case. The c measure of the Poincaré map is thus ill defined. From this example it is clear that the simple correspondence $n\langle t_{coll}\rangle_c \mapsto t$ between the physical time t and the number of iterations n of the map is not able to explain the qualitative difference between the (physically meaningful) survival probability $P(t)$ and the *discrete-time* survival probability $P(n)$, defined as the fraction of initial conditions that survive inside the system up to n collisions at least. From Fig. 43 one can have the impression that the differences appear only for long times. In Fig. 44 we present, however, ρ_c of the Poincaré map numerically obtained as usual, which should be compared to the true-time map result shown in Fig. 6. There is a

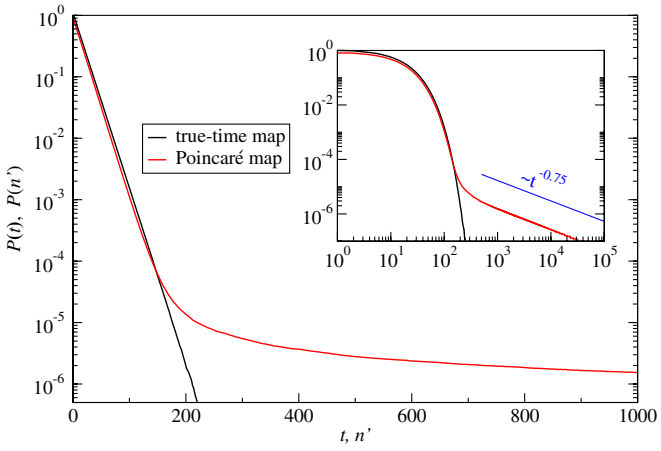

FIG. 43 (color online). Difference between the true-time and the Poincaré map of the cardioid billiard. Survival probability $P(t)$ as a function of the physical time t (black) and the discrete-time survival probability $P(n)$ given in terms of iteration number n of the Poincaré map (gray), multiplied by the average collision time $\langle t_{\rm coll}\rangle_c$ for comparison, $n' = n\langle t_{\rm coll}\rangle_c$. The leak is as in Fig. 4 and Table II. 10^8 initial conditions have been taken, uniformly distributed in $[-0.9, 0.9]\times[-0.9, 0.9]$, to avoid sliding initial conditions. The log-log inset highlights the power-law tail of the Poincaré map.

disagreement which can be clearly seen in (but is not restricted to) the region of the sliding orbits ($|p| \approx 1$).

The c measures of the Poincaré map and of the true-time map are generically different (even in the absence of sliding orbits) $\kappa \neq \gamma_{\rm Pmap}/\langle t_{\rm coll}\rangle_c$, and there is no simple relationship between κ of the flow and $\gamma_{\rm Pmap}$. For the cardioid billiard

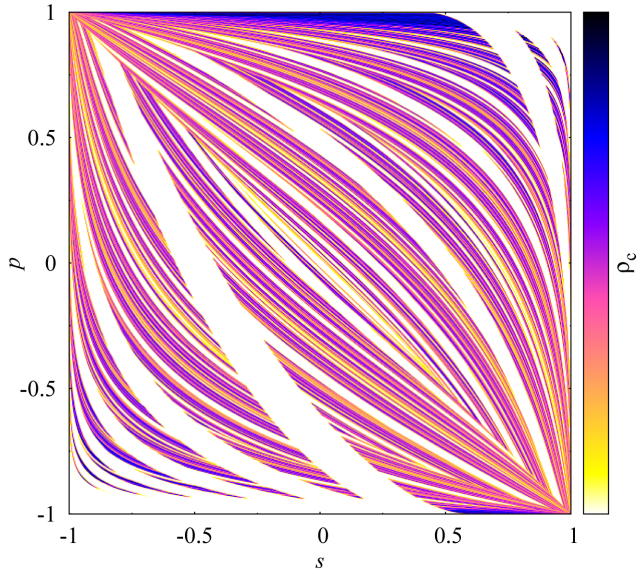

FIG. 44 (color online). Conditionally invariant measure for the Poincaré map of the cardioid billiard obtained for initial conditions uniformly distributed in $[-0.9, 0.9]\times[-0.9, 0.9]$. This measure was obtained by recording, during an interval $\Delta n^* = 30$, the coordinates of the orbits that survived at least $n^* = 10$ iterations. In comparison to the corresponding true-time map measure, Fig. 6, obtained with $t^* = \Delta t^* = 80$, points in the sliding-orbit region ($|p| \approx 1$) have a bigger weight, although in the range $10 < n < 40$, escape is essentially exponential (cf. Fig. 43).

$\gamma_{\rm Pmap}$ is not even defined, as $P(n)$ decays asymptotically as a power law. If, nevertheless, we consider an effective $\gamma_{\rm Pmap}$ extracted from the intermediate-time behavior in Fig. 43, we obtain that $\gamma_{\rm Pmap}$ and $\kappa\langle t_{\rm coll}\rangle_c$ differ by about 2%, as can be seen from Table II and the data reported in the caption.

REFERENCES

Abdullaev, S. S., T. Eich, and K. H. Finken, 2001, Phys. Plasmas **8**, 2739.
Afraimovich, V., and L. A. Bunimovich, 2010, Nonlinearity **23**, 643.
Aguirre, J., and M. A. F. Sanjuán, 2003, Phys. Rev. E **67**, 056201.
Aguirre, J., R. L. Viana, and M. A. F. Sanjuán, 2009, Rev. Mod. Phys. **81**, 333.
Akaishi, A., and A. Shudo, 2009, Phys. Rev. E **80**, 066211.
Alt, H., H. D. Gräf, H. L. Harney, R. Hofferbert, H. Lengeler, A. Richter, P. Schardt, and H. A. Weidenmüller, 1995, Phys. Rev. Lett. **74**, 62.
Alt, H., H.-D. Gräf, H. Harney, R. Hofferbert, H. Rehfeld, A. Richter, and P. Schardt, 1996, Phys. Rev. E **53**, 2217.
Altmann, E., and T. Tél, 2008, Phys. Rev. Lett. **100**, 174101.
Altmann, E., and T. Tél, 2009, Phys. Rev. E **79**, 016204.
Altmann, E. G., 2009, Phys. Rev. A **79**, 013830.
Altmann, E. G., E. C. da Silva, and I. L. Caldas, 2004, Chaos **14**, 975.
Altmann, E. G., and A. Endler, 2010, Phys. Rev. Lett. **105**, 255102.
Altmann, E. G., T. Friedrich, A. E. Motter, H. Kantz, and A. Richter, 2008, Phys. Rev. E **77**, 016205.
Altmann, E. G., and H. Kantz, 2007, Europhys. Lett. **78**, 10008.
Altmann, E. G., J. C. Leitao, and J. V. Lopes, 2012, Chaos **22**, 026114.
Altmann, E. G., G. Del Magno, and M. Hentschel, 2008, Europhys. Lett. **84**, 10008.
Altmann, E. G., A. E. Motter, and H. Kantz, 2005, Chaos **15**, 033105.
Altmann, E. G., A. E. Motter, and H. Kantz, 2006, Phys. Rev. E **73**, 026207.
Altmann, E. G., J. S. E. Portela, and T. Tél, 2013, unpublished.
Aref, H., 1984, J. Fluid Mech. **143**, 1.
Aref, H., and M. E. Naschie, 1995, *Chaos Applied to Fluid Mixing* (Pergamon, New York), 1st ed.
Ares, N., and D. A. Wisniacki, 2009, Phys. Rev. E **80**, 046216.
Armstead, D. N., B. R. Hunt, and E. Ott, 2004, Physica (Amsterdam) **193D**, 96.
Arnoldi, J.-F., F. Faure, and T. S. Weich, 2013, arXiv:1302.3087.
Artuso, R., E. Aurell, and P. Cvitanovic, 1990, Nonlinearity **3**, 361.
Artuso, R., L. Cavallasca, and G. Cristadoro, 2008, Phys. Rev. E **77**, 046206.
Artuso, R., and C. Manchein, 2009, Phys. Rev. E **80**, 036210.
Artuso, R., and A. Prampolini, 1998, Phys. Lett. A **246**, 407.
Bäcker, A., and H. Dullin, 1997, J. Phys. A **30**, 1991.
Bahsoun, W., and S. Vaienti, 2012, arXiv:1206.3654v1.
Bakhtin, Y., and L. Bunimovich, 2011, J. Stat. Phys. **143**, 943.
Barthélemy, J., O. Legrand, and F. Mortessagne, 2005, Europhys. Lett. **70**, 162.
Bauer, W., and G. Bertsch, 1990, Phys. Rev. Lett. **65**, 2213.
Berry, M., 1981, Eur. J. Phys. **2**, 91.
Berry, M., N. Balazs, M. Tabor, and A. Voros, 1979, Ann. Phys. (N.Y.) **122**, 26.
Berry, M. V., 1987, Proc. R. Soc. A **413**, 183.
Berry, M. V., 2009, J. Phys. A **42**, 165208.

Berry, M. V., 2010, in *New Directions in Linear Acoustics and Vibration*, edited by M. Wright, and R. Weaver (Cambridge University Press, Cambridge, England), pp. vii–ix.
Bittner, S., E. Bogomolny, B. Dietz, M. Miski-Oglu, P. Oria Iriarte, A. Richter, and F. Schäfer, 2010, Phys. Rev. E **81**, 066215.
Bittner, S., B. Dietz, R. Dubertrand, J. Isensee, M. Miski-Oglu, and A. Richter, 2012, Phys. Rev. E **85**, 056203.
Bleher, S., C. Grebogi, E. Ott, and R. Brown, 1988, Phys. Rev. A **38**, 930.
Bodai, T., E. G. Altmann, and A. Endler, 2013, Phys. Rev. E **87**, 042902.
Bogomolny, E., R. Dubertrand, and C. Schmit, 2008, Phys. Rev. E **78**, 056202.
Buljan, H., and V. Paar, 2001, Phys. Rev. E **63**, 066205.
Bunimovich, L., 2012, Contemp. Math. **567**, 11 236.
Bunimovich, L., and A. Yurchenko, 2011, Isr. J. Math. **182**, 229.
Bunimovich, L. A., 2008, Nonlinearity **21**, T13.
Bunimovich, L. A., and C. P. Dettmann, 2005, Phys. Rev. Lett. **94**, 100201.
Bunimovich, L. A., and C. P. Dettmann, 2007, Europhys. Lett. **80**, 40 001.
Bunimovich, L. A., and B. Z. Webb, 2012, arXiv:1211.4617.
Buric, N., A. Rampioni, G. Turchetti, and S. Vaienti, 2003, J. Phys. A **36**, L209.
Casati, G., G. Maspero, and D. L. Shepelyansky, 1997, Phys. Rev. E **56**, R6233.
Casati, G., G. Maspero, and D. L. Shepelyanski, 1999a, Physica (Amsterdam) **131D**, 311.
Casati, G., G. Maspero, and D. L. Shepelyansky, 1999b, Phys. Rev. Lett. **82**, 524.
Chappell, D. J., and G. Tanner, 2013, J. Comput. Phys. **234**, 487.
Chappell, D. J., G. Tanner, N. Sondergaard, and D. Loechel, 2013, arXiv:1303.4249.
Chernov, N., and R. Markarian, 2006, *Chaotic Billiards*, Mathematical Surveys and Monographs (American Mathematical Society, Providence), Vol. 112.
Chirikov, B. V., and D. L. Shepelyansky, 1984, Physica (Amsterdam) **13D**, 395.
Chirikov, B. V., and D. L. Shepelyansky, 1999, Phys. Rev. Lett. **82**, 528.
Chirikov, B. V., and D. L. Shepelyansky, 2002, Phys. Rev. Lett. **89**, 239402.
Christiansen, F., and P. Grassberger, 1993, Phys. Lett. A **181**, 47.
Cioffi, F., F. Gallerano, and E. Napoli, 2005, J. Hydraul. Res. **43**, 290.
Claus, I., and P. Gaspard, 2001, Phys. Rev. E **63**, 036227.
Collet, S., Pierre Martínez, and V. Maume-Deschamps, 2000, Nonlinearity **13**, 1263.
Cristadoro, G., G. Knight, and M. Degli Esposti, 2012, arXiv:1212.0673v1.
Cristadoro, G., and R. Ketzmerick, 2008, Phys. Rev. Lett. **100**, 184101.
Custódio, M. S., and M. W. Beims, 2011, Phys. Rev. E **83**, 056201.
Cvitanović, P., R. Artuso, P. Dahlquist, R. Mainieri, G. Tanner, G. Vattay, N. Whelan, and A. Wirzba, 2004, "Chaos: Classical and Quantum," http://chaosbook.org.
da Silva, E. C., I. L. Caldas, R. L. Viana, and M. A. F. Sanjuán, 2002, Phys. Plasmas **9**, 4917.
Dembowski, C., B. Dietz, T. Friedrich, H.-D. Gräf, A. Heine, C. Mejía-Monasterio, M. Miski-Oglu, A. Richter, and T. Seligman, 2004, Phys. Rev. Lett. **93**, 134102.
Demers, M., and P. Wright, 2011, arXiv:1112.4812.
Demers, M., P. Wright, and L.-S. Young, 2010, Commun. Math. Phys. **294**, 353.
Demers, M. F., and L.-S. Young, 2006, Nonlinearity **19**, 377.
de Moura, A. P. S., and P. S. Letelier, 1999, Phys. Lett. A **256**, 362.
Dennis, M. R., 2010, in *New Directions in Linear Acoustics and Vibration*, edited by M. Wright, and R. Weaver (Cambridge University Press, Cambridge, England), pp. 65–84.
Dettmann, C. P., 2011, in *Frontiers in the Study of Chaotic Dynamical Systems with Open Problems*, edited by Z. Elhadj, and J. C. Sprott (World Scientific, Singapore), pp. 195–218.
Dettmann, C. P., 2013, Nonlinearity **26**, 307.
Dettmann, C. P., and O. Georgiou, 2009, Physica (Amsterdam) **238D**, 2395.
Dettmann, C. P., and O. Georgiou, 2011a, J. Phys. A **44**, 195102.
Dettmann, C. P., and O. Georgiou, 2011b, Phys. Rev. E **83**, 036212.
Dettmann, C. P., and O. Georgiou, 2012, Chaos **22**, 026113.
Dettmann, C. P., and T. B. Howard, 2009, Physica (Amsterdam) **238D**, 2404.
Dettmann, C. P., and E. D. Leonel, 2012, Physica (Amsterdam) **241D**, 403.
Dettmann, C. P., G. V. Morozov, M. Sieber, and H. Waalkens, 2009, Phys. Rev. A **80**, 063813.
Dietz, B., T. Friedrich, M. Miski-Oglu, A. Richter, T. H. Seligman, and K. Zapfe, 2006, Phys. Rev. E **74**, 056207.
Dietz, B., A. Heine, A. Richter, O. Bohigas, and P. Leboeuf, 2006, Phys. Rev. E **73**, 035201.
Ding, M., T. Bountis, and E. Ott, 1990, Phys. Lett. A **151**, 395.
Dorfman, J. R., 1999, *An Introduction to Chaos in Nonequilibrium Statistical Mechanics* (Cambridge University Press, Cambridge, England), 1st ed.
Doron, E., and U. Smilansky, 1992a, Chaos **2**, 117.
Doron, E., and U. Smilansky, 1992b, Phys. Rev. Lett. **68**, 1255.
Dullin, H. R., and A. Baecker, 2001, Nonlinearity **14**, 1673.
Dumont, R., and P. Brumer, 1992, Chem. Phys. Lett. **188**, 565.
Eberspächer, A., J. Main, and G. Wunner, 2010, Phys. Rev. E **82**, 046201.
Eckhardt, B., 2003, J. Phys. A **36**, 371.
Engelhardt, W., and W. Feneberg, 1978, J. Nucl. Mater. **76–77**, 518.
Ermann, L., G. Carlo, and M. Saraceno, 2009, Phys. Rev. Lett. **103**, 054102.
Ermann, L., G. G. Carlo, J. M. Pedrosa, and M. Saraceno, 2012, Phys. Rev. E **85**, 066204.
Ermann, L., and D. L. Shepelyansky, 2010, Eur. Phys. J. B **75**, 299.
Evans, T. E., R. A. Moyer, and P. Monat, 2002, Phys. Plasmas **9**, 4957.
Ezra, G. S., H. Waalkens, and S. Wiggins, 2009, J. Chem. Phys. **130**, 164118.
Faisst, H., and B. Eckhardt, 2003, Phys. Rev. E **68**, 026215.
Falconer, K., 1985, *The Geometry of Fractal Sets*, Falconer-book (Cambridge University Press, Cambridge, England), 1st ed.
Faure, F., N. Roy, and J. Sjoestrand, 2008, Open Mat. J. **1**, 35 [http://www.benthamscience.com/open/tomatj/articles/V001/35TOMATJ.htm].
Fendrik, A. J., A. M. F. Rivas, and M. J. Sánchez, 1994, Phys. Rev. E **50**, 1948.
Fendrik, A. J., and M. J. Sánchez, 1995, Phys. Rev. E **51**, 2996.
Fendrik, A. J., and D. A. Wisniacki, 1997, Phys. Rev. E **55**, 6507.
Ferguson, A., and M. Pollicott, 2012, Ergod. Theory Dyn. Syst. **32**, 961.
Friedman, N., A. Kaplan, D. Carasso, and N. Davidson, 2001, Phys. Rev. Lett. **86**, 1518.
Froyland, G., and K. Pradberg, 2009, Physica (Amsterdam) **238D**, 1507.

Froyland, G., and O. Stancevic, 2010, Discrete Contin. Dyn. Syst. Series B **14**, 457.
Fyodorov, Y. V., D. V. Savin, and H.-J. Sommers, 2005, J. Phys. A **38**, 10731.
García-Mata, I., and D. A. Wisniacki, 2011, J. Phys. A **44**, 315101.
Gaspard, P., 1996, Phys. Rev. E **53**, 4379.
Gaspard, P., 1998, *Chaos, Scattering and Statistical Mechanics*, Cambridge Nonlinear Science Series (Cambridge University Press, Cambridge, England), Vol. 9.
Gaspard, P., and J. R. Dorfman, 1995, Phys. Rev. E **52**, 3525.
Geisel, T., A. Zacherl, and G. Radons, 1988, Z. Phys. B **71**, 117.
Georgiou, O., C. P. Dettmann, and E. G. Altmann, 2012, Chaos **22**, 043115.
Gmachl, C., F. Capasso, E. E. Narimanov, J. U. Nöckel, A. D. Stone, J. Faist, and D. L. Sivco, 1998, Science **280**, 1556.
Gorin, T., T. Prosen, T. H. Seligman, and M. Znidaric, 2006, Phys. Rep. **435**, 33.
Goussev, A., and K. Richter, 2007, Phys. Rev. E **75**, 015201(R).
Goussev, A., D. Waltner, K. Richter, and R. Jalabert, 2008, New J. Phys. **10**, 093010.
Grete, P., and M. Markus, 2007, Phys. Rev. E **75**, 036207.
Gutiérrez, M., and A. Goussev, 2009, Phys. Rev. E **79**, 046211.
Gutiérrez, M., D. Waltner, J. Kuipers, and K. Richter, 2009, Phys. Rev. E **79**, 046212.
Harayama, T., and S. Shinohara, 2011, Laser Photonics Rev. **5**, 247.
Haydn, N., Y. Lacroix, and S. Vaienti, 2005, Ann. Probab. **33**, 2043.
Höhmann, R., U. Kuhl, and H.-J. Stöckmann, 2008, Phys. Rev. Lett. **100**, 124101.
Hu, H., A. Rampioni, L. Rossi, G. Turchetti, and S. Vaienti 2004, Chaos **14**, 160.
Jacobs, J., E. Ott, and B. Hunt, 1998, Phys. Rev. E **57**, 6577.
Jacquod, P., and C. Petitjean, 2009, Adv. Phys. **58**, 67.
Joyce, W. B., 1975, J. Acoust. Soc. Am. **58**, 643.
Joyce, W. B., 1978, J. Acoust. Soc. Am. **64**, 1429.
Jung, C., T. Tél, and E. Ziemniak, 1993, Chaos **3**, 555.
Kac, M., 1959, *Probability and Related Topics in Physical Sciences* (Interscience, New York).
Kantz, H., and P. Grassberger, 1985, Physica (Amsterdam) **17D**, 75.
Kantz, H., and P. Grassberger, 1987, Phys. Lett. A **123**, 437.
Kaplan, A., N. Friedman, M. Andersen, and N. Davidson, 2001, Phys. Rev. Lett. **87**, 274101.
Karney, C. F. F., 1983, Physica (Amsterdam) **8D**, 360.
Károlyi, G., M. Pattanyús-Ábrahám, T. Krámer, J. Józsa, and T. Tél, 2010, Engineering Comp. Mech. **163**, 251.
Katok, A., and B. Hasselblatt, 1995, *Introduction to the Modern Theory of Dynamical Systems*, Encyclopedia of Mathematics and its Applications (Cambridge University Press, Cambridge, England).
Kaufmann, Z., and H. Lustfeld, 2001, Phys. Rev. E **64**, 055206.
Keating, J., M. Novaes, S. Prado, and M. Sieber, 2006, Phys. Rev. Lett. **97**, 150406.
Keller, G., and C. Liverani, 2009, J. Stat. Phys. **135**, 519.
Ketzmerick, R., L. Hufnagel, F. Steinbach, and M. Weiss, 2000, Phys. Rev. Lett. **85**, 1214.
Klages, R., 2007, *Microscopic Chaos, Fractals and Transport in Nonequilibrium Statistical Mechanics*, Advanced Series in Nonlinear Dynamics (World Scientific, Singapore).
Knight, G., O. Georgiou, C. Dettmann, and R. Klages, 2012, Chaos **22**, 023132.
Köber, B., U. Kuhl, H.-J. Stöckmann, A. Goussev, and K. Richter, 2011, Phys. Rev. E **83**, 016214.
Kokshenev, V., and M. Nemes, 2000, Physica (Amsterdam) **275A**, 70.
Kokshenev, V., and E. Vicentini, 2003, Phys. Rev. E **68**, 016221.
Kopp, M., and H. Schomerus, 2010, Phys. Rev. E **81**, 026208.
Körber, M. J., M. Michler, A. Bäcker, and R. Ketzmerick, 2013, arXiv:1304.2662.
Kovács, Z., and T. Tél, 1992, Phys. Rev. A **45**, 2270.
Kuhl, U., H.-J. Stöckmann, and R. Weaver, 2005, J. Phys. A **38**, 10433.
Lai, Y.-C., and T. Tél, 2011, *Transient Chaos: Complex Dynamics in Finite Time Scales*, Applied Mathematical Sciences (Springer, New York), Vol. 173.
Lai, Y.-C., K. Życzkowski, and C. Grebogi, 1999, Phys. Rev. E **59**, 5261.
Laskar, J., and M. Gastineau, 2009, Nature (London) **459**, 817.
Lau, Y.-T., J. M. Finn, and E. Ott, 1991, Phys. Rev. Lett. **66**, 978.
Lebental, M., J. S. Lauret, J. Zyss, C. Schmit, and E. Bogomolny, 2007, Phys. Rev. A **75**, 033806.
Lee, S.-Y., S. Rim, J.-W. Ryu, T.-Y. Kwon, M. Choi, and C.-M. Kim, 2004, Phys. Rev. Lett. **93**, 164102.
Legrand, O., and D. Sornette, 1990a, Physica (Amsterdam) **44D**, 229.
Legrand, O., and D. Sornette, 1990b, Europhys. Lett. **11**, 583.
Legrand, O., and D. Sornette, 1991a, Phys. Rev. Lett. **66**, 2172.
Legrand, O., and D. Sornette, 1991b, in *Large Scale Structures in Nonlinear Physics*, edited by J.-D. Fournier, and P.-L. Sulem, Lecture Notes in Physics (Springer, Berlin/Heidelberg), Vol. 392, pp. 267–274.
Leonel, E. D., M. W. Beims, and L. A. Bunimovich, 2012, Chaos **22**, 026101.
Leonel, E. D., and C. P. Dettmann, 2012, arXiv:1203.6235v1.
Lippolis, D., J.-W. Ryu, S.-Y. Lee, and S. W. Kim, 2012, Phys. Rev. E **86**, 066213.
Liu, Z., and Y.-C. Lai, 2002, Phys. Rev. E **65**, 046204.
Lu, W. T., S. Sridhar, and M. Zworski, 2003, Phys. Rev. Lett. **91**, 154101.
Matyas, L., and I. F. Barna, 2011, Chaos, Solitons and Fractals **44**, 1111.
Matyas, L., and P. Gaspard, 2005, Phys. Rev. E **71**, 036147.
Matyas, L., and R. R. Klages, 2004, Physica (Amsterdam) **187D**, 66.
Meiss, J. D., 1992, Rev. Mod. Phys. **64**, 795.
Meiss, J. D., 1997, Chaos **7**, 139.
Meiss, J. D., and E. Ott, 1985, Phys. Rev. Lett. **55**, 2741.
Meiss, J. D., and E. Ott, 1986, Physica (Amsterdam) **20D**, 387.
Mekis, A., J. U. Nöckel, G. Chen, A. D. Stone, and R. K. Chang, 1995, Phys. Rev. Lett. **75**, 2682.
Miyaguchi, T., 2007, Phys. Rev. E **75**, 066215.
Morrison, P. J., 2000, Phys. Plasmas **7**, 2279.
Mortessagne, F., O. Legrand, and D. Sornette, 1992, Europhys. Lett. **20**, 287.
Mortessagne, F., O. Legrand, and D. Sornette, 1993, Chaos **3**, 529.
Motter, A., 2001, Phys. Lett. A **285**, 127.
Nagler, J., 2002, Das eingeschränkte Drei-Körper-Problem im Crashtest, Ph.D. thesis, Bremen University.
Nagler, J., 2004, Phys. Rev. E **69**, 066218.
Nagler, J., 2005, Phys. Rev. E **71**, 026227.
Nagler, J., M. Krieger, M. Linke, J. Schönke, and J. Wiersig, 2007, Phys. Rev. E **75**, 046204.
Nándori, P., and D. Szász, 2012, Chaos **22**, 026115.
Neufeld, Z., P. H. Haynes, and G. Picard, 2000, Phys. Fluids **12**, 2506.
Neufeld, Z., and E. Hernández-Garcia, 2009, *Chemical and Biological Processes in Fluid Fows: A Dynamical Systems Approach* (Imperial College Press, Cambridge), 1st ed.
Ngan, K., and R. Pierrehumbert, 2000, Phys. Fluids **12**, 822.
Nöckel, J. U., and A. D. Stone, 1997, Nature (London) **385**, 45.

Nonnenmacher, S., 2011, Nonlinearity **24**, R123.
Nonnenmacher, S., and E. Schenk, 2008, Phys. Rev. E **78**, 045202R.
Nonnenmacher, S., and M. Zworski, 2005, J. Phys. A **38**, 10 683.
Novaes, M., 2012, arXiv:1211.7248v1.
Novaes, M., J. M. Pedrosa, D. Wisniacki, G. G. Carlo, and J. P. Keating, 2009, Phys. Rev. E **80**, 035202.
Ott, E., 1993, *Chaos in Dynamical Systems* (Cambridge University Press, Cambridge, England).
Ottino, J. M., 1989, *The Kinematics of Mixing: Stretching, Chaos and Transport* (Cambridge University Press, Cambridge, England), 1st ed.
Paar, V., and H. Buljan, 2000, Phys. Rev. E **62**, 4869.
Paar, V., and N. Pavin, 1997, Phys. Rev. E **55**, 4112.
Pedrosa, J. M., G. G. Carlo, D. A. Wisniacki, and L. Ermann, 2009, Phys. Rev. E **79**, 016215.
Pedrosa, J. M., D. Wisniacki, G. G. Carlo, and M. Novaes, 2012, Phys. Rev. E **85**, 036203.
Peres, A., 1984, Phys. Rev. A **30**, 1610.
Pianigiani, G., and J. A. Yorke, 1979, Trans. Am. Math. Soc. **252**, 351.
Pierrehumbert, R., H. Brogniez, and R. Roca, 2007, in *The Global Circulation of the Atmosphere*, edited by T. Schneider, and A. Sobel (Princeton University Press, Princeton, NJ).
Pierrehumbert, R. T., 1994, Chaos Solitons Fractals **4**, 1091.
Pikovsky, A., and O. Popovich, 2003, Europhys. Lett. **61**, 625.
Pikovsky, A. S., 1992, J. Phys. A **25**, L477.
Poli, C., B. Dietz, O. Legrand, F. Mortessagne, and A. Richter, 2009, Phys. Rev. E **80**, 035204.
Poli, C., G. A. Luna-Acosta, and H.-J. Stöckmann, 2012, Phys. Rev. Lett. **108**, 174101.
Portela, J. S., I. L. Caldas, and R. L. Viana, 2008, Eur. Phys. J. Special Topics **165**, 195.
Portela, J. S. E., I. L. Caldas, R. L. Viana, and M. A. F. Sanjuán, 2007, Int. J. Bifurcation Chaos Appl. Sci. Eng. **17**, 4067.
Potzuweit, A., T. Weich, S. Barkhofen, U. Kuhl, H.-J. Stöckmann, and M. Zworski, 2012, Phys. Rev. E **86**, 066205.
Puhlmann, M., H. Schanz, T. Kottos, and T. Geisel, 2005, Europhys. Lett. **69**, 313.
Ramilowski, J. A., S. D. Prado, F. Borondo, and D. Farrelly, 2009, Phys. Rev. E **80**, 055201(R)
Redding, B., L. Ge, Q. Song, J. Wiersig, G. S. Solomon, and H. Cao, 2012, Phys. Rev. Lett. **108**, 253902.
Ree, S., and L. Reichl, 2002, Phys. Rev. E **65**, 055205.
Richter, A., 1999, in *The IMA Volumes in Mathematics and its Applictaions* (Springer-Verlag, New York), Vol. 109, p. 479.
Robnik, M., 1983, J. Phys. A **16**, 3971.
Rotter, I., 2009, J. Phys. A **42**, 153001.
Ryu, J.-W., S.-Y. Lee, C.-M. Kim, and Y.-J. Park, 2006, Phys. Rev. E **73**, 036207.
Sadurní, E., and T. H. Seligman, 2008, J. Phys. A **41**, 102002.
Saito, N., H. Hirooka, J. Ford, F. Vivaldi, and G. Walker, 1982, Physica (Amsterdam) **5D**, 273.
Sanjuán, M. A. F., T. Horita, and K. Aihara, 2003, Chaos **13**, 17.
Savin, D. V., O. Legrand, and F. Mortessagne, 2006, Europhys. Lett. **76**, 774.
Savin, D. V., and V. V. Sokolov, 1997, Phys. Rev. E **56**, R4911.
Schelin, A., I. Caldas, R. Viana, and S. Benkadda, 2011, Phys. Lett. A **376**, 24.
Schenck, E., 2009, Ann. Henri Poincaré **10**, 711.
Schmitz, O., 2012, Nucl. Fusion **52**, 054001.
Schneider, J., V. Fernández, and E. Hernández-Garcia, 2005, J. Mar. Syst. **57**, 111.
Schneider, J., J. Schmalzl, and T. Tél, 2007, Chaos **17**, 033115.
Schneider, J., and T. Tél, 2003, Ocean Dynamics **53**, 64.
Schneider, J., T. Tél, and Z. Neufeld, 2002, Phys. Rev. E **66**, 066218.
Schomerus, H., and M. Hentschel, 2006, Phys. Rev. Lett. **96**, 243903.
Schomerus, H., and J. Tworzydło, 2004, Phys. Rev. Lett. **93**, 154102.
Schwefel, H. G. L., N. B. Rex, H. E. Tureci, R. K. Chang, A. D. Stone, T. Ben-Messaoud, and J. Zyss, 2004, J. Opt. Soc. Am. B **21**, 923.
Shen, Y., M. Miyake, S. Takamura, T. Kuroda, and T. Okuda, 1989, J. Nucl. Mater. **168**, 295.
Shepelyansky, D. L., 2008, Phys. Rev. E **77**, 015202(R).
Shinohara, S., T. Harayama, T. Fukushima, M. Hentschel, T. Sasaki, and E. E. Narimanov, 2010, Phys. Rev. Lett. **104**, 163902.
Shinohara, S., T. Harayama, T. Fukushima, M. Hentschel, S. Sunada, and E. Narimanov, 2011, Phys. Rev. A **83**, 053837.
Shinohara, S., M. Hentschel, J. Wiersig, T. Sasaki, and T. Harayama, 2009, Phys. Rev. A **80**, 031801.
Sieber, M., and K. Richter, 2001, Phys. Scr. **2001** T90, 128.
Skipetrov, S. E., and B. A. van Tiggelen, 2006, Phys. Rev. Lett. **96**, 043902.
Song, Q., W. Fang, B. Liu, S.-T. Ho, G. S. Solomon, and H. Cao, 2009, Phys. Rev. A **80**, 041807.
Song, Q., L. Ge, B. Redding, and H. Cao, 2012, Phys. Rev. Lett. **108**, 243902.
Song, Q. H., L. Ge, A. D. Stone, H. Cao, J. Wiersig, J.-B. Shim, J. Unterhinninghofen, W. Fang, and G. S. Solomon, 2010, Phys. Rev. Lett. **105**, 103902.
Spina, M. A., I. Garcia-Mata, and M. Saraceno, 2010, J. Phys. A **43**, 392003.
Stockmann, H.-J., 1999, *Quantum Chaos—An Introduction* (Cambridge University Press, Cambridge, England), 1st ed.
Szanyi, S., 2012, in *Proceedings of the Conference of Junior Researchers in Civil Engineering*, edited by J. Jozsa, T. Lovas, and R. Nemeth (Budapest University of Technology and Economics, Budapest), pp. 225–232.
Taddese, B. T., T. M. Antonsen, E. Ott, and S. M. Anlage, 2010, J. Appl. Phys. **108**, 114911.
Takamura, S., Y. Shen, H. Yamada, M. Miyake, T. Tamakoshi, and T. Okuda, 1989, J. Nucl. Mater. **162–164**, 643.
Tanaka, H., and A. Shudo, 2006, Phys. Rev. E **74**, 036211.
Tanaka, T., M. Hentschel, T. Fukushima, and T. Harayama, 2007, Phys. Rev. Lett. **98**, 033902.
Tanner, G., 2009, J. Sound Vib. **320**, 1023.
Tél, T., 1987, Phys. Rev. A **36**, 1502.
Tél, T., A. P. S. de Moura, C. Grebogi, and G. Károlyi, 2005, Phys. Rep. **413**, 91.
Tél, T., and M. Gruiz, 2006, *Chaotic Dynamics: An Introduction Based on Classical Mechanics* (Cambridge University Press, Cambridge, England).
Tuval, I., J. Schneider, O. Piro, and T. Tél, 2004, Europhys. Lett. **65**, 633.
Ullmann, K., and I. L. Caldas, 2000, Chaos, Solitons & Fractals **11**, 2129.
Vahala, K., 2003, Nature (London) **424**, 839.
Venegeroles, R., 2009, Phys. Rev. Lett. **102**, 064101.
Viana, R. L., E. C. D. Silva, T. Kroetz, I. L. Caldas, M. Roberto, and M. A. F. Sanjuán, 2011, Phil. Trans. R. Soc. A **369**, 371.
Vicentini, E., and V. B. Kokshenev, 2001, Physica (Amsterdam) **295A**, 391.
Vivaldi, F., G. Casati, and I. Guarneri, 1983, Phys. Rev. Lett. **51**, 727.
Waltner, D., M. Gutierrez, A. Goussev, and K. Richter, 2008, Phys. Rev. Lett. **101**, 4.

Weiss, M., L. Hufnagel, and R. Ketzmerick 2002, Phys. Rev. Lett. **89**, 239401.
Wesson, J., 1987, *Tokamaks* (Oxford University Press, Oxford, UK).
Wiersig, J., and M. Hentschel, 2008, Phys. Rev. Lett. **100**, 033901.
Wiersig, J., and J. Main, 2008, Phys. Rev. E **77**, 036205.
Wimberger, S., A. Krug, and A. Buchleitner, 2002, Phys. Rev. Lett. **89**, 263601.
Wingen, A., M. Jakubowski, K. H. Spatschek, S. S. Abdullaev, K. H. Finken, M. Lehnen, and TEXTOR team, 2007, Phys. Plasmas **14**, 042502.
Wojtkowski, M., 1986, Commun. Math. Phys. **105**, 391.
Xeridat, O., C. Poli, O. Legrand, F. Mortessagne, and P. Sebbah, 2009, Phys. Rev. E **80**, 035201.
Yan, C., Q. J. Wang, L. Diehl, M. Hentschel, J. Wiersig, N. Yu, C. Pflügl, M. A. Belkin, T. Edamura, M. Yamanishi, H. Kan, and F. Capasso, 2009 Appl. Phys. Lett. **94**, 251101.
Zaslavsky, G. M., 2002, Phys. Rep. **371**, 461.
Zaslavsky, G. M., 2005, *Hamiltonian Chaos and Fractional Dynamics* (Oxford University Press, Oxford).
Życzkowski, K., and E. M. Bollt, 1999, Physica (Amsterdam) **132D**, 392.